7-26-2016 12:00 AM

Application of Molecular Layer Deposition for Graphite Anodes in Lithium-ion Batteries and Porous Thin-film Materials

Craig L. Langford, *The University of Western Ontario*

Supervisor: Dr. Xueliang (Andy) Sun, *The University of Western Ontario*

A thesis submitted in partial fulfillment of the requirements for the Master of Engineering Science degree in Mechanical and Materials Engineering

Abstract

With climate change occurring because of greenhouse gas emissions, the demand for emission free transportation has led to the development of electric vehicles. Improving the batteries' cycling stability, capacity and safety have been the leading challenges to compete with gasoline and diesel engines. With advances in thin-film deposition techniques via atomic and molecular layer deposition, ultrathin films can be deposited to control the surface chemistry of the battery's active materials. This thesis aims to understand two main aspects of molecular layer deposition. First, how it can influence solid electrolyte interface formation on the graphite surface during cycling in a lithium-ion battery. Utilizing physical and electrochemical testing it is shown that a conformal coating can be deposited on the graphite electrode, and graphite's characteristic capacity decay can be eliminated increasing the battery's longevity. Second, how the organic chain length in the hybrid organic-inorganic thin-films can influence the thin films structure after annealing in an oxygen rich atmosphere. Utilizing chemical and physical characterization techniques it is shown that a controllable surface area can be achieved.

Keywords

Nanomaterials, molecular layer deposition, lithium-ion battery, graphite, thin-film coatings, porous materials, renewable energy

Co-Authorship Statement

Chapter 3

Graphite anode fabrication and testing was performed by C. Langford under the guidance of Dr. Xueliang Sun and Dr. Xifei Li. Atomic and molecular layer deposition was performed with the guidance of Andrew Lushington.

Chapter 4

BET surface area measurements were performed under the guidance of Xia Li.

Acknowledgments

First, I would like to thank Prof. Xueliang (Andy) Sun for his support throughout my graduate studies at Western University. Since he first took me as a research assistant for an internship during my undergraduate studies, he has been an incredible mentor and has helped guide my career and studies beyond what I deemed possible. Along the way, he has provided excellent support and I am proud to have worked as his graduate student. I would also like to thank Kathy Li, the laboratory manager, who kept everything running smoothly in the laboratories. Furthermore, she was always around for personal support outside of my studies. Thanks for making my time at Western so enjoyable.

Throughout my studies a number post-doctoral fellows were of great assistance to my work. In particular, I would like to thank Dr. Xifei Li for his extensive knowledge and guidance in battery fabrication and theory, Dr. Jian Liu, for his mentorship in atomic and molecular layer deposition, and Dr. Qian Sun for his tremendously in-depth understanding of LIB materials. Without all of their help, much of my research would not have been possible.

I would like to extend my gratitude to Dr. Fang Dai and Dr. Mei Cai who supervised my research during my time at General Motors. In particular, Dr. Dai was a wealth of information with respect to rechargeable systems for electric vehicles. He helped shape my understanding of the technology landscape, as well as understand the possibilities and limitations of these advanced technologies for future application.

I would like to thank all the fellow researchers in our group. Particularly those in the ALD/MLD sub-group: Andrew Lushington, Biqiong Wang and Yang Zhao. Your assistance meant a great deal. Without the love and support from my parents and sisters, this would not have been possible. Andrew, Adam, Anastasia and Steve for the beers and many talks on electric vehicle technologies and beyond. Finally, I would like to thank my girlfriend Mudi for her lasting love and support throughout my studies.

Table of Contents

List of Tables

List of Figures

Glossary

ALD – atomic layer deposition

BET – Brunaur, Emmet and Teller

CV – cyclic voltammetry

CVD – chemical vapor deposition

DEC – diethyl carbonate

DMC – dimethyl carbonate

DSC – differential scanning calorimetry

EC – ethylene carbonate

EDX – energy-dispersive X-ray

EG – ethylene glycol

EIS – electroimpedance spectroscopy

EMC – ethyl methyl carbonate

FTIR – Fourier transform infrared spectroscopy

LIB – lithium-ion battery

LIPON – lithium phosphorous oxynitride

MLD – molecular layer deposition

PC – propylene carbonate

PLD – pulsed laser deposition

PVD – physical vapor deposition

QCM – quartz crystal microbalance

RF – radio frequency

SEI – solid electrolyte interface

SEM – scanning electron microscopy

TC – terphthalyoyl chloride

TGA – thermogravimetric analysis

TMA – trimethylaluminum

VC – vinylene carbonate

1 Introduction and Literature Review

1.1 Lithium-ion Batteries

The rechargeable lithium-ion battery (LIB) was first commercialized by Sony in 1991 [1], quickly overtaking portable nickel-metal-hydride and nickel-cadmium batteries [2], becoming the leading rechargeable battery system. This is due to its high energy density, high power density, long life-time, low self-discharge, and relative environmental friendliness [1], [3]. These properties also make LIBs a viable alternative to fossil fuels for electric vehicles. There has been a recent shift towards using sustainable energy to reduce greenhouse gas emissions. Transportation was Canada's second largest greenhouse gas contributor in 2012, accounting for 24% the total greenhouse gas emissions [4]. To reduce and eliminate transportation emissions a portable energy storage system is essential, an excellent application for LIBs. Nevertheless, despite their aforementioned advantages, when utilized in electric vehicles and compared to a conventional combustion engine, LIBs still have to address a number of issues including energy density, safety, durability, uniformity and cost [3].

1.1.1 Fundamentals of Lithium-ion Batteries

LIBs are electrochemical cells, which are composed of three main components: the cathode, anode, and an intermediary electrolyte, that can be connected in series or parallel to create a LIB pack. During charging of the battery, electrons are removed from the cathode, which is oxidized, and travel through the external circuit to the anode, which is reduced (Figure 1.1). Meanwhile, Li-ions travel across the electrolyte from the cathode to the anode to complete the electric circuit. Once the anode is fully reduced, and/or the cathode fully oxidized, the battery is fully charged. When the cell is connected to an external load, the electron-rich anode oxidizes and the resulting electrons flow through the external load producing electric current. Again, the lithium ions travel across the electrolyte from the anode to the cathode completing the circuit.

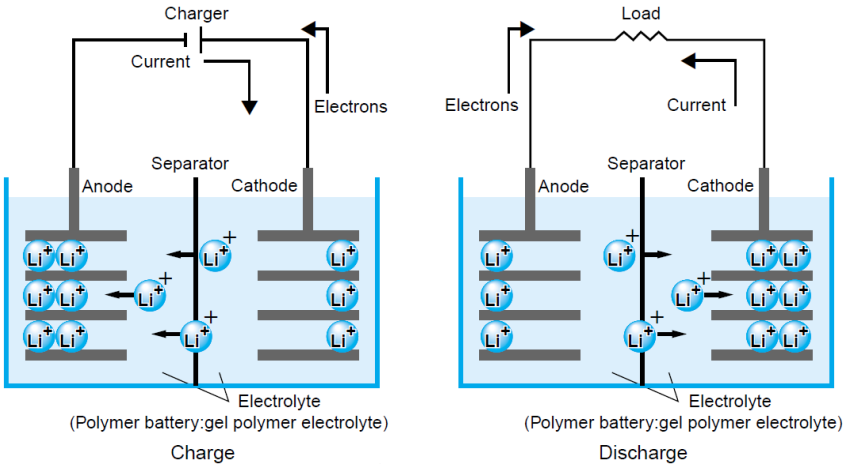

Figure 1.1. Schematic depicting the charge and discharge of a LIB [5].

In commercial LIBs, the anode and cathode are both composed of layered intercalation compounds which have been shown to be safe with a high cyclability [1]. A metal oxide is normally used as the cathode material with the half reaction:

$$Li_{1-x}MO_2 + xLi^+ + xe^- \leftrightarrow LiMO_2 \quad \textbf{(1.1)}$$

And graphite as the anode with the half reaction:

$$xLiC_6 \leftrightarrow xLi^+ + xe^- + xC_6 \quad \textbf{(1.2)}$$

Resulting in the overall reaction:

$$LiMO_2 + C_6 \leftrightarrow Li_{1-x}MO_2 + xLiC_6 \quad \textbf{(1.3)}$$

The difference of the potentials between reactions 1.1 and 1.2 determines the maximum energy density which can be delivered from the LIB. Ideally all of the electrochemical energy from these reactions would convert to electrical energy, however, this is not the case. Energy is lost within the cell as a result of the following factors:

(1) **The charge transfer overpotential.** The energy needed to be overcome for the reactions to occur at the electrodes' surfaces.

(2) **The concentration polarization.** A result of a concentration gradient of products and reactants at the electrode surface and bulk due to limited mass transfer.

(3) **Internal resistances in the cell.** Includes any resistance through the current collectors, interface resistance between the current collectors and the active material, etc.

Connecting the cell to an external load R results in a voltage of:

$$E = E_0 - [(\eta_{ct})_a + (\eta_c)_a] - [(\eta_{ct})_c + (\eta_c)_c] - iR_i = iR \quad \textbf{(1.4)}$$

Where E_0 = open-circuit voltage of cell

$(\eta_{ct})_a, (\eta_{ct})_c$ = charge transfer overvoltage at anode and cathode

$(\eta_{ct})_a, (\eta_c)_c$ = concentration polarization at anode and cathode

i = operating current of cell on load

R_i = internal resistances of the cell

These resistances follow Ohm's law and result in a linear relationship between the battery's output current and resulting voltage drop. Therefore, at higher current densities the voltage drop of LIBs will be more pronounced.

A number of different battery configurations have developed for LIBs since their introduction. The most popular commercial designs used today are made from wound Li-ion cells [1]. In these cells, a porous polyolefin polymer separates the anode and cathode, which are wound to the desired configuration. This method is used to create cylindrical cells (Figure 1.2a), prismatic cells and pouch cells (both of which are folded in a flat configuration). The cathode and anode current collectors, typically aluminum and copper foil respectively, are coated on each side by the battery's active material. Tabs are attached to the current collectors to connect to the battery's terminals. This configuration maximizes the relative mass of the battery's active materials increasing the overall specific capacity. The wound lithium-ion cell design is advantageous in minimizing the mass of the battery housing and enhancing safety features. Looking at the mass distribution of commercial cells from Sony in Figure 1.2b, it can be seen that the active anode and cathode electrode materials compromise a majority of the battery's total mass. Pouch cells, those typically used for smart-phones and other mobile devices, use a thin plastic/aluminum casing instead of a hard metal casing decreasing the relative mass of the packaging even further [6]. For

further improvement of the specific capacity of the battery it is evident that the specific capacity of the active materials (positive and negative electrodes) must be improved.

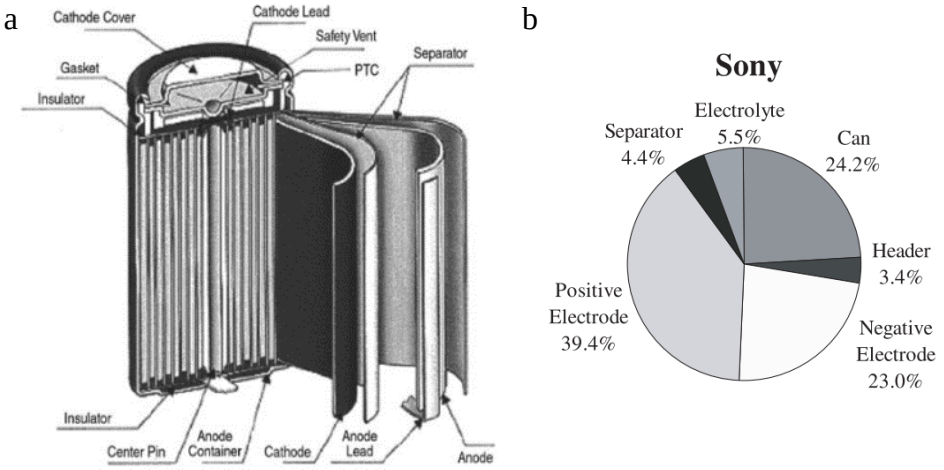

Figure 1.2. (a) Schematic [7] and (b) mass distribution of different components [1] in a commercial cylindrical cell.

The demand for smaller LIBs is increasing for a number of wireless consumer and medical products [8]. Despite the above efforts, the wound LIB design becomes impractical when miniaturized as the relative packaging mass increases [9]. The packaging is responsible for the containment of the liquid electrolyte, ensuring its safety. Therefore, over the past several decades a number of studies have focused on the development of practical micro-batteries without a liquid electrolyte [8]. The thin-film LIB was developed from these works which is an all-solid-state battery composed of several electrochemical cells that are connected in series and/or parallel with each other. These batteries are deposited via thin film techniques over a substrate with a total thickness of less than 15 μm [9]. A typical schematic of such a thin-film battery configuration can be seen in Figure 1.3. In this configuration the mass of the packaging makes up an even smaller portion of the total mass, therefore, the battery performance is even more dependent upon the active anode and cathode materials.

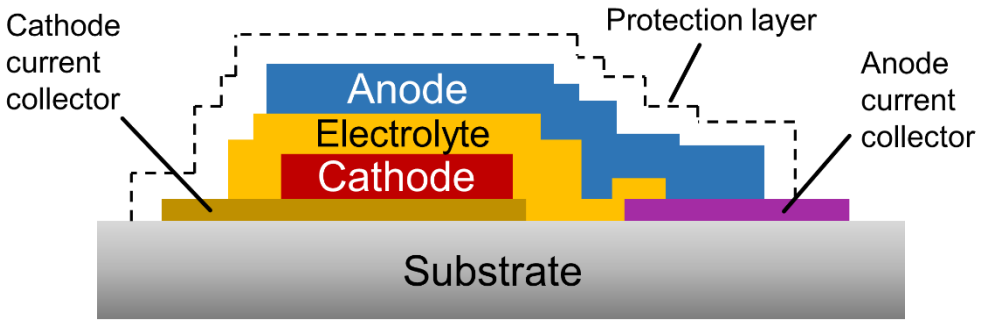

Figure 1.3: Configuration of an all-solid-state thin-film battery.

This thesis focuses on improving the cycling capacity of graphite, the commercial lithium-ion battery anode material, to improve the overall specific capacity of the battery. The decreasing specific capacity can be attributed to instabilities of the graphite-electrolyte interface. Conventional techniques to improve the interface stability are introduced here as their understanding is critical to developing a superior method to address this issue. To improve the stability this thesis focuses on utilizing a thin film technique which is introduced in detail in Chapter 1.2.

1.1.2 Graphite for Lithium-ion Batteries

Pure lithium anodes were briefly commercialized in the early 1980s but this was short lived. They proved highly dangerous due to lithium's high volatility as well as lithium dendrite formation, which could short the battery causing thermal runaway [10]. An anode material which lithiated and delithiated safely and consistently was needed. Graphite was found to be a possible lithium intercalation compound in the 1970s [11], however, this was typically done via crude techniques such as mixing lithium with graphite, and not achieved electrochemically. It wasn't until 1983 that Yazami demonstrated that, with a solid electrolyte, graphite could be intercalated electrochemically [12]. This lead to increasing research interest in graphite as a LIB anode material despite its impractical cyclability, it only exhibited 10% of its initial capacity after 5 cycles [10]. It wasn't until 1991 when Sony announced a battery claiming to have greater than 1200 cycles that graphite's practicality was demonstrated [10]. This high cyclability is attributed to graphite's distinct intercalation properties and is enabled by the use of an organic electrolyte discussed further in this chapter.

Intercalation of lithium into graphite is periodic, that is, when fully lithiated every layer is lithiated, at half lithiation every second layer is lithiated, etc (Figure 1.4). These different stages exhibit different reduction potentials due to slightly different energies needed for its reduction. These voltage plateaus in which the phase change occurs have been well documented and occur at a low voltage vs Li/Li+, ideal for a LIB anode material [12], [13]. Fully lithiating the graphite to stage one results in a final composition of LiC_6 with a theoretical capacity of 372 mAh/g.

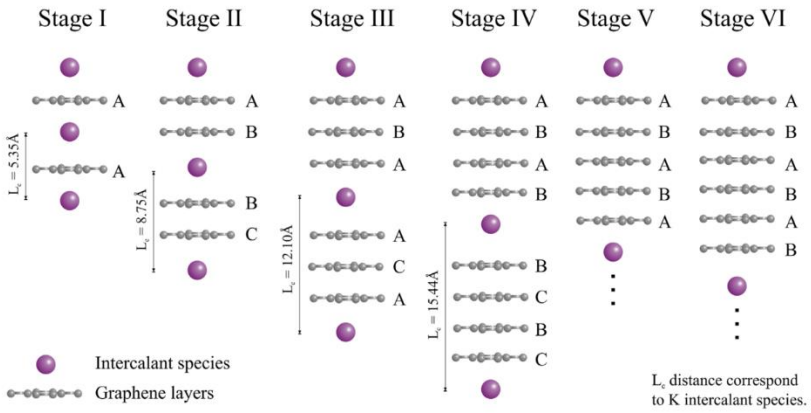

Figure 1.4. Schematic of phases graphite forms during delithiation [14].

What makes the pairing of graphite with a carbonate-based electrolyte so unique is that the potential of the graphite is above the voltage window of the electrolyte. In an ideal battery configuration (Figure 1.5a) the potential of the anode would be below that of the electrolyte's potential window, therefore, reduction of the electrolyte is avoided. In the graphite-carbonate based system, the higher graphite potential enables reduction of the electrolyte on the graphite's surface (Figure 1.5b). This process occurs on the cathode as well due to the cathode oxidizing the electrolyte. The products formed from these reactions create a thin, solid coating on the electrodes' surfaces called the solid-electrolyte-interphase (SEI).

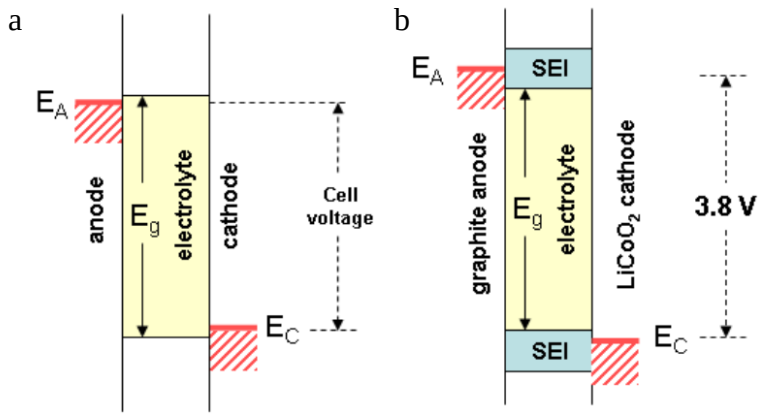

Figure 1.5. Voltage window of (a) a desired electrolyte and (b) a carbonate based electrolyte paired with a graphite/$LiCoO_2$ system [15].

The SEI between the graphite and electrolyte is the key to graphite's practicality. The requirements for the SEI are as follows:

(1) **An electron transference number of zero.** There must be no electrons allowed through the SEI, otherwise reduction of the electrolyte would continuously occur.

(2) **High lithium-ion conductivity.** Allows the diffusion of lithium-ions to intercalate/deintercalate easily to/from the graphite.

(3) **Uniform morphology and chemical composition.** Enables a uniform current distribution.

(4) **Good adhesion to the graphite's surface.** Deters delamination, which would expose and reduce fresh electrolyte on the graphite's surface.

(5) **Good mechanical strength and flexibility.** Allows the expansion and contraction of the graphite during lithiation and delithiation.

(6) **Low electrolyte solubility.** Stops the continuous dissolution of the SEI into the electrolyte.

Early reports used propylene carbonate (PC) as an electrolyte [16] which resulted in a poorly adhering SEI which led to continuous decomposition of the electrolyte. It wasn't until an ethylene carbonate (EC) containing electrolyte was developed that a stable SEI

was achieved [17]. The SEI created by EC based electrolytes met the requirements listed above for practical use, leading to a large amount of research into its composition [18].

Despite graphite's high reduction potential, the electron transfer from the graphite to the electrolyte is not favourable without the aid of (1) lithium-ions and (2) an applied voltage [19]. The decreased reduction potential for popular carbonates is depicted in Figure 1.6a, where lithium is shown to decrease the energy needed for the reduction process in all cases. It should be noted that the oxidation potential on the cathode is similarly oxidized as a result of the anions. The reduction of the electrolyte is complex, involving the solvent as well as lithium-salt anions and has been summarized by Yan *et al* [20] describing over 30 reactions occurring in the graphite-$LiPF_6$/EC/DMC (dimethyl carbonate) system. This decomposition results in a number of both lithium and carbon based products as depicted in Figure 1.6b. Depth profiling on the SEI has revealed that the outermost surface is mainly composed of organic species in contrast to the inner surface's inorganic composition [21].

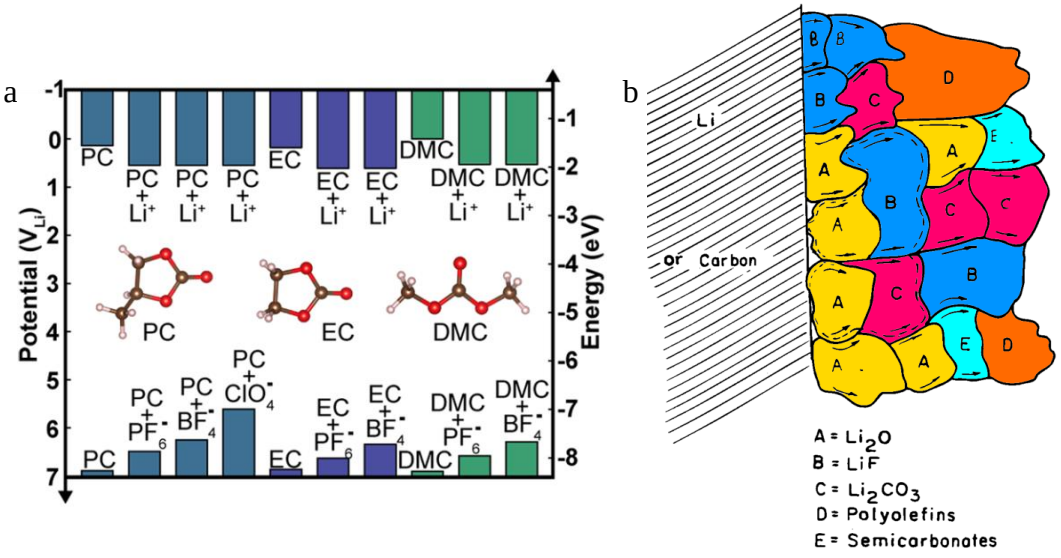

Figure 1.6. (a) Reduction and oxidation potentials of polypropylene carbonate, ethylene carbonate and dimethyl carbonate and (b) SEI composition after reduction of the electrolyte [22], [23].

The resulting SEI's ability to meet the aforementioned requirements will impact the battery's performance, therefore, researchers have focused on controlling the composition of the SEI, which can be approached in three main ways:

(1) **Choosing the electrolyte and salt composition.** The development of an EC based electrolyte enabled graphite's use as a practical anode material.
(2) **Using additives in the electrolyte.** This method typically differs from (1) in that the additives typically make up no more than 5% (weight or volume) of the electrolyte [24].
(3) **Surface treatment of graphite.** The additional surface functional groups on the graphite impact the resulting SEI formation.

This thesis focuses on the use of ultrathin films on graphite deposited via atomic layer deposition and molecular layer deposition (introduced in Chapter 1.2); therefore, a thorough understanding of these methods will reveal the requirements of the deposited films. The development of the carbonate-based electrolyte was thoroughly explained through the development of graphite for LIBs, however, graphite still exhibits a characteristic capacity decay and the side reactions which occur during SEI formation and consumes a large amount of electrolyte and lithium. The following sections focus on the use of additives and surface treatments to address these issues. This will provide insight as to what thin-film compositions may create the most stable SEI.

1.1.2.1 Additives to Control the SEI on Graphite

The reduction of the electrolyte typically occurs in two steps [25]. The first step occurs at a low reduction potential, before the potential is high enough for the insertion of lithium ions. During this step an unstable inorganic film formulates which can produce gaseous products. The second step, on the other hand, occurs at a potential similar to the insertion of lithium ions into graphite and produces a stable polymeric film which has a high lithium conductivity. Therefore, focus has been on using additives which will produce a continuous, stable organic film at a low reduction potential, before the inorganic film has the opportunity to be created. These SEI improving additives include: those which

polymerize upon reduction, those which improve the adhesion to the graphite's surface and those which combine with final products formed by the reduction process.

Research of various additives which polymerize at a low reduction potential led to the development of vinylene carbonate (VC) which was found to improve the SEI [26]. The polymerization of this compound is attributed to the reduction of the double bond found in the vinyl group (-CH=CH_2) described by the following general reaction:

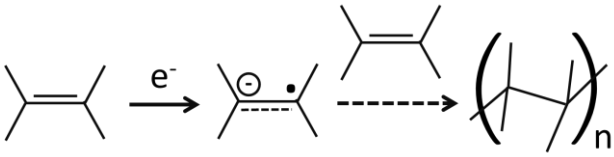

(1.5)

This polymerization could be extended to other vinyl containing compounds and led to a number of works on these types of additives [24]. Furan derivatives, which contain two double carbon bonds, are reported to follow a similar polymerization reaction [27]. These additives promote polymerization via promoted electrons from the graphite's surface, however, the polymers produced must also adhere well to the surface of the graphite.

To improve the adherence of the reduced products to the surface of the graphite, reductive agents have been developed. Once reduced these additives adhere to the graphite's surface and create sites with high affinity for the polymeric compounds. Reductive agents typically are composed of sulfur based compounds [28]–[30], though, a number of other additives have been shown to increase the SEI's adhesion including nitrogen based groups [31]–[33] and halogenated groups (chlorine and fluorine typically) [34]–[37]. With the addition of these additives batteries were found to have lower carbonate consumption as well as a higher lithium ion conductivity. This can be attributed to a reduction of the first step in electrolyte reduction, due to the improved adhesion of the polymer formed by the additives.

Additives which stabilize and improve the ionic conduction of the SEI, by scavenging radical anions and intermediate compounds, have been an important aspect of the development of a stable SEI. Added carbon dioxide was first found to help this process

[33], [38] as it was shown to react both with EC radicals as well as with the reduction products via the following reactions :

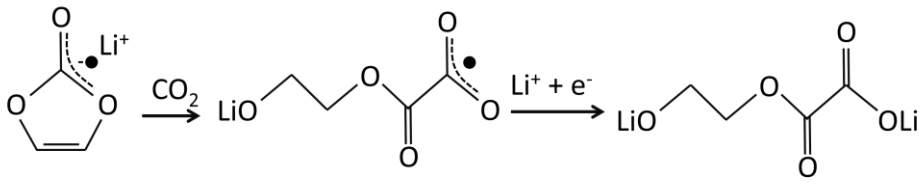

(1.6)

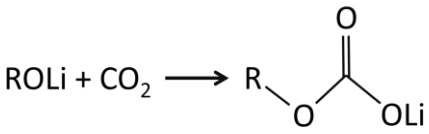

(1.7)

Reacting with these radical anions stops further electrolyte decomposition and has been shown to produce a thinner more compact SEI which decreases the gas evolution in the cell, increases the SEI's ionic conductivity and increases the battery life [39]. Various other additives have demonstrated to be able to stabilize the radicals, typically composed of a well conjugated structure to distribute the radical [40], [41].

Additives have been shown to be a powerful tool in improving the performance of LIBs. Despite only being a small portion of the electrolyte these additives can increase the stability of the SEI, suppress electrolyte decomposition, decrease gas evolution and improve the SEI's ionic conductivity. Furthermore, other additives have been shown to bring many other benefits to the LIB such as protecting the cathode [42], stabilizing the lithium salt [43] as well as increasing the safety of the battery [44]. Table 1.1 shows a summary of the techniques used specifically to enhance the graphite-electrolyte interface and demonstrates their breadth of use. However, despite these advantages, the additives in the electrolyte can produce undesired effects on the cathode or even within the electrolyte itself [24]. Therefore, this thesis focuses on designing the SEI and improving its performance while avoiding these potential disadvantages.

Table 1.1. Application of additives for the graphite-electrolyte interface.

Additive Goal	Mechanism	Additive Compounds
Produce stable SEI	C=C bond is reduced promoting polymerization	Vinyl derivatives [26], [45]–[47], furan derivatives[27]
Increase adhesion of reduction products	Reduces and adsorbs onto graphite active sites attracting reduction products	Sulfur derivatives [28]–[30], [48], nitrogen derivatives [33], [48]
Stabilize reduction products	Scavenges radical anions from reduction products or intermediate compounds	CO_2 [38], CO_2 producing compounds [49], highly-conjugated compounds [40], [41]
Adhere to graphite reduction sites	Strongly adheres to graphite reduction sites reducing electrolyte reduction	Halogenated compounds [34], silicon derivatives [50], [51]
Improve SEI performance	Introduces boron into the SEI which has been shown to improve its performance	Boron containing compounds [52]–[54]

1.1.2.2 Control of SEI via Surface Modification of Graphite

Another technique that has been used to control the SEI of the graphite-electrolyte interface is the surface treatment of graphite before battery fabrication. By controlling the surface of the graphite its reactivity and morphology can be controlled, ultimately tuning the resulting SEI to improve its ionic conductivity, stability and electrolyte compatibility. Graphite's layered structure creates an anisotropic surface composed of basal and edge planes. This results in variance in both the reactivity and ionic conductivity on the planes. Due to the edge planes having hanging bonds the carbon atoms on the edge plane have been shown to be more reactive compared to those on the surface of the basal plane [55]. Furthermore, the lithium ions enter between the graphite layers through the edge plane [56], therefore, the composition of this plane is important.

To control the reactivity and surface morphology of graphite a number of different techniques have been used. This includes mild oxidation [57], surface modification with metals and metal oxides [58]–[60], polymeric coatings [61] and coating with amorphous

carbon [62]. Table 1.2 summarizes the various methods used. Typically, these methods attempt to physically or chemically bond to the active sites on the graphite to decrease its activity. Furthermore, in some cases the films increase the capacity of the graphite due to the film having lithium storage capabilities as well. This is the case with Sn, which is a well-known alloying anode material [63], and amorphous carbon which has been shown to contain pores in which lithium storage occurs [64]. Overall, surface treatment has been shown to be a viable method to increase the performance of the graphite-electrolyte interface and unlike the use of additives it has a higher selectivity, avoiding any impact on the electrolyte or cathode. This thesis focuses on coating the surface of the graphite with an ultrathin film, effectively changing the surface chemistry of the graphite anode.

Table 1.2. Methods to treat graphite to improve the graphite-electrolyte interface.

Method	Aim	Technique/Compounds
Mild oxidation	Create a dense layer of oxides on graphite's surface to decrease reactivity	Thermal oxidation [65], chemical oxidation [66]–[69]
Metal coating	Block electrolyte exposure to active sites	Ni [70], Ag, Sn, Zn [58]
Metal oxide coating	Increase ionic conductivity and battery capacity	SnO [60], SnO_2 [60], CuO, NiO, FeO, PbO [59]
Polymeric coating	Suppression of electrolyte decomposition and solvent intercalation and increase capacity	Polyacrylic acid, polymethacrylic acid, polyvinyl alchol [61], polyethylene oxide [71]
Carbon coating	Decrease electrolyte decomposition and increase capacity	Heating polymer coatings [71], thermal vapour deposition [62]

1.2 Atomic and Molecular Layer Deposition

1.2.1 Atomic Layer Deposition

Moore's Law, a simple observation made by Gordon Moore in 1965 stated that the density of the transistor of an integrated circuit would double at regular intervals and continue to do so in the future [72]. Largely, this has held true, due to the development of new methods

that have enabled the continuous miniaturization of the transistor. In the search for techniques to create smaller features, focus shifted towards atomic layer deposition (ALD). ALD is a thin film deposition technique in which chemicals are sequentially exposed to a surface which was referred to as atomic layer epitaxy in early reports [73]. Early application of ALD was focused on the creation of dielectric ZnS thin for thin film display devices leading to the commercialization of a number of electroluminescent devices in Finland in the 1980s [74]. This technique demonstrated a unique ability to have highly precise control of the thin-film's thickness as well as an unmatched conformity on high aspect structures. These unique abilities made ALD a very attractive technique to deposit dielectrics for transistors and resulted in a large increase in research interest starting in the late 80s to present.

ALD stemmed from chemical vapour deposition (CVD), a thin film deposition technique in which chemical gases chemically react on a substrates surface. CVD overcomes issues found with physical deposition (PVD) techniques, namely, it is not restricted to line-of-site deposition, a characteristic of sputtering, evaporation and other PVD techniques (Figure 1.7a). Despite this, CVD has several drawbacks, particularly when applied to high aspect structures: it is mass transport-limited which can cause a thicker coating to develop in regions with higher chemical concentration (Figure 1.7b) and the thickness of the film is difficult to control on the angstrom level [75], [76]. ALD is a method, which overcomes these limitations providing a uniform coating on high aspect structures with excellent thickness control (Figure 1.7c). In addition, ALD typically has a growth temperature below 400 ºC which is much lower than a typical CVD deposition (normally 600-1000 ºC) [77], allowing deposition on a wider range of substrates.

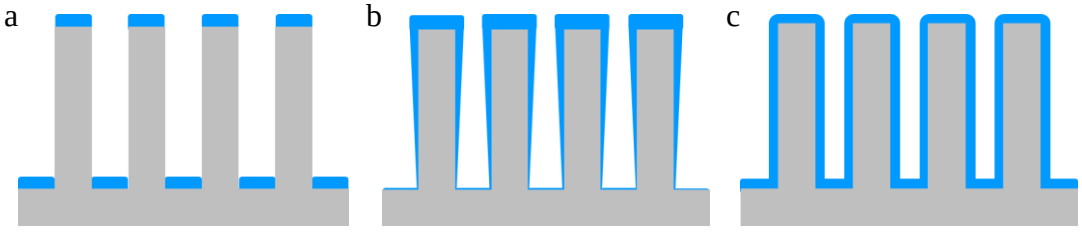

Figure 1.7. Thin films formed on high aspect substrates via (a) a line of sight method, (b) chemical vapour deposition and (c) atomic layer deposition.

As previously mentioned, ALD overcomes the limitations of CVD via the sequential exposure of precursor gases to the surface. In this process, the exposed precursor reacts with the surface groups fully saturating the surface, creating a new layer. The ALD process follows four main steps:

(1) Introduction of the first precursor (Reactant A), which reacts with the surface in a self-terminating manner.
(2) Purge system to remove remaining reactant and gaseous by-products.
(3) Introduction of the second precursor (Reactant B), which reacts with the surface in a self-terminating manner.
(4) Purge system to remove remaining reactant and gaseous by-product from second precursor.

Repeating steps 1-4 creates a stepwise growth of the thin film. An ALD reaction cycle produces a single layer of the resulting thin film as depicted in

Figure 1.8. Often times steps 1 and 3 are described as half reactions [78] and are highly dependent on the surface chemistry of the substrate.

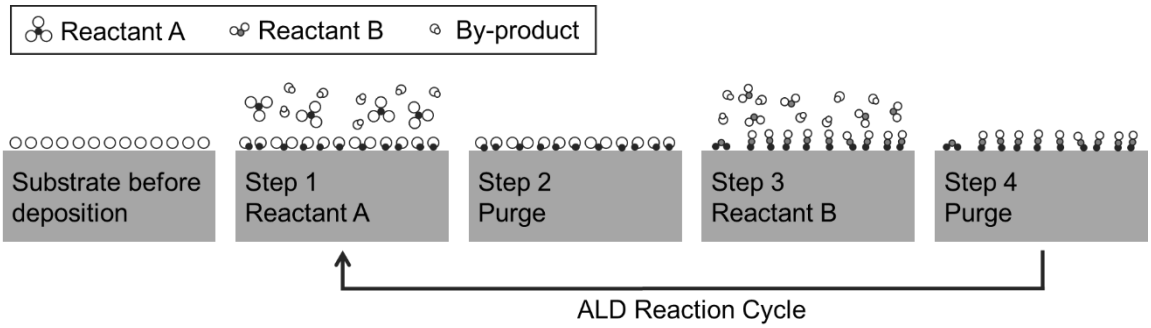

Figure 1.8. Schematic of typical steps in an ALD reaction cycle.

Due to its excellent dielectric properties, aluminum oxide has been intensively studied for semiconductor applications [79] and is a good example of the ALD process. For the deposition of aluminum oxide, exposure of trimethylaluminum (TMA) induces reactions with the surface groups as per the following half reaction:

$$AlOH* + Al(CH_3)_3 \rightarrow AlOAl(CH_3)_2* + CH_4 \quad \textbf{(1.8)}$$

Following the TMA exposure, the system is purged to remove any remaining precursor and by-product. Once purged the complementary oxidizing precursor, water, is introduced to react with the surface groups producing the following reaction:

$$AlCH_3* + H_2O \rightarrow AlOH* + CH_4 \quad \textbf{(1.9)}$$

Upon the completion of the aluminum's oxidation, the system is purged again to remove any remaining precursors or by-products. This completes the first ALD cycle, which can be repeated indefinitely. The complete reaction of the system is:

$$2\,Al(CH_3)_3 + 3\,H_2O \rightarrow Al_2O_3 + 6\,CH_4 \quad \textbf{(1.10)}$$

By controlling the number of cycles precise control of the film thickness is achieved. For example, the thickness of ALD deposited aluminum oxide grows in the range of 1.1 – 1.2 angstroms per cycle [80], [81]. These films are highly conformal and can be created at temperatures as low as room temperature [80]–[82].

The ALD process is dependent upon a number of different aspects, including the precursor used, temperature, pressure, exposure time and purge time. In selecting a precursor for an ALD process, it must fulfil a number of requirements. The requirements of the precursors are as follows:

(1) **Sufficient volatility at the deposition temperature.** The precursor must be in gaseous form for the process to occur.
(2) **Cannot self-decompose or self-react at deposition temperature.** Self-decomposition or self-reactions result in an uncontrollable CVD process.
(3) **Must be able to react with surface sites.** This allows initial deposition of the precursor on the surface of the substrate.
(4) **Must react with the complementary precursors.** This allows sequential reactions allowing growth of the thin film.
(5) **Does not etch the substrate or film.** This also applies to the by-products of the reactions; which one must account for.
(6) **Reasonably priced.**

(7) **Safe handling and preferably non-toxic.** Typically, highly reactive precursors are dangerous and one must handle them with care and with a number of safety guards.

Due to these strict requirements, precursor design has become a large area of interest with many precursors specifically designed for ALD [79], [81]. Generally, researchers have developed and classified ALD precursors as inorganic and organometallic. Inorganic precursors normally provide low-cost methods for numerous ALD processes, which include elemental precursors [83], halide precursors [84]–[87], oxygen-coordinated compounds [88], [89], nitrogen-coordinated compounds [90], [91] as well as precursors coordinated through other inorganic elements [92]. The well-known volatility and reactivity of organometallic precursors has enabled their application for ALD. These compounds, such as TMA, typically contain a metal-carbon bond and include metal alkyls [93], cyclopentadienyl-type compounds [94], [95], as well as other similar structures [96].

During the ALD process, a number of different parameters are controlled to influence the resulting reaction. This includes the pressure, temperature and exposure time during the deposition. Typically, ALD reactors are composed of a lateral flow system with the precursors upstream from the deposition chamber, an inert carrier gas, and a high vacuum pump creating a low pressure environment [73]. An inert gas carries the precursors as well as helps remove remaining precursors and by-products during the purging steps. Utilizing a high vacuum allows the use of precursors with less volatility, creates a higher probability of precursor–substrate interaction and aids in complete removal of the remaining precursor and by-products during the purging steps. For the practical use of most ALD precursors the optimum pressure for this type of reactor is around ~1 Torr [81], however, atmospheric pressure ALD systems have been demonstrated given the precursor has a sufficient vapour pressure [73].

The ALD growth rate is dependent upon the deposition temperature; however, there is a temperature range, known as the ALD “window” in which the deposition rate is constant (Figure 1.9). Below the ALD window, the reaction may not have enough energy to complete resulting in a decrease of the reaction rate, or if the precursor vapour has a high affinity for the substrate’s surface, condensation can occur creating a higher deposition

rate. Similarly, above the ALD window the rate may decrease as the precursor has too much energy and desorbs from the surface, or the rate may increase as the gaseous precursor decomposes onto the surface of the substrate. Staying within this window ensures linear ALD growth. Other important parameters include the precursor exposure time and the purge time. The exposure time must be sufficient to allow full saturation of the surface and the purge time must be sufficient to completely remove any remaining precursor and by-product from the system. Special care must be taken with the purge time during low temperature deposition [97]. Due to the lower temperature surface, the precursor is more prone to physical absorption and condensation, therefore, a longer purge time is used.

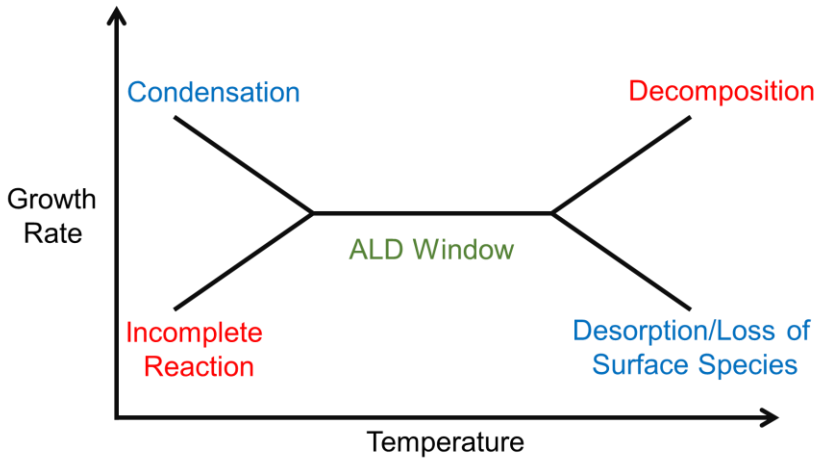

Figure 1.9. Temperature dependence of ALD growth.

ALD has become well established for its use in the semiconductor industry to create high-k oxides. In this realm, Al_2O_3, ZrO_2 and HfO_2 have been the most intently studied due to their dielectric properties [98]. These thin films have been used for a number of products including magnetic recording heads, metal oxide semiconductor field effect transistors (MOSFETS), dynamic random access memory (DRAM) capacitors, nonvolatile ferroeletric memories as well as a number of other applications [82]. With ALD's ability to deposit highly uniform films on high aspect structures with excellent thickness precision a number of promising applications have been recently investigated including those in biomedical devices [99], [100], nanodevices [101], sensors [102], nanophotovoltaics [102] as well as lithium-ion batteries [77]. This thesis focuses on the comparison of ALD and

molecular layer deposition thin-films influence on the SEI layer of graphite anodes. Molecular layer deposition is discussed in the following section.

1.2.2 Molecular Layer Deposition

Further research in ALD in the 1990s led to the development of various types of precursors, including larger functionalized molecules. For this, investigations utilized many techniques from polymerization chemistry, in which complementary molecules reacted with one another to create a polymer chain with an ABAB structure. By heating of the monomer precursors, a sufficient vapour pressure could be created to follow an ALD type process. The thin film deposition process, deposited molecule by molecule, was referred to as alternating vapour deposition polymerization (AVDP) [103], as well as molecular layer deposition (MLD) [104], [105], however, MLD eventually became the accepted nomenclature. Early work resulted in the development of a number of polymers including polyimides [104], [105], alkyl polyamide [103], nylon 66 [106] and more complex nylon structures [107]. This technique exploited many of the advantages of ALD including conformal growth on high aspect structures as well as excellent thickness control.

Due to the larger molecules used for MLD a number of different phenomena occur in comparison to ALD. The first and most distinguishing difference between the two apart from their respective compositions is their growth rates. Due to the larger molecules being deposited via MLD growth rates can vary from 2-6Å/cycle in comparison to ~1Å/cycle for Al_2O_3 via ALD [108], [109]. This growth rate, however, is lower than anticipated and is normally lower than the length of the monomer units. This is due to two phenomena that occur due to the larger molecules. First, the added bulk from the molecules sterically hinder each other. This can result in molecules on the surface blocking reaction sites as seen Figure 1.10 [110]. Second, due to the flexibility of the monomer units, the reactant may react twice with the surface as seen in Figure 1.10, terminating the growth of the chain. As a result of the steric hindrance and double reactions, the films formed by the MLD deposition can be highly porous resulting in densities much lower thin-films from ALD [97], [111].

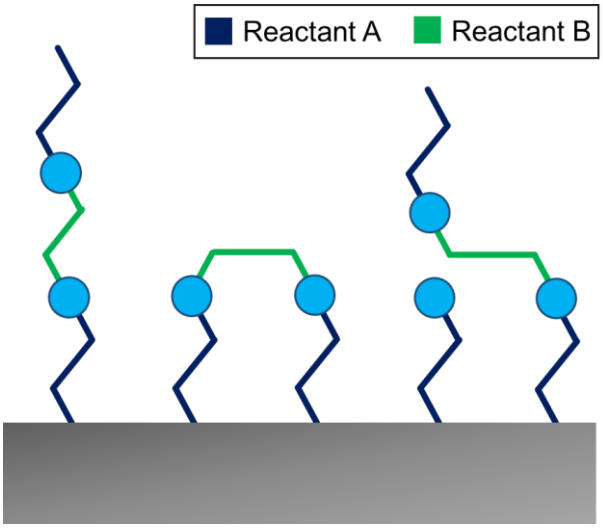

Figure 1.10. Schematic of ideal MLD deposition, double bonding and steric hindrance.

Purely organic MLD films were developed through the 1990s and the early 2000 and in the late 2000s the techniques of MLD and ALD were combined to create organic-inorganic hybrid films [111]–[114]. These films allowed the combination of the flexibility from the organic component as well as the electrically insulating properties of the inorganic constituent. In addition, hybrid organic-inorganic films have demonstrated electrical properties completely unique than those found individually with the inorganic or organic portions [115]. Most of this work has involved aluminum-based hybrid systems called alucone [116]–[120], however, studies also have included those of titanicone [121], [122], zincone [123], [124], and zircone [125].

Development of alucone has led to the capability to control the carbon content of the film [126]. This was achieved with the use of TMA, ethylene glycol (EG) and terphthalyoyl chloride (TC), as seen in Figure 1.11. By alternating TMA-EG for a number of subcycles the aluminum content could be increased, and alternatively, the carbon content could be increased by alternating TC-EG subcycles. The combination of each subcycle is called a supercycle which were shown to be able to tune the electrical conductivity after pyrolysis of the films in an inert atmosphere.

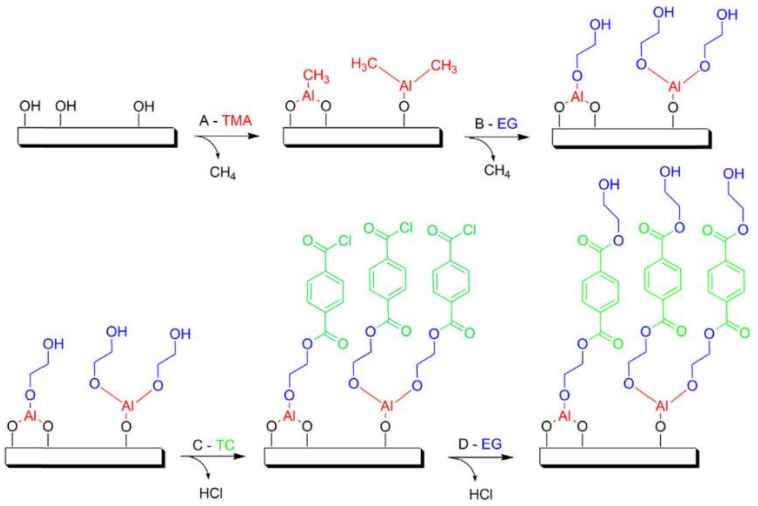

Figure 1.11. Process to develop alucone films with controlled carbon content [126].

Though ALD and MLD are very similar in technique, they have several subtle differences that helps distinguish them. A summary of these differences can be seen in Table 1.3. The most obvious difference between the two is the resulting composition of the thin films. ALD produces exclusively inorganic thin-films. These thin-films are typically composed of metal oxides and metal nitrides, however, elimination chemistry has allowed the development of pure metals. MLD on the other hand utilizes larger organic molecules as precursors resulting in either a purely organic or a hybrid organic-inorganic thin-film.

Due to the different precursors and chemistries, ALD and MLD vary in deposition temperature as well. Typically, higher temperatures are used in ALD than MLD due to the required energy for the reactions to occur. Furthermore, the larger MLD molecules used in MLD desorb more rapidly at higher temperature, resulting in lower growth rates. Therefore, MLD typically uses deposition temperatures <200 °C. As ALD occurs atom by atom the growth rate is in the angstrom range, whereas MLD growth can occur in the nanometer scale. Despite this, many MLD growth rates have been shown to be similar to ALD growth rates. This is due to the reactive groups on the larger MLD molecules having a lower probability of reacting with the surface, steric hindrance between the molecules and double reactions. As a result of the larger MLD molecules having higher van der Waals forces a larger purge time is normally needed to remove physisorbed molecules from the surface of the substrate.

Table 1.3. Comparison of various differences between ALD and MLD. Information gathered from sources in reviews [81] and [108].

	ALD	**MLD**
Composition	Metal-oxides, metal nitrides, metals	Organic, hybrid organic-inorganic
Deposition temperature (°C)	25-425	25-400
Deposition rate (Å/cycle)	0.2-3	0.1-25
Purge time (s)	0.5-15	5-120

1.2.3 ALD and MLD for LIB electrodes

As research into various applications for ALD & MLD has developed beyond the semiconductor industry, it has become clear that these techniques are excellent for electrodes in LIBs. In particular, ALD & MLD's application for surface coatings on the LIB's electrodes to control SEI formation has gained increasing traction over the past decade. This is due to these techniques offering a number of advantages specifically applicable to the LIB electrodes, including:

(1) **Low temperature deposition.** This allows deposition on electrode-binder (polymer) composites, after electrode fabrication.
(2) **High conformity.** The high aspect ratio and porous nature of LIB electrodes requires a conformal coating, otherwise exposed surfaces will react during cycling.
(3) **Highly precise thickness control.** The SEI which forms on the electrodes are in the order of nanometers [55], the range in which ALD & MLD films are developed.
(4) **Stoichiometric control.** The breadth of compositions developed via ALD & MLD allow tuning of the SEI.

These features have resulted in research on utilizing ALD for the protection of the cathode [127]–[129], anode [127], [130]–[133], and future battery electrode materials [134]–[138]. The deposition of electrode and solid-state-electrolyte materials via ALD is also an

interesting focus which may have application in future thin film batteries [134], [139]–[142].

The use of ALD for the LIB cathode focuses on addressing a number of key issues. In cobalt based cathode materials such as $LiCoO_2$ and $LiNi_{1/3}Mn_{1/3}Co_{1/3}O_2$ cobalt is subject to dissolution due to attack from HF species in the electrolyte (a side product of H_2O and $LiPF_6$) [143]. By using ALD of a thin Al_2O_3 layer, HF attack on the bulk material was reduced improving the cycling performance [127], [129], [143]. An increase in the rate performance was also found with the ALD coating suggesting improvement in the SEI formation [143]. Furthermore, the resulting electrochemical performance from ALD coatings on the composite electrode was compared to that of an electrode with an ALD coating directly on the powder [133]. A large over-potential, in addition to a decreased capacity occurred with the direct deposition of the ALD thin film on the powder. This was attributed to poor contact between the active electrode particles and the added electron-conducting agents as seen in Figure 1.12. Due to the composite containing a polymeric binder as well as the copper current collector oxidizing at high temperatures, this technique shows the excellent low temperature capabilities of ALD for the LIB electrode.

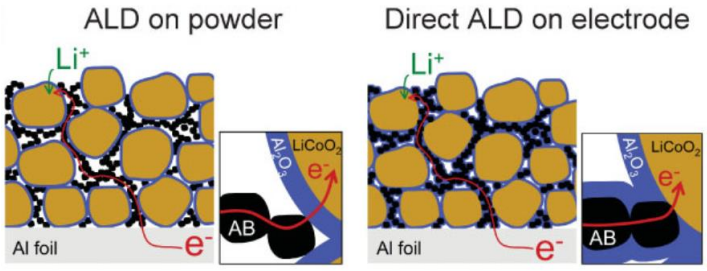

Figure 1.12. Schematic of electrical conduction with ALD coating on powder vs ALD coating on the electrode [133].

ALD of Al_2O_3 [127], [132], [133] and TiO_2 [144] on graphite LIB anodes has also been investigated to improve the SEI formation and decrease electrolyte decomposition. It was shown that, similarly to deposition on the cathode, that the performance of the anode with ALD deposition on the composite was superior to that on the powder [133]. The electrode with ALD deposition on the composite showed an improved cycling performance as well as an increase in Coulombic efficiency during the first charge-discharge cycle [127]. This

suggests that the ALD coating decreases the number of side reactions to create the SEI, resulting in less electrolyte and lithium loss. The SEI of the bare and coated graphite was also analyzed after cycling and revealed that a thinner SEI was produced when the graphite was coated with an ALD thin film [127]. The SEI produced with an ALD coating also showed a decreased formation of LiF and Li_2O, both inorganic compounds that impede the SEI's performance. The resulting improvements in the SEI demonstrates the practical use of ALD for coating the LIB's anode.

Investigation of MLD to control the surface chemistry of LIB electrode materials has only recently begun. Silicon, a high capacity anode material, was shown to have an increased stability with an alucone coating [145]. This increase in stability was largely attributed to the alucone coating expanding and contracting with the silicon nanoparticles during lithiation and delithiation. This flexibility allowed the alucone to keep contact between the silicon and conducting agents maintaining conductivity throughout the electrode composite. Our group has recently shown that MLD can be further applied to sulfur cathodes to stabilize their cycling performance [146], [147]. In this work the stability of the alucone coated cathode was superior to the ALD Al_2O_3 coated cathode. Furthermore, the alucone coating enabled cycling of the sulfur cathodes in a carbonate electrolyte. This capability allows the cycling of the batteries at high temperatures, something not possible with the previously used ether based electrolyte. One final study, by Loebl *et al*, investigated the effect of ALD and MLD coatings on carbon nanofibers [131]. At the end of their study they found the MLD coatings decreased the cycling capacity of the electrodes, however, the stability increased. No work has been done to date on the use of an MLD thin-film alucone coating for the present day commercial anode material, graphite. This thesis focuses on utilizing MLD to change the composition of the coating on the graphite and investigate the resulting electrochemical performance.

1.2.4 Porous thin-films via MLD

Microporous materials are attractive due to their high surface area to volume ratio. Due to this property, they have potential use for applications such as catalysis, gas-adsorption technologies and gas sensors [148], [149]. For the development of many porous metal oxides, a hybrid metal oxide – organic structure is calcined to remove the organic linker

resulting in the porous metal oxide [149]. This technique has been extended to the development of porous thin-films via the sol-gel coating method. This consists of dipping the substrate in a solution where a hydrolysis reaction produces a metal oxide product, which deposits on the substrate's surface. Evaporating the remaining solvent from the thin-film results in a porous metal oxide coating. This method has been demonstrated to have a wide range of possible applications including selectivity [150], anti-corrosion [151], anti-reflection [152] and drug encapsulation [153]. From these works, it is clear that a thin-film with a conformal thickness and porosity has numerous applications. Furthermore, it may prove beneficial to be used as an electrode coating, as the porous structure would promote lithium ion diffusion pathways.

Research on ALD materials has led to the development of porous thin-films. Work by Qin *et al* [154] investigated the effect of annealing copper nanowires which were coated with an ALD Al_2O_3 thin-film. From their work they discovered that by annealing the coated nanowires in air the copper migrated through the Al_2O_3 to the outer surface of the ALD coating as seen in Figure 1.13a. This unique phenomenon was speculated to be due to high stresses developing as the copper oxidized and formed Cu_2O. To minimize energy in the system during this oxidation process the copper oxide diffused through the Al_2O_3 coating resulting in a hollow core, thereby Al_2O_3 nanotubes. This method, albeit novel and interesting, is not possible on other substrates as it requires the diffusion of copper through the thin film. Therefore, researchers have investigated more direct and universal methods to produce porous thin-films, leading to investigations involving MLD.

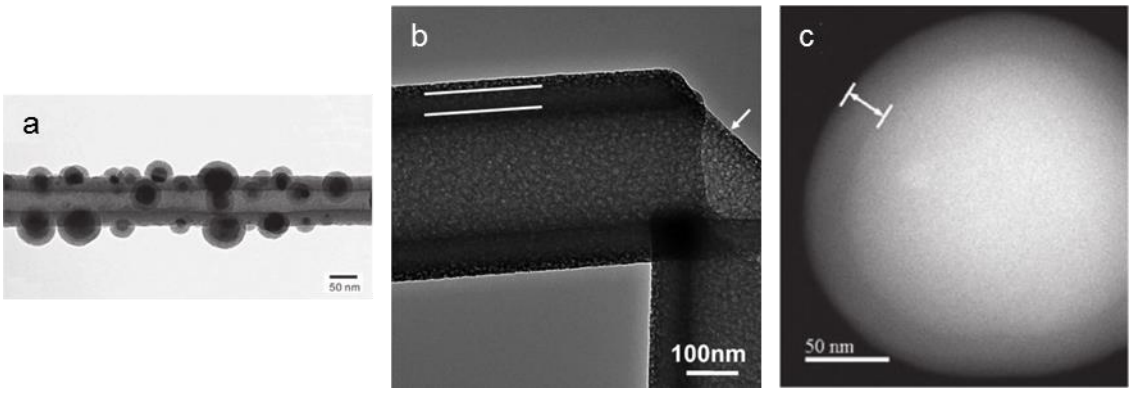

Figure 1.13. TEM images of (a) a porous Al_2O_3 nanotube with Cu nanoparticles on the surface [154], (b) a porous ZnO nanotube [155] and (c) a porous Al_2O_3 thin-film on an SiO_2 nanoparticle [156].

To create porous thin-films, regardless of the substrate, an interesting method involves the treatment of hybrid organic-inorganic MLD thin-films. To accomplish this the hybrid thin-films are deposited followed by either a water treatment or thermal treatment to remove its organic component. In both cases a porous metal oxide structure remains, however, delamination of the thin-film from the substrate has been shown to occur during the water treatment. Therefore, for a conformal thin-film coating an annealing treatment is ideal and was shown to produce a microporous thin-film with a narrow pore size distribution. This has been achieved for both alucone [156] and zincone [155] thin films as seen in Figure 1.13. Unlike work with bulk microporous materials, no method has been found to control the porosity or surface area of these thin-films. This thesis focuses on controlling the surface area of porous thin-films derived by MLD by varying the organic chain-length in the MLD thin-film structure.

1.2.5 Physical Vapour Deposition Techniques

A number of chemical and physical vapour deposition techniques have been applied to lithium-ion battery development including chemical vapor deposition (CVD) [157], electrodeposition [158], pulsed laser deposition (PLD) [159] and sputtering [8]. Sputtering, in particular, is a popular thin-film deposition technique, which has been used for thin-film LIBs. A full understanding of this technique is necessary in understanding the advantages

and limitations of ALD/MLD. Furthermore, this section provides insight as to the various applications in LIBs that sputtering can provide.

1.2.5.1 Sputter Deposition

Sputtering is a process in which high energy particles bombard a solid material's surface to eject particles from the surface [160]. Sputtering of atoms via ionic bombardment has been long investigated, as it created undesired deterioration of the anodic surface, with early reports of this phenomena occurring over 100 years ago [161]. It wasn't until the late 1900s that this phenomena was taken advantage of utilizing the ejected particles as a thin film deposition technique, thereby sputter deposition [162]. This technique has been shown to have a number of coating applications including: improvement of the mechanical wear resistance of metals [163], improvement of the corrosion resistance of metals [164], coatings for computer disc drives [165], as well as a the deposition of a number of materials for integrated circuits [166]. Sputter deposition's ability to create a uniform, thin film with a controlled thickness and stoichiometry at a low temperature [167], has allowed its commercialization.

In a typical direct current (DC) sputter deposition configuration an anode and cathode are positioned to allow an inert gas pass between them (such as Ar or Xe [166]), as seen in Figure 1.14a. Applying a voltage across the electrodes results in gas molecules ionizing, however, the ionization efficiency is very low in an electrode only system which is dependent upon ion collisions [167]. A higher pressure and voltage is needed in this case, which results in poor film formation [160], therefore, a method to increase the local ion density is needed. By using magnets, ions and electrons are constrained to the magnetic field, as depicted by the dashed lines in Figure 1.14a, creating a high-density region of ions, producing a plasma. A lower pressure is required to maintain the plasma (10^{-3} mbar vs 10^{-2} mbar) and a lower voltage is needed to accelerate the ions as well (500 V vs 2-3 kV) [162]. The higher ionic density results in a higher flux of ions accelerating towards the anode. Placing a target in front of the anode enables accelerated ions to bombard its surface, sputtering off the target material. Placing the substrate in line with the target allows the deposition of the target material onto the substrate. The thickness of the deposited film on the substrate can be directly controlled by the voltage applied, time and ion density

(pressure) [166]. By creating a cathode with an open hole through which the target can be ejected (Figure 1.14b), a sputtering configuration can be produced in which the cathode is not behind the substrate, called a sputtering gun [168]. In this case the cathode-anode distance is much shorter, therefore, a much lower voltage needs to be applied to result in the same electric field strength. Interestingly, researchers are investigating this configuration without a gas, which is an interesting avenue for space propulsion [169].

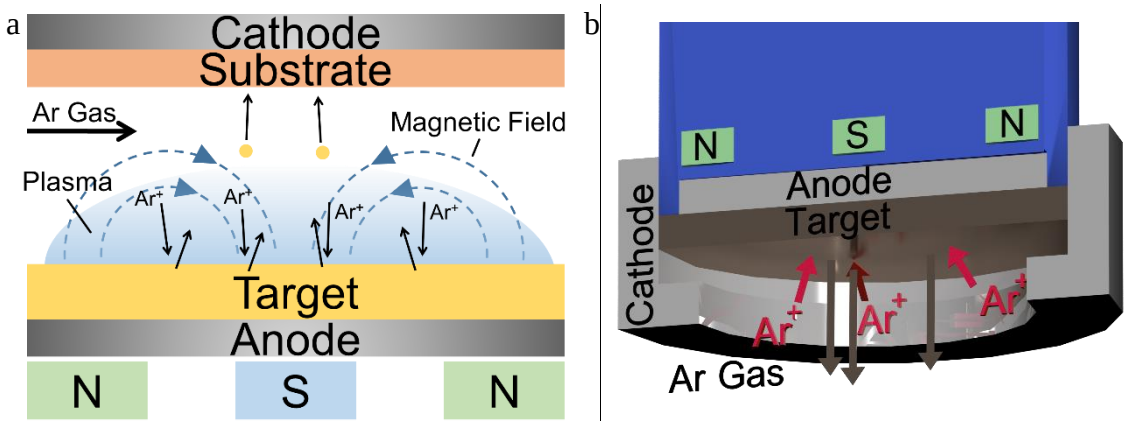

Figure 1.14: Schematic of (a) typical sputter deposition configuration and (b) a sputtering gun configuration.

Any charges building on the target are normally dispersed when a conductive target is used, however, these charges accumulate if one desires to use an insulating target material [166]. Furthermore, the accumulation of the charges will produce a layer of ionic species on the surface decreasing the deposition rate. To allow the sputtering of insulating targets, radio-frequency (RF) sputtering was developed. In this method an alternating voltage is applied to the electrodes, normally with a frequency of 13.56 MHz [162]. The alternating voltage allows the sputtering of the insulating material, however, this is at the expense of a reduced deposition rate (typically in the order of μm/h) [170]. By utilizing an RF – magnetron sputtering system, virtually any material can be deposited in a uniform manner, at a low temperature and with a controlled thickness.

1.2.5.2 Sputtering Lithium-ion Battery Electrolyte Thin Films

Sputtering has become a fundamental component in the development of thin-film LIBs due to the capabilities of RF-magnetron sputtering. Producing conformal thin films of any

composition with a tuned thickness has enabled deposition of anode materials [171], [172], solid-electrolyte materials [173]–[175] and cathode materials [176]–[178]. Sputtered anode and cathode materials have been shown to have comparable performances to their bulk LIB counterparts, however, the performance of a solid electrolyte is far below its organic liquid counterpart.

The investigation of solid-state electrolytes has led to the development of both crystalline and amorphous lithium-ion conducting thin films. Amorphous materials have demonstrated their practical use and have been developed for commercial thin film batteries [8]. One of the most promising materials, lithium phosphorous oxynitride (LIPON), has been heavily investigated for its use as a thin film solid electrolyte via sputtering [175], [179], [180]. This is due to its ionic conductivity of 2.3×10^{-6} S cm^{-1}, superior to other amorphous materials, however, this is still over 4 magnitudes lower than the conductivity of a liquid electrolyte. Due to its low ionic conductivity researchers have looked into crystalline materials as they exhibit ionic conductivities considerably higher than amorphous materials.

Crystalline materials are of particular interest as their ionic conductivity approaches that of a liquid electrolyte. Garnet based structures and sulfide based structures have demonstrated ionic conductivities approaching that of liquid electrolytes (10^{-5} [181] and 10^{-3} S cm^{-1} [182] respectively). This is due to their crystalline structure forming lithium ion conducting channels as seen in Figure 1.15.

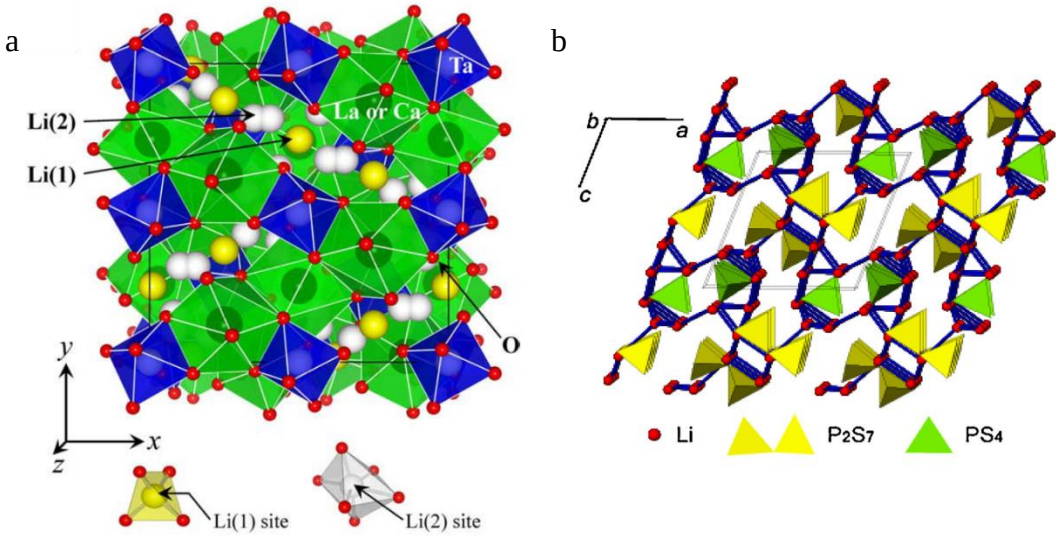

Figure 1.15:Schematic depicting the crystalline structure of (a) garnet [183] and (b) sulfide [181] crystalline structures.

Studies have demonstrated deposition of these compositions via sputtering [184], [185], however, this has been achieved with some limitations. To achieve a crystalline thin film the materials must be sputtered at a high temperature (~700 ºC [184]), however, to deposit on active electrode materials a much lower temperature must be used to avoid 1) side reactions with the active material and 2) oxidation of the current collector 3) cracks forming from varying thermal expansion coefficients of the materials. The resulting amorphous thin film has a much lower conductivity than its crystalline counterpart. Nonetheless, if this limitation can be addressed, sputtered thin-film crystalline electrolytes are promising candidates for thin film batteries.

Sputtering has proven to be a powerful tool in depositing thin-films for LIBs, however, it differs from ALD and MLD drastically. Sputtering is a line-of-site method, therefore, it is not practical to be used on high aspect or porous structures. In addition, sputtering achieves a lower control of thickness and conformity. This is due to inconsistencies in the system including variances in the electric field strength, ion concentrations and impurities on the surface of the substrate. Therefore, for developing thin-films for LIB interfaces ALD and MLD are highly advantageous.

1.3 Thesis Objectives

MLD is a powerful tool that has gained popularity in recent years, however, its application and capabilities are still yet to be fully realized. Due to its ability to create homogenous, ultrathin films, with excellent control of thickness, MLD provides an excellent avenue to coat highly porous structures. In addition, excellent control of the stoichiometry of the thin-films provides a possibility to further control various other physical aspects. However, investigation of the application and capabilities of MLD thin-films have just begun leaving much for exploration.

Therefore, the main objectives of this thesis revolved around (1) the application and (2) the capabilities of the MLD technique. First, the ultrathin SEI that forms on the LIB's graphite anode heavily depends on the graphite's surface chemistry and can be improved by metal oxide coatings via ALD. This, however, fails to address a number of requirements for a stable SEI, particularly good flexibility, making it difficult for the thin-film to expand and contract with the graphite during charge and discharge. The added flexibility of the organic-inorganic MLD thin-films would provide an excellent avenue to improve the graphite coating.

Secondly, controlling the organic content of MLD thin-films is a well-documented method to control the resulting conductivity of the thin-films after an annealing treatment in argon. In addition, porous thin-films result when the MLD coatings are annealed in air, effectively burning out the organic content of the films leaving behind a porous metal oxide film. By annealing MLD thin-films in air which have a controlled organic content there arises a possibility to control the surface area of the remaining metal oxide thin-film. Therefore, the objectives of this thesis are as follows:

(1) Demonstrate that MLD is superior to ALD as a coating method to improve the stability of graphite anodes in LIBs

This is achieved in two steps. The first is the confirmation that the MLD and ALD thin-films followed step-wise growth on the graphite electrodes. By combining QCM and EDX characterization techniques, it is possible to confirm conformal and continuous growth of

the thin-films. Furthermore, it is important to confirm that the thin-film techniques do not affect the morphology of the electrode, particularly the binding polymer, which has a relatively low melting temperature. Therefore, a comparison of the morphology of the electrodes before and after deposition was performed via SEM characterization.

Secondly, electrochemical investigation of the coated graphite electrodes was performed. By utilizing a relatively high charge-discharge cycling rate, I hoped to examine the characteristic capacity decay of the graphite and how the thin-film coatings influenced its performance. Furthermore, I hoped to gain insight into the ionic resistances created by the thin-films on the electrodes. This is accomplished by analysis of the lithiation and delithiation voltage plateaus as well as EIS measurements.

(2) Develop a MLD derived porous thin-film with a controlled surface area by controlling the thin-film's inorganic-organic ratio

This is achieved in two main steps. The first is the development of an MLD sequence in which the organic content could be controlled. By using both an organic and inorganic exposure sequence the number of organic sequences could be increased to increase the organic content of the thin-films. Step-wise growth could be confirmed by QCM, and thickness measurements could be achieved via TEM. Furthermore, confirmation of the increasing carbon content is necessary. This is accomplished by a combination of TGA and FTIR methods, which allows direct analysis of the organic content of the coatings.

The second major step is the surface area analysis of the films after their annealing process in air. Gas sorption is an excellent technique as it sheds insight to the surface morphology of the thin-films. Additionally, confirmation of the removal of the organic content is necessary to confirm little effect on the remaining metal oxide structure. From this, I hoped to demonstrate the increasing organic content results in a higher surface area of the thin-films.

1.4 Thesis Organization

This thesis contains five chapters organized in an integrated article format: an introduction, a summary of the experimental methods, two articles, and a concluding chapter. It is

organized in accordance to the Thesis Regulation Guide from the School of Graduate and Postdoctoral Studies at Western University. The outline of each chapter is as follows:

Chapter 1 is an introduction to the fundamentals of LIBs including the workings of graphite, the LIB's commercial anode material with a detailed review of previous methods to stabilize graphite's performance. This is followed by a detailed introduction to ALD and MLD, the uses of ALD and MLD for LIBs as well as the development of porous thin-films derived from MLD thin-films are explored. Finally, ALD and MLD are compared to other thin-film deposition techniques.

Chapter 2 provides a detailed description of the experimental methods for the ALD and MLD processes to produce the thin-films and details the fabrication process to produce LIBs. This is followed by a description of the physical, chemical and electrochemical characterization methods used for testing of the thin-films and battery materials.

Chapter 3 reports on the development of graphite anodes with ALD and MLD thin-film coatings. Specifically, Al_2O_3 and alucone thin-films are deposited via ALD and MLD respectively with 10 and 20 deposition cycles. Several characterization methods are used to confirm their deposition and that the ALD and MLD coating process does not affect the morphology of the electrodes. The effect of the different coatings on the electrodes electrochemical performance are examined in detail.

Chapter 4 investigates the use of hybrid organic-inorganic MLD thin-films to produce high surface area thin-films. This is accomplished by utilizing 20 cycles composed of a single inorganic deposition sub-cycle followed by 1, 3 and 5 organic sub-cycles. Characterization reveals the increasing organic content of the thin-films and the films are annealed under air to burn out the organic content. Further surface area measurements of the annealed thin-films demonstrate an increasing surface area with organic content.

Chapter 5 discusses the objectives of the thesis and summarizes the results presented in Chapters 3 and 4. The capabilities of MLD as a thin-film technique to improve LIB electrode material as well as its ability to produce porous thin-films are discussed and future work based on this thesis is suggested.

References

[1] D. Linden and T. Reddy, *Handbook of batteries*, 4th ed. New York: The McGraw-Hill Companies, Inc., 2010.

[2] M. Armand and J.-M. Tarascon, "Building better batteries," *Nature*, vol. 451, no. 7179, pp. 652–657, Feb. 2008.

[3] L. Lu, X. Han, J. Li, J. Hua, and M. Ouyang, "A review on the key issues for lithium-ion battery management in electric vehicles," *J. Power Sources*, vol. 226, pp. 272–288, Mar. 2013.

[4] E. Canada, "Canada's Emissions Trends," *Environ. Canada*, no. July, pp. 1–60, 2011.

[5] *Lithium Ion Rechargeable Batteries: Technical Handbook*. San Jose: Sony Electronics Inc.

[6] E. Sahraei, R. Hill, and T. Wierzbicki, "Calibration and finite element simulation of pouch lithium-ion batteries for mechanical integrity," *J. Power Sources*, vol. 201, pp. 307–321, Mar. 2012.

[7] C. Daniel, "Materials and processing for lithium-ion batteries," *JOM*, vol. 60, no. 9, pp. 43–48, Sep. 2008.

[8] J. Bates, "Thin-film lithium and lithium-ion batteries," *Solid State Ionics*, vol. 135, no. 1–4, pp. 33–45, Nov. 2000.

[9] N. J. Dudney, "Thin Film Micro-Batteries," *Electrochem. Soc.*, vol. 17, no. 1, pp. 44–48, 2008.

[10] D. Fauteux and R. Koksbang, "Rechargeable lithium battery anodes: alternatives to metallic lithium," *J. Appl. Electrochem.*, vol. 23, no. 1, pp. 1–10, Jan. 1993.

[11] D. Guerard and A. Herold, "Intercalation of lithium into graphite and other carbons," *Carbon N. Y.*, vol. 13, no. 4, pp. 337–345, Aug. 1975.

[12] R. Yazami and P. Touzain, "A reversible graphite-lithium negative electrode for electrochemical generators," *J. Power Sources*, vol. 9, no. 3, pp. 365–371, Jan. 1983.

[13] J. R. Dahn, "Phase diagram of LixC6," *Phys. Rev. B*, vol. 44, no. 17, pp. 9170–9177, Nov. 1991.

[14] J. C. Chacón-Torres, L. Wirtz, and T. Pichler, "Raman spectroscopy of graphite intercalation compounds: Charge transfer, strain, and electron-phonon coupling in graphene layers," *Phys. Status Solidi B*, vol. 251, no. 12, pp. 2337–2355, Dec. 2014.

[15] C. M. Julien, A. Mauger, K. Zaghib, and H. Groult, "Comparative Issues of Cathode Materials for Li-Ion Batteries," *Inorganics*, vol. 2, pp. 132–154, 2014.

[16] M. Arakawa and J.-I. Yamaki, "The cathodic decomposition of propylene carbonate in lithium batteries," *J. Electroanal. Chem. Interfacial Electrochem.*, vol. 219, no. 1–2, pp. 273–280, Mar. 1987.

[17] R. Fong, "Studies of Lithium Intercalation into Carbons Using Nonaqueous Electrochemical Cells," *J. Electrochem. Soc.*, vol. 137, no. 7, p. 2009, 1990.

[18] T. Marks, S. Trussler, a. J. Smith, D. Xiong, and J. R. Dahn, "A Guide to Li-Ion

Coin-Cell Electrode Making for Academic Researchers," *J. Electrochem. Soc.*, vol. 158, no. 1, p. A51, 2011.

[19] E. Endo, "Electron Spin Resonance Study of the Electrochemical Reduction of Electrolyte Solutions for Lithium Secondary Batteries," *J. Electrochem. Soc.*, vol. 145, no. 11, p. 3757, 1998.

[20] J. Yan, B.-J. Xia, Y.-C. Su, X.-Z. Zhou, J. Zhang, and X.-G. Zhang, "Phenomenologically modeling the formation and evolution of the solid electrolyte interface on the graphite electrode for lithium-ion batteries," *Electrochim. Acta*, vol. 53, no. 24, pp. 7069–7078, Oct. 2008.

[21] A. Zaban, E. Zinigrad, and D. Aurbach, "Impedance Spectroscopy of Li Electrodes. 4. A General Simple Model of the Li−Solution Interphase in Polar Aprotic Systems," *J. Phys. Chem.*, vol. 100, no. 8, pp. 3089–3101, Jan. 1996.

[22] M. Gauthier, T. J. Carney, A. Grimaud, L. Giordano, N. Pour, H.-H. Chang, D. P. Fenning, S. F. Lux, O. Paschos, C. Bauer, F. Maglia, S. Lupart, P. Lamp, and Y. Shao-Horn, "Electrode–Electrolyte Interface in Li-Ion Batteries: Current Understanding and New Insights," *J. Phys. Chem. Lett.*, vol. 6, no. 22, pp. 4653–4672, Nov. 2015.

[23] E. Peled, "Advanced Model for Solid Electrolyte Interphase Electrodes in Liquid and Polymer Electrolytes," *J. Electrochem. Soc.*, vol. 144, no. 8, p. L208, 1997.

[24] S. S. Zhang, "A review on electrolyte additives for lithium-ion batteries," *J. Power Sources*, vol. 162, no. 2, pp. 1379–1394, Nov. 2006.

[25] S. Zhang, M. S. Ding, K. Xu, J. Allen, and T. R. Jow, "Understanding Solid Electrolyte Interface Film Formation on Graphite Electrodes," *Electrochem. Solid-State Lett.*, vol. 4, no. 12, p. A206, 2001.

[26] D. Aurbach, J. S. Gnanaraj, W. Geissler, and M. Schmidt, "Vinylene Carbonate and Li Salicylatoborate as Additives in LiPF3(CF2CF3)3 Solutions for Rechargeable Li-Ion Batteries," *J. Electrochem. Soc.*, vol. 151, no. 1, p. A23, 2004.

[27] C. Korepp, H. J. Santner, T. Fujii, M. Ue, J. O. Besenhard, K.-C. Möller, and M. Winter, "2-Cyanofuran—A novel vinylene electrolyte additive for PC-based electrolytes in lithium-ion batteries," *J. Power Sources*, vol. 158, no. 1, pp. 578–582, Jul. 2006.

[28] M. W. Wagner, C. Liebenow, and J. O. Besenhard, "Effect of polysulfide-containing electrolyte on the film formation of the negative electrode," *J. Power Sources*, vol. 68, no. 2, pp. 328–332, Oct. 1997.

[29] Y. Ein-Eli, "Dithiocarbonic anhydride (CS2)—a new additive in Li-ion battery electrolytes," *J. Electroanal. Chem.*, vol. 531, no. 1, pp. 95–99, Aug. 2002.

[30] Y. Ein-Eli, "New Electrolyte System for Li-Ion Battery," *J. Electrochem. Soc.*, vol. 143, no. 9, p. L195, 1996.

[31] H. Gan and E. S. Takeuchi, "Nitrate additives for nonaqueous electrolyte rechargeable cells." Google Patents, 2000.

[32] H. Gan and E. S. Takuchi, "Organic nitrite additives for nonaqueous electrolyte in

alkali metal electrochemical cells.” Google Patents, 2000.

[33] J. O. Besenhard, M. W. Wagner, M. Winter, A. D. Jannakoudakis, P. D. Jannakoudakis, and E. Theodoridou, “Inorganic film-forming electrolyte additives improving the cycling behaviour of metallic lithium electrodes and the self-discharge of carbon—lithium electrodes,” *J. Power Sources*, vol. 44, no. 1–3, pp. 413–420, Apr. 1993.

[34] A. Naji, J. Ghanbaja, P. Willmann, and D. Billaud, “New halogenated additives to propylene carbonate-based electrolytes for lithium-ion batteries,” *Electrochim. Acta*, vol. 45, no. 12, pp. 1893–1899, Feb. 2000.

[35] Z. X. Shu, “Use of Chloroethylene Carbonate as an Electrolyte Solvent for a Graphite Anode in a Lithium-Ion Battery,” *J. Electrochem. Soc.*, vol. 143, no. 7, p. 2230, 1996.

[36] Z. X. Shu, “Use of Chloroethylene Carbonate as an Electrolyte Solvent for a Graphite Anode in a Lithium-Ion Battery,” *J. Electrochem. Soc.*, vol. 143, no. 7, p. 2230, 1996.

[37] X. Zhao, Q. C. Zhuang, S. D. Xu, Y. X. Xu, Y. L. Shi, and X. X. Zhang, “A new insight into the content effect of fluoroethylene carbonate as a film forming additive for lithium-ion batteries,” *Int. J. Electrochem. Sci.*, vol. 10, no. 3, pp. 2515–2534, 2015.

[38] G. V. Zhuang, H. Yang, B. Blizanac, and P. N. Ross, “A Study of Electrochemical Reduction of Ethylene and Propylene Carbonate Electrolytes on Graphite Using ATR-FTIR Spectroscopy,” *Electrochem. Solid-State Lett.*, vol. 8, no. 9, p. A441, 2005.

[39] J. Shin, C. Han, U. Jung, and S. Lee, “Effect of Li2CO3 additive on gas generation in lithium-ion batteries,” *J. Power Sources*, vol. 109, pp. 47–52, 2002.

[40] C. Wang, H. Nakamura, H. Komatsu, M. Yoshio, and H. Yoshitake, “Electrochemical behaviour of a graphite electrode in propylene carbonate and 1,3-benzodioxol-2-one based electrolyte system,” *J. Power Sources*, vol. 74, no. 1, pp. 142–145, Jul. 1998.

[41] J.-T. Lee, M.-S. Wu, F.-M. Wang, Y.-W. Lin, M.-Y. Bai, and P.-C. J. Chiang, “Effects of Aromatic Esters as Propylene Carbonate-Based Electrolyte Additives in Lithium-Ion Batteries,” *J. Electrochem. Soc.*, vol. 152, no. 9, p. A1837, 2005.

[42] E. Wang, D. Ofer, W. Bowden, N. Iltchev, R. Moses, and K. Brandt, “Stability of Lithium Ion Spinel Cells. III. Improved Life of Charged Cells,” *J. Electrochem. Soc.*, vol. 147, no. 11, p. 4023, 2000.

[43] S. S. Zhang, K. Xu, and T. R. Jow, “A Thermal Stabilizer for LiPF6-Based Electrolytes of Li-Ion Cells,” *Electrochem. Solid-State Lett.*, vol. 5, no. 9, p. A206, 2002.

[44] W. K. Behl, “Electrochemical Overcharge Protection of Rechargeable Lithium Batteries,” *J. Electrochem. Soc.*, vol. 135, no. 1, p. 21, 1988.

[45] S. S. Zhang, K. Xu, and T. R. Jow, “EIS study on the formation of solid electrolyte interface in Li-ion battery,” *Electrochim. Acta*, vol. 51, no. 8–9, pp. 1636–1640, Jan.

2006.

[46] U. S. Patent, “Date of Patent : Related US Application Data PDatent1 ? bit9rgc3 : ts,” 2000.

[47] J.-T. Lee, Y.-W. Lin, and Y.-S. Jan, “Allyl ethyl carbonate as an additive for lithium-ion battery electrolytes,” *J. Power Sources*, vol. 132, no. 1–2, pp. 244–248, May 2004.

[48] N. Electrolyte and I. N. Alkali, “Nitrate additives for nonaqueous electrolyte rechargeable cells,” 2000.

[49] M. D. Levi, E. Markevich, C. Wang, M. Koltypin, and D. Aurbach, “The effect of dimethyl pyrocarbonate on electroanalytical behavior and cycling of graphite electrodes,” *J. Electrochem. Soc.*, vol. 151, no. 6, p. A848, 2004.

[50] Y. Cao, L. Xiao, X. Ai, and H. Yang, “Surface-Modified Graphite as an Improved Intercalating Anode for Lithium-Ion Batteries,” *Electrochem. Solid-State Lett.*, vol. 6, no. 2, p. A30, 2003.

[51] G. Schroeder, B. Gierczyk, D. Waszak, and M. Walkowiak, “Impact of ethyl tris-2-methoxyethoxy silane on the passivation of graphite electrode in Li-ion cells with PC-based electrolyte,” *Electrochem. commun.*, vol. 8, no. 10, pp. 1583–1587, Oct. 2006.

[52] H. Mao and J. N. Reimers, “Use of B2 O3 additive in non-aqueous rechargeable lithium batteries.” Google Patents, 1999.

[53] U. Heider, M. Schmidt, A. Amann, M. Niemann, and A. Kühner, “Use of additives in electrolyte for electrochemical cells.” Google Patents, 2003.

[54] H. Mao, U. Von Sacken, and J. N. Reimers, “Additives for improving cycle life of non-aqueous rechargeable lithium batteries.” Google Patents, 1999.

[55] L. J. Fu, H. Liu, C. Li, Y. P. Wu, E. Rahm, R. Holze, and H. Q. Wu, “Surface modifications of electrode materials for lithium ion batteries,” *Solid State Sci.*, vol. 8, no. 2, pp. 113–128, Feb. 2006.

[56] A. Funabiki, M. Inaba, and Z. Ogumi, “A.c. impedance analysis of electrochemical lithium intercalation into highly oriented pyrolytic graphite,” *J. Power Sources*, vol. 68, no. 2, pp. 227–231, Oct. 1997.

[57] Y. P. Wu, C. Jiang, C. Wan, and R. Holze, “Anode materials for lithium ion batteries from mild oxidation of natural graphite,” *J. Appl. Electrochem.*, vol. 32, no. 9, pp. 1011–1017, 2002.

[58] T. Takamura, K. Sumiya, J. Suzuki, C. Yamada, and K. Sekine, “Enhancement of Li doping/undoping reaction rate of carbonaceous materials by coating with an evaporated metal film,” *J. Power Sources*, vol. 81–82, pp. 368–372, Sep. 1999.

[59] H. Huang, E. . Kelder, and J. Schoonman, “Graphite–metal oxide composites as anode for Li-ion batteries,” *J. Power Sources*, vol. 97–98, pp. 114–117, Jul. 2001.

[60] J. K. Lee, D. H. Ryu, J. B. Ju, Y. G. Shul, B. W. Cho, and D. Park, “Electrochemical characteristics of graphite coated with tin-oxide and copper by fluidised-bed chemical vapour deposition,” *J. Power Sources*, vol. 107, no. 1, pp. 90–97, Apr.

2002.

[61] S. Komaba, T. Ozeki, and K. Okushi, “Functional interface of polymer modified graphite anode,” *J. Power Sources*, vol. 189, no. 1, pp. 197–203, Apr. 2009.

[62] M. Yoshio, H. Wang, K. Fukuda, Y. Hara, and Y. Adachi, “Effect of Carbon Coating on Electrochemical Performance of Treated Natural Graphite as Lithium-Ion Battery Anode Material,” *J. Electrochem. Soc.*, vol. 147, no. 4, p. 1245, 2000.

[63] M. Winter and J. O. Besenhard, “Electrochemical lithiation of tin and tin-based intermetallics and composites,” *Electrochim. Acta*, vol. 45, no. 1–2, pp. 31–50, Sep. 1999.

[64] Y. Wu, C.-R. Wan, C.-Y. Jiang, S.-B. Fang, and Y.-Y. Jiang, “Mechanism of lithium storage in low temperature carbon,” *Carbon N. Y.*, vol. 37, no. 12, pp. 1901–1908, 1999.

[65] J. Shim and K. A. Striebel, “Electrochemical characterization of thermally oxidized natural graphite anodes in lithium-ion batteries,” *J. Power Sources*, vol. 164, no. 2, pp. 862–867, Feb. 2007.

[66] Y. P. Wu, C. Jiang, C. Wan, and R. Holze, “Mild preparation of anode materials by a salt-free green method,” *Electrochem. commun.*, vol. 4, no. 6, pp. 483–487, Jun. 2002.

[67] Y. Wu, C. Jiang, C. Wan, and E. Tsuchida, “A green method for the preparation of anode materials for lithium ion batteries,” *J. Mater. Chem.*, vol. 11, no. 4, pp. 1233–1236, 2001.

[68] Y. Wu, “Modified natural graphite as anode material for lithium ion batteries,” *J. Power Sources*, vol. 111, no. 2, pp. 329–334, Sep. 2002.

[69] Y. Ein-Eli, “Chemical Oxidation: A Route to Enhanced Capacity in Li-Ion Graphite Anodes,” *J. Electrochem. Soc.*, vol. 144, no. 9, p. 2968, 1997.

[70] P. Yu, J. a Ritter, R. E. White, and B. N. Popov, “Ni-Composite Microencapsulated Graphite as the Negative Electrode in Lithium-Ion Batteries I. Initial Irreversible Capacity Study,” *J. Electrochem. Soc.*, vol. 147, no. 4, p. 1280, 2000.

[71] T. Tsumura, “Surface modification of natural graphite particles for lithium ion batteries,” *Solid State Ionics*, vol. 135, no. 1–4, pp. 209–212, Nov. 2000.

[72] R. R. Schaller, “Moore’s law: past, present and future,” *IEEE Spectr.*, vol. 34, no. 6, pp. 52–59, Jun. 1997.

[73] T. Suntola, “Atomic layer epitaxy,” *Mater. Sci. Reports*, vol. 4, no. 5, pp. 261–312, Jan. 1989.

[74] T. Suntola, J. Antson, A. Pakkala, and S. Lindfors, “Thin Film Electroluminescent device,” *Soc. Inf. Disp. 80 Dig.*, 1980.

[75] K. Choy, “Chemical vapour deposition of coatings,” *Prog. Mater. Sci.*, vol. 48, no. 2, pp. 57–170, 2003.

[76] H. O. Pierson and W. A. Publishing, *Handbook of chemical vapor deposition: principles, technology and applications*, 2nd ed. New York: Noyes Publications, 1999.

[77] X. Meng, X.-Q. Yang, and X. Sun, “Emerging Applications of Atomic Layer Deposition for Lithium-Ion Battery Studies,” *Adv. Mater.*, vol. 24, no. 27, pp. 3589–3615, Jul. 2012.

[78] R. L. Puurunen, “Surface chemistry of atomic layer deposition: A case study for the trimethylaluminum/water process,” *J. Appl. Phys.*, vol. 97, no. 12, p. 121301, 2005.

[79] K. Ahn and L. Forbes, “Methods, systems, and apparatus for atomic-layer deposition of aluminum oxides in integrated circuits.” Google Patents, 2003.

[80] B. Xu, D. Qian, Z. Wang, and Y. S. Meng, “Recent progress in cathode materials research for advanced lithium ion batteries,” *Mater. Sci. Eng. R Reports*, vol. 73, no. 5–6, pp. 51–65, May 2012.

[81] S. M. George, “Atomic Layer Deposition: An Overview,” *Chem. Rev.*, vol. 110, no. 1, pp. 111–131, Jan. 2010.

[82] N. Pinna and M. Knez, *Atomic Layer Deposition of Nanostructured Materials*. Weinheim, Germany: Wiley-VCH Verlag GmbH & Co. KGaA, 2011.

[83] R. L. Puurunen, “A Short History of Atomic Layer Deposition: Tuomo Suntola’s Atomic Layer Epitaxy,” *Chem. Vap. Depos.*, vol. 20, no. 10–11–12, pp. 332–344, Dec. 2014.

[84] M. Ritala, M. Leskelä, E. Nykänen, P. Soininen, and L. Niinistö, “Growth of titanium dioxide thin films by atomic layer epitaxy,” *Thin Solid Films*, vol. 225, no. 1–2, pp. 288–295, Mar. 1993.

[85] M. Ritala, M. Leskelä, L. Niinistö, T. Prohaska, G. Friedbacher, and M. Grasserbauer, “Development of crystallinity and morphology in hafnium dioxide thin films grown by atomic layer epitaxy,” *Thin Solid Films*, vol. 250, no. 1–2, pp. 72–80, Oct. 1994.

[86] M. Ritala and M. Leskelä, “Zirconium dioxide thin films deposited by ALE using zirconium tetrachloride as precursor,” *Appl. Surf. Sci.*, vol. 75, no. 1–4, pp. 333–340, Jan. 1994.

[87] H. Tiznado, M. Bouman, B.-C. Kang, I. Lee, and F. Zaera, “Mechanistic details of atomic layer deposition (ALD) processes for metal nitride film growth,” *J. Mol. Catal. A Chem.*, vol. 281, no. 1–2, pp. 35–43, Feb. 2008.

[88] M. Tammenmaa, H. Antson, M. Asplund, L. Hiltunen, M. Leskelä, L. Niinistö, and E. Ristolainen, “Alkaline earth sulfide thin films grown by atomic layer epitaxy,” *J. Cryst. Growth*, vol. 84, no. 1, pp. 151–154, Jul. 1987.

[89] M. Tammenmaa, M. Leskelä, T. Koskinen, and L. Niinistö, “Zinc sulphide thin films doped with rare earth ions,” *J. Less Common Met.*, vol. 126, pp. 209–214, Dec. 1986.

[90] D. M. Hausmann, E. Kim, J. Becker, and R. G. Gordon, “Atomic Layer Deposition of Hafnium and Zirconium Oxides Using Metal Amide Precursors,” *Chem. Mater.*, vol. 14, no. 10, pp. 4350–4358, Oct. 2002.

[91] J. S. Becker, E. Kim, and R. G. Gordon, “Atomic Layer Deposition of Insulating Hafnium and Zirconium Nitrides,” *Chem. Mater.*, vol. 16, no. 18, pp. 3497–3501,

Sep. 2004.

[92] M. J. Saly, F. Munnik, R. J. Baird, and C. H. Winter, “Atomic Layer Deposition Growth of BaB2O4 Thin Films from an Exceptionally Thermally Stable Tris(pyrazolyl)borate-Based Precursor,” *Chem. Mater.*, vol. 21, no. 16, pp. 3742–3744, Aug. 2009.

[93] a. C. Dillon, A. W. Ott, J. D. Way, and S. M. George, “Surface chemistry of Al2O3 deposition using Al(CH3)3 and H2O in a binary reaction sequence,” *Surf. Sci.*, vol. 322, no. 1–3, pp. 230–242, Jan. 1995.

[94] H. L. Lu, G. Scarel, C. Wiemer, M. Perego, S. Spiga, M. Fanciulli, and G. Pavia, “Atomic Layer Deposition of NiO Films on Si(100) Using Cyclopentadienyl-Type Compounds and Ozone as Precursors,” *J. Electrochem. Soc.*, vol. 155, no. 10, p. H807, 2008.

[95] C. Brahim, A. Ringuedé, M. Cassir, M. Putkonen, and L. Niinistö, “Electrical properties of thin yttria-stabilized zirconia overlayers produced by atomic layer deposition for solid oxide fuel cell applications,” *Appl. Surf. Sci.*, vol. 253, no. 8, pp. 3962–3968, Feb. 2007.

[96] M. Schuisky, K. Kukli, M. Ritala, A. Hårsta, and M. Leskelä, “Atomic Layer CVD in the Bi–Ti–O System,” *Chem. Vap. Depos.*, vol. 6, no. 3, pp. 139–145, Jun. 2000.

[97] M. D. Groner, F. H. Fabreguette, J. W. Elam, and S. M. George, “Low-Temperature Al 2 O 3 Atomic Layer Deposition,” *Chem. Mater.*, vol. 16, no. 4, pp. 639–645, Feb. 2004.

[98] M. Leskelä and M. Ritala, “Atomic Layer Deposition Chemistry: Recent Developments and Future Challenges,” *Angew. Chemie Int. Ed.*, vol. 42, no. 45, pp. 5548–5554, Nov. 2003.

[99] C. Pang, C. Lee, and K.-Y. Suh, “Recent advances in flexible sensors for wearable and implantable devices,” *J. Appl. Polym. Sci.*, vol. 130, no. 3, pp. 1429–1441, Nov. 2013.

[100] A. Purniawan, P. J. French, G. Pandraud, and P. M. Sarro, “TiO2 ALD nanolayer as evanescent waveguide for biomedical sensor applications,” *Procedia Eng.*, vol. 5, pp. 1131–1135, 2010.

[101] H. Kim, H.-B.-R. Lee, and W.-J. Maeng, “Applications of atomic layer deposition to nanofabrication and emerging nanodevices,” *Thin Solid Films*, vol. 517, no. 8, pp. 2563–2580, Feb. 2009.

[102] L. Niinist, M. Nieminen, J. Pivsaari, J. Niinist, M. Putkonen, and M. Nieminen, “Advanced electronic and optoelectronic materials by Atomic Layer Deposition: An overview with special emphasis on recent progress in processing of high-k dielectrics and other oxide materials,” *Phys. status solidi*, vol. 201, no. 7, pp. 1443–1452, May 2004.

[103] A. Kubono, N. Yuasa, H.-L. Shao, S. Umemoto, and N. Okui, “In-situ study on alternating vapor deposition polymerization of alkyl polyamide with normal molecular orientation,” *Thin Solid Films*, vol. 289, no. 1–2, pp. 107–111, Nov. 1996.

[104] T. Yoshimura, S. Tatsuura, and W. Sotoyama, “Polymer films formed with

monolayer growth steps by molecular layer deposition," *Appl. Phys. Lett.*, vol. 59, no. 4, p. 482, 1991.

[105] T. Yoshimura, S. Tatsuura, W. Sotoyama, A. Matsuura, and T. Hayano, "Quantum wire and dot formation by chemical vapor deposition and molecular layer deposition of one-dimensional conjugated polymer," *Appl. Phys. Lett.*, vol. 60, no. 3, p. 268, 1992.

[106] H.-I. Shao, S. Umemoto, T. Kikutani, and N. Okui, "Layer-by-layer polycondensation of nylon 66 by alternating vapour deposition polymerization," *Polymer (Guildf).*, vol. 38, no. 2, pp. 459–462, Jan. 1997.

[107] A. Nagai, H. Shao, S. Umemoto, and T. Kikutani, "Quadruple aliphatic polyamide systems prepared by a layer-by-layer alternating vapour deposition method," *High Perform. Polym.*, vol. 13, no. 2, pp. 169–179, Jun. 2001.

[108] P. Sundberg and M. Karppinen, "Organic and inorganic–organic thin film structures by molecular layer deposition: A review," *Beilstein J. Nanotechnol.*, vol. 5, pp. 1104–1136, Jul. 2014.

[109] J. Meyer and T. Riedl, "Low-Temperature Atomic Layer Deposition," 2012.

[110] S. M. George, B. Yoon, and A. a Dameron, "Surface Chemistry for Molecular Layer Deposition of Organic and Hybrid Organic−Inorganic Polymers," *Acc. Chem. Res.*, vol. 42, no. 4, pp. 498–508, Apr. 2009.

[111] A. A. Dameron, D. Seghete, B. B. Burton, S. D. Davidson, A. S. Cavanagh, J. A. Bertrand, and S. M. George, "Molecular Layer Deposition of Alucone Polymer Films Using Trimethylaluminum and Ethylene Glycol," *Chem. Mater.*, vol. 20, no. 10, pp. 3315–3326, May 2008.

[112] E. C. Constable, "Coordination Polymers," in *Supramolecular Chemistry*, vol. 6, no. 4, Chichester, UK: John Wiley & Sons, Ltd, 2012, pp. 3073–3086.

[113] V. M. Smirnov, E. G. Zemtsova, A. A. Belikov, I. L. Zheldakov, P. . E. Morozov, O. G. Polyachonok, and V. B. Aleskovskii, "Chemical design of quasi-one-dimensional organoiron nanostructures fixed on an inorganic matrix and study of their magnetic properties," *Dokl. Phys. Chem.*, vol. 413, no. 2, pp. 95–98, Apr. 2007.

[114] B. H. Lee, M. K. Ryu, S.-Y. Choi, K.-H. Lee, S. Im, and M. M. Sung, "Rapid Vapor-Phase Fabrication of Organic−Inorganic Hybrid Superlattices with Monolayer Precision," *J. Am. Chem. Soc.*, vol. 129, no. 51, pp. 16034–16041, Dec. 2007.

[115] B. H. Lee, K. H. Lee, S. Im, and M. M. Sung, "Monolayer-precision fabrication of mixed-organic–inorganic nanohybrid superlattices for flexible electronic devices," *Org. Electron.*, vol. 9, no. 6, pp. 1146–1153, Dec. 2008.

[116] a. a. Dameron, D. Seghete, B. B. Burton, S. D. Davidson, a. S. Cavanagh, J. a. Bertrand, and S. M. George, "Molecular Layer Deposition of Alucone Polymer Films Using Trimethylaluminum and Ethylene Glycol," *Chem. Mater.*, vol. 20, no. 10, pp. 3315–3326, May 2008.

[117] M. Park, S. Oh, H. Kim, D. Jung, D. Choi, and J.-S. Park, "Gas diffusion barrier characteristics of Al2O3/alucone films formed using trimethylaluminum, water and ethylene glycol for organic light emitting diode encapsulation," *Thin Solid Films*,

vol. 546, pp. 153–156, Nov. 2013.

[118] D. Seghete, B. D. Davidson, R. a. Hall, Y. J. Chang, V. M. Bright, and S. M. George, "Sacrificial layers for air gaps in NEMS using alucone molecular layer deposition," *Sensors Actuators A Phys.*, vol. 155, no. 1, pp. 8–15, Oct. 2009.

[119] B. Yoon, D. Seghete, A. S. Cavanagh, and S. M. George, "Molecular Layer Deposition of Hybrid Organic−Inorganic Alucone Polymer Films Using a Three-Step ABC Reaction Sequence," *Chem. Mater.*, vol. 21, no. 22, pp. 5365–5374, Nov. 2009.

[120] A. A. Lushington, J. Liu, M.N. Bannis, B. Xiao, S. Lawes, R. Li, X. Sun, "A Novel Approach in Controlling the Conductivity of Thin Films using Molecular Layer Deposition," *Appl. Surf. Sci.*, 2015.

[121] K. Van de Kerckhove, F. Mattelaer, D. Deduytsche, P. M. Vereecken, J. Dendooven, and C. Detavernier, "Molecular layer deposition of 'titanicone', a titanium-based hybrid material, as an electrode for lithium-ion batteries," *Dalt. Trans.*, vol. 45, no. 3, pp. 1176–1184, 2016.

[122] A. I. Abdulagatov, R. a Hall, J. L. Sutherland, B. H. Lee, A. S. Cavanagh, and S. M. George, "Molecular Layer Deposition of Titanicone Films using TiCl4 and Ethylene Glycol or Glycerol: Growth and Properties," *Chem. Mater.*, vol. 24, no. 15, pp. 2854–2863, Aug. 2012.

[123] J. Liu, B. Yoon, E. Kuhlmann, M. Tian, J. Zhu, S. M. George, Y.-C. Lee, and R. Yang, "Ultralow Thermal Conductivity of Atomic/Molecular Layer-Deposited Hybrid Organic–Inorganic Zincone Thin Films," *Nano Lett.*, vol. 13, no. 11, pp. 5594–5599, Nov. 2013.

[124] D. Choudhury and S. K. Sarkar, "The ALD-MLD Growth of a ZnO-Zincone Heterostructure," *Chem. Vap. Depos.*, vol. 20, no. 4–5–6, pp. 130–137, Jun. 2014.

[125] B. H. Lee, V. R. Anderson, and S. M. George, "Molecular Layer Deposition of Zircone and ZrO2 /Zircone Alloy Films: Growth and Properties," *Chem. Vap. Depos.*, vol. 19, no. 4–6, pp. 204–212, Jun. 2013.

[126] A. Lushington, J. Liu, M. N. Bannis, B. Xiao, S. Lawes, R. Li, and X. Sun, "A novel approach in controlling the conductivity of thin films using molecular layer deposition," *Appl. Surf. Sci.*, vol. 357, pp. 1319–1324, Dec. 2015.

[127] Y. S. Jung, P. Lu, A. S. Cavanagh, C. Ban, G.-H. Kim, S.-H. Lee, S. M. George, S. J. Harris, and A. C. Dillon, "Unexpected Improved Performance of ALD Coated LiCoO 2 /Graphite Li-Ion Batteries," *Adv. Energy Mater.*, vol. 3, no. 2, pp. 213–219, Feb. 2013.

[128] J. W. Kim, J. J. Travis, E. Hu, K. Nam, S. C. Kim, C. S. Kang, J. Woo, X. Yang, S. M. George, K. H. Oh, S.-J. Cho, and S. Lee, "Unexpected high power performance of atomic layer deposition coated Li[Ni1/3Mn1/3Co1/3]O2 cathodes," *J. Power Sources*, vol. 254, no. 2014, pp. 190–197, May 2014.

[129] I. D. Scott, Y. S. Jung, A. S. Cavanagh, Y. Yan, A. C. Dillon, S. M. George, and S.-H. Lee, "Ultrathin Coatings on Nano-LiCoO2 for Li-Ion Vehicular Applications," *Nano Lett.*, vol. 11, no. 2, pp. 414–418, Feb. 2011.

[130] P. Lichty, M. Wirz, P. Kreider, O. Kilbury, D. Dinair, D. King, A. Steinfeld, and A. W. Weimer, “Surface Modification of Graphite Particles Coated by Atomic Layer Deposition and Advances in Ceramic Composites,” *Int. J. Appl. Ceram. Technol.*, vol. 10, no. 2, pp. 257–265, Mar. 2013.

[131] a. J. Loebl, C. J. Oldham, C. K. Devine, B. Gong, S. E. Atanasov, G. N. Parsons, and P. S. Fedkiw, “Solid Electrolyte Interphase on Lithium-Ion Carbon Nanofiber Electrodes by Atomic and Molecular Layer Deposition,” *J. Electrochem. Soc.*, vol. 160, no. 11, pp. A1971–A1978, Sep. 2013.

[132] a. Tokranov, B. W. Sheldon, P. Lu, X. Xiao, and A. Mukhopadhyay, “The Origin of Stress in the Solid Electrolyte Interphase on Carbon Electrodes for Li Ion Batteries,” *J. Electrochem. Soc.*, vol. 161, no. 1, pp. A58–A65, Nov. 2013.

[133] Y. S. Jung, A. S. Cavanagh, L. a Riley, S.-H. Kang, A. C. Dillon, M. D. Groner, S. M. George, and S.-H. Lee, “Ultrathin Direct Atomic Layer Deposition on Composite Electrodes for Highly Durable and Safe Li-Ion Batteries,” *Adv. Mater.*, vol. 22, no. 19, pp. 2172–2176, Apr. 2010.

[134] C. Ban, M. Xie, X. Sun, J. J. Travis, G. Wang, H. Sun, A. C. Dillon, J. Lian, and S. M. George, “Atomic layer deposition of amorphous TiO2 on graphene as an anode for Li-ion batteries,” *Nanotechnology*, vol. 24, no. 42, p. 424002, Oct. 2013.

[135] E. Kazyak, K. N. Wood, and N. P. Dasgupta, “Improved Cycle Life and Stability of Lithium Metal Anodes through Ultrathin Atomic Layer Deposition Surface Treatments,” *Chem. Mater.*, vol. 27, no. 18, pp. 6457–6462, Sep. 2015.

[136] H. Kim, J. T. Lee, D.-C. Lee, A. Magasinski, W. Cho, and G. Yushin, “Plasma-Enhanced Atomic Layer Deposition of Ultrathin Oxide Coatings for Stabilized Lithium-Sulfur Batteries,” *Adv. Energy Mater.*, vol. 3, no. 10, pp. 1308–1315, Oct. 2013.

[137] A. Kohandehghan, P. Kalisvaart, K. Cui, M. Kupsta, E. Memarzadeh, and D. Mitlin, “Silicon nanowire lithium-ion battery anodes with ALD deposited TiN coatings demonstrate a major improvement in cycling performance,” *J. Mater. Chem. A*, vol. 1, no. 41, p. 12850, 2013.

[138] A. C. Kozen, C. Lin, A. J. Pearse, M. A. Schroeder, X. Han, L. Hu, S.-B. Lee, G. W. Rubloff, and M. Noked, “Next-Generation Lithium Metal Anode Engineering via Atomic Layer Deposition,” *ACS Nano*, vol. 9, no. 6, pp. 5884–5892, Jun. 2015.

[139] K. B. Gandrud, A. Pettersen, O. Nilsen, and H. Fjellvåg, “High-performing iron phosphate for enhanced lithium ion solid state batteries as grown by atomic layer deposition,” *J. Mater. Chem. A*, vol. 1, no. 32, pp. 9054–9059, 2013.

[140] J. Liu, M. N. Banis, X. Li, A. Lushington, M. Cai, R. Li, T.-K. Sham, and X. Sun, “Atomic Layer Deposition of Lithium Tantalate Solid-State Electrolytes,” *J. Phys. Chem. C*, vol. 117, no. 39, pp. 20260–20267, Oct. 2013.

[141] J. Liu, M. N. Banis, Q. Sun, A. Lushington, R. Li, T.-K. Sham, and X. Sun, “Rational Design of Atomic-Layer-Deposited LiFePO4 as a High-Performance Cathode for Lithium-Ion Batteries,” *Adv. Mater.*, vol. 26, no. 37, pp. 6472–6477, Oct. 2014.

[142] V. Miikkulainen, A. Ruud, E. Østreng, O. Nilsen, M. Laitinen, T. Sajavaara, and H.

Fjellvåg, “Atomic Layer Deposition of Spinel Lithium Manganese Oxide by Film-Body-Controlled Lithium Incorporation for Thin-Film Lithium-Ion Batteries,” *J. Phys. Chem. C*, vol. 118, no. 2, pp. 1258–1268, Jan. 2014.

[143] J. W. Kim, J. J. Travis, E. Hu, K.-W. Nam, S. C. Kim, C. S. Kang, J.-H. Woo, X.-Q. Yang, S. M. George, K. H. Oh, S.-J. Cho, and S.-H. Lee, “Unexpected high power performance of atomic layer deposition coated Li[Ni1/3Mn1/3Co1/3]O2 cathodes,” *J. Power Sources*, vol. 254, pp. 190–197, May 2014.

[144] M.-L. Lee, C.-Y. Su, Y.-H. Lin, S.-C. Liao, J.-M. Chen, T.-P. Perng, J.-W. Yeh, and H. C. Shih, “Atomic layer deposition of TiO2 on negative electrode for lithium ion batteries,” *J. Power Sources*, vol. 244, pp. 410–416, Dec. 2013.

[145] D. M. Piper, J. J. Travis, M. Young, S.-B. Son, S. C. Kim, K. H. Oh, S. M. George, C. Ban, and S.-H. Lee, “Reversible High-Capacity Si Nanocomposite Anodes for Lithium-ion Batteries Enabled by Molecular Layer Deposition,” *Adv. Mater.*, vol. 26, no. 10, pp. 1596–1601, Mar. 2014.

[146] X. Li, A. Lushington, J. Liu, R. Li, and X. Sun, “Superior stable sulfur cathodes of Li–S batteries enabled by molecular layer deposition,” *Chem. Commun.*, vol. 50, no. 68, p. 9757, Jul. 2014.

[147] X. Li, A. Lushington, Q. Sun, W. Xiao, J. Liu, B. Wang, Y. Ye, K. Nie, Y. Hu, Q. Xiao, R. Li, J. Guo, T.-K. Sham, and X. Sun, “Safe and Durable High-Temperature Lithium–Sulfur Batteries via Molecular Layer Deposited Coating,” *Nano Lett.*, vol. 16, no. 6, pp. 3545–3549, Jun. 2016.

[148] F. Schüth and W. Schmidt, “Microporous and Mesoporous Materials,” *Adv. Mater.*, vol. 14, no. 9, pp. 629–638, May 2002.

[149] Y. Ma, W. Tong, H. Zhou, and S. L. Suib, “A review of zeolite-like porous materials,” *Microporous Mesoporous Mater.*, vol. 37, no. 1–2, pp. 243–252, May 2000.

[150] C.-Y. Tsai, S.-Y. Tam, Y. Lu, and C. J. Brinker, “Dual-layer asymmetric microporous silica membranes,” *J. Memb. Sci.*, vol. 169, no. 2, pp. 255–268, May 2000.

[151] S. V. Lamaka, M. L. Zheludkevich, K. A. Yasakau, R. Serra, S. K. Poznyak, and M. G. S. Ferreira, “Nanoporous titania interlayer as reservoir of corrosion inhibitors for coatings with self-healing ability,” *Prog. Org. Coatings*, vol. 58, no. 2–3, pp. 127–135, Feb. 2007.

[152] J. Hiller, J. D. Mendelsohn, and M. F. Rubner, “Reversibly erasable nanoporous anti-reflection coatings from polyelectrolyte multilayers,” *Nat. Mater.*, vol. 1, no. 1, pp. 59–63, Sep. 2002.

[153] J.-F. Chen, H.-M. Ding, J.-X. Wang, and L. Shao, “Preparation and characterization of porous hollow silica nanoparticles for drug delivery application,” *Biomaterials*, vol. 25, no. 4, pp. 723–727, Feb. 2004.

[154] Y. Qin, Y. Yang, R. Scholz, E. Pippel, X. Lu, and M. Knez, “Unexpected Oxidation Behavior of Cu Nanoparticles Embedded in Porous Alumina Films Produced by Molecular Layer Deposition,” *Nano Lett.*, vol. 11, no. 6, pp. 2503–2509, Jun. 2011.

[155] Q. Peng, B. Gong, R. M. VanGundy, and G. N. Parsons, "'Zincone' Zinc Oxide−Organic Hybrid Polymer Thin Films Formed by Molecular Layer Deposition," *Chem. Mater.*, vol. 21, no. 5, pp. 820–830, Mar. 2009.

[156] X. Liang, M. Yu, J. Li, Y.-B. Jiang, and A. W. Weimer, "Ultra-thin microporous–mesoporous metal oxide films prepared by molecular layer deposition (MLD)," *Chem. Commun.*, no. 46, p. 7140, Dec. 2009.

[157] L. B. Chen, J. Y. Xie, H. C. Yu, and T. H. Wang, "An amorphous Si thin film anode with high capacity and long cycling life for lithium ion batteries," *J. Appl. Electrochem.*, vol. 39, no. 8, pp. 1157–1162, Aug. 2009.

[158] R. Epur, M. Ramanathan, F. R. Beck, A. Manivannan, and P. N. Kumta, "Electrodeposition of amorphous silicon anode for lithium ion batteries," *Mater. Sci. Eng. B*, vol. 177, no. 14, pp. 1157–1162, Aug. 2012.

[159] N. Kuwata, R. Kumar, K. Toribami, T. Suzuki, T. Hattori, and J. Kawamura, "Thin film lithium ion batteries prepared only by pulsed laser deposition," *Solid State Ionics*, vol. 177, no. 26–32, pp. 2827–2832, Oct. 2006.

[160] H. Oechsner, "Sputtering - A review of some recent experimental and theoretical aspects," *Appl. Phys.*, vol. 8, pp. 185–198, 1975.

[161] G. K. Wehner, "Sputtering by Ion Bombardment," in *Advances in Electronics and Electron Physics*, vol. 7, Elsevier, 1955, pp. 239–298.

[162] P. Kelly and R. Arnell, "Magnetron sputtering: a review of recent developments and applications," *Vacuum*, vol. 56, no. 3, pp. 159–172, Mar. 2000.

[163] V. Fox, J. Hampshire, and D. Teer, "MoS2/metal composite coatings deposited by closed-field unbalanced magnetron sputtering: tribological properties and industrial uses," *Surf. Coatings Technol.*, vol. 112, no. 1–3, pp. 118–122, Feb. 1999.

[164] J. Pan, C. Leygraf, D. Thierry, and A. M. Ektessabi, "Corrosion resistance for biomaterial applications of TiO2 films deposited on titanium and stainless steel by ion-beam-assisted sputtering," *J. Biomed. Mater. Res.*, vol. 35, no. 3, pp. 309–318, Jun. 1997.

[165] Y. Liu, "Disc drive with wear-resistant ramp coating of carbon nitride or metal nitride." Google Patents, 2002.

[166] K. Wasa and S. Hayakawa, *Handbook of sputter deposition technology*, 2nd ed. Yokohama City: Matsushita Electric, Ltd., 2012.

[167] K. Sarakinos, J. Alami, and S. Konstantinidis, "High power pulsed magnetron sputtering: A review on scientific and engineering state of the art," *Surf. Coatings Technol.*, vol. 204, no. 11, pp. 1661–1684, Feb. 2010.

[168] D. B. Fraser, "Film deposition with the Sputter Gun," *J. Vac. Sci. Technol.*, vol. 14, no. 1, p. 147, Jan. 1977.

[169] J. Andersson and A. Anders, "Gasless sputtering: Opportunities for ultraclean metallization, coatings in space, and propulsion," *Appl. Phys. Lett.*, vol. 92, no. 22, p. 221503, 2008.

[170] F. M. D'Heurle, "Aluminum films deposited by rf sputtering," *Metall. Mater. Trans.*

B, vol. 1, no. 3, pp. 725–732, Mar. 1970.

[171] V. Baranchugov, E. Markevich, E. Pollak, G. Salitra, and D. Aurbach, "Amorphous silicon thin films as a high capacity anodes for Li-ion batteries in ionic liquid electrolytes," *Electrochem. commun.*, vol. 9, no. 4, pp. 796–800, Apr. 2007.

[172] W. J. Zhang, "A review of the electrochemical performance of alloy anodes for lithium-ion batteries," *J. Power Sources*, vol. 196, no. 1, pp. 13–24, 2011.

[173] P. Knauth, "Inorganic solid Li ion conductors: An overview," *Solid State Ionics*, vol. 180, no. 14–16, pp. 911–916, Jun. 2009.

[174] J. B. Goodenough and P. Singh, "Review—Solid Electrolytes in Rechargeable Electrochemical Cells," *J. Electrochem. Soc.*, vol. 162, no. 14, pp. A2387–A2392, 2015.

[175] X. Yu, "A Stable Thin-Film Lithium Electrolyte: Lithium Phosphorus Oxynitride," *J. Electrochem. Soc.*, vol. 144, no. 2, p. 524, 1997.

[176] C.-L. Liao and K.-Z. Fung, "Lithium cobalt oxide cathode film prepared by rf sputtering," *J. Power Sources*, vol. 128, no. 2, pp. 263–269, Apr. 2004.

[177] M. Köhler, F. Berkemeier, T. Gallasch, and G. Schmitz, "Lithium diffusion in sputter-deposited lithium iron phosphate thin-films," *J. Power Sources*, vol. 236, pp. 61–67, Aug. 2013.

[178] H.-S. Moon, K.-S. Ji, J.-W. Park, W. Il Cho, and Y. S. Yoon, "Electrochemical Characteristics of Sputtered Lithium Manganese Oxide Thin Film for Micropower Systems," *J. Korean Phys. Soc.*, vol. 40, no. 1, pp. 22–25, 2002.

[179] C. H. Choi, W. I. Cho, B. W. Cho, H. S. Kim, Y. S. Yoon, and Y. S. Tak, "Radio-Frequency Magnetron Sputtering Power Effect on the Ionic Conductivities of Lipon Films," *Electrochem. Solid-State Lett.*, vol. 5, no. 1, p. A14, 2002.

[180] C. S. Nimisha, K. Y. Rao, G. Venkatesh, G. M. Rao, and N. Munichandraiah, "Sputter deposited LiPON thin films from powder target as electrolyte for thin film battery applications," *Thin Solid Films*, vol. 519, no. 10, pp. 3401–3406, Mar. 2011.

[181] M. Tatsumisago, M. Nagao, and A. Hayashi, "Recent development of sulfide solid electrolytes and interfacial modification for all-solid-state rechargeable lithium batteries," *J. Asian Ceram. Soc.*, vol. 1, no. 1, pp. 17–25, Mar. 2013.

[182] Y. Seino, K. Takada, B.-C. Kim, L. Zhang, N. Ohta, H. Wada, M. Osada, and T. Sasaki, "Synthesis of phosphorous sulfide solid electrolyte and all-solid-state lithium batteries with graphite electrode," *Solid State Ionics*, vol. 176, no. 31–34, pp. 2389–2393, Oct. 2005.

[183] J. Awaka, N. Kijima, Y. Takahashi, H. Hayakawa, and J. Akimoto, "Synthesis and crystallographic studies of garnet-related lithium-ion conductors Li6CaLa2Ta2O12 and Li6BaLa2Ta2O12," *Solid State Ionics*, vol. 180, no. 6–8, pp. 602–606, May 2009.

[184] D. J. Kalita, S. H. Lee, K. S. Lee, D. H. Ko, and Y. S. Yoon, "Ionic conductivity properties of amorphous Li–La–Zr–O solid electrolyte for thin film batteries," *Solid State Ionics*, vol. 229, pp. 14–19, Dec. 2012.

[185] K. Joo, “Thin film lithium ion conducting LiBSO solid electrolyte,” *Solid State Ionics*, vol. 160, no. 1–2, pp. 51–59, May 2003.

2 Experimental and Characterization Methods

This chapter describes the methods for fabrication and characterization of the electrodes and ALD/MLD thin-films described in this thesis. Due to the nanometer-scale thickness of the thin-films, a number of different characterization techniques allow their characterization. This includes methods such as scanning electron microscopy (SEM), energy-dispersive X-ray (EDX) spectroscopy, Fourier transform infrared (FTIR) spectroscopy, thermogravimetric analysis (TGA) and differential scanning calorimetry (DSC), as well as quartz crystal microbalance (QCM) mass measurements. Furthermore, for the electrochemical characterization of the electrode materials techniques including galvanostatic charge-discharge cycling, cyclic voltammetry (CV) and electroimpedance spectroscopy (EIS) can be used. This chapter provides a general overview of the fabrication and characterization methods, however, specific details of the studies are found in the methods section of their respective chapter.

2.1 Fabrication Methods

2.1.1 ALD and MLD Deposition

A Gemstar Arradiance 8 tool was used for the ALD and MLD thin film coatings. Substrates were placed in the reaction chamber, which was pumped down to ~0.6 mTorr and heated to the desired temperature. Precursor bottles and the manifold (the valves leading to the reaction chamber) were heated to their respective temperatures. An argon gas flow was passed through the manifolds and the chamber and the system was left to stabilize for 1 hour before deposition.

A typical precursor exposure involved the following steps: (1) pulsing of the precursor into the system and closing the pump to “bathe” the substrate in the precursor, (2) opening the pump and purging the system with argon gas to remove the remaining precursor and reactants, (3) decreasing argon gas flow and allowing the system to stabilize. Once the pressure in the chamber stabilized, repeating the process with the complementary precursor completed a single deposition cycle. Discussion of the parameters for the ALD/MLD thin-film deposition are in detail in their respective sections.

Figure 2.1. Photo of the Gemstar Arradiance 8 atomic layer deposition tool.

2.1.2 Electrode Preparation

Electrode slurries were prepared with three main components: (1) the active material, (2) a conducting agent and (3) a polymeric binder. Asbury Carbons HPM850 natural flake graphite was used as the electroactive material with a mean particle size of 5 μm and a surface area of 18.0 m^2/g. Cabot Black Pearls® 2000 (BP2000) conductive carbon black was used as the conducting agent and Alpha Aesar polyvinylidene fluoride (PVdF) was used as the binder. The graphite, carbon black, PVdF mixture ratio used was 8:1:1 respectively as seen in Figure 2.2a.

The mixture was dry ground for 5 minutes to disperse the particles followed by the addition of 3 hours of wet grinding in n-methyl-2pyrrolidone (NMP), to create the slurry (Figure 2.2b). The NMP was added in a 25:1 w/w ratio to the carbon black. The slurry was tape cast with two pieces of tape onto the copper foil collector (Figure 2.2c) and dried overnight at 60 °C under vacuum.

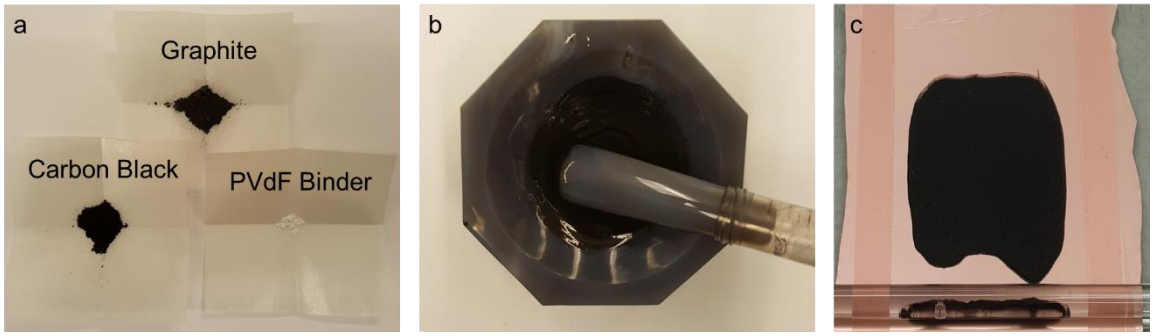

Figure 2.2. Photos of (a) the materials used for electrode fabrication, (b) wet grinding of the slurry and (c) slurry tape cast onto copper foil.

2.2 Characterization Methods

2.2.1 Physical Characterization Methods

A number of techniques were used to characterize the coated battery materials and thin film coatings. This included quartz crystal microbalance (QCM) mass measurements, scanning electron microscopy (SEM), transmission electron microscopy (TEM), thermogravimetric analysis (TGA) and Fourier transform infrared spectroscopy (FTIR).

To confirm ALD and MLD growth during the thin-film deposition process a Colnatec quartz crystal microbalance (QCM) measured the mass gain per cycle in the deposition chamber. This method relies on the use of a quartz crystal, which has excellent piezoelectric properties. In this system, the quartz crystal resonates at its resonance frequency. Any mass variation on the surface of the quartz crystal results in a change in its frequency. As the frequency is highly sensitive to any mass change, this method is exceptionally accurate at measuring mass changes. The dependence of the frequency on the mass change is in accordance with the equation:

$$\Delta f = -\frac{2f_0^2 \Delta m}{A\sqrt{\mu\rho}} = -C\Delta m \qquad \textbf{(2.1)}$$

Where Δf is the resonant frequency change of the quartz crystal, f_0 is the fundamental frequency of the bare quartz crystal, Δm is the mass change, A is the surface area, μ is the shear modulus of the quartz crystal, and ρ is the density of the quartz. As f_0, A, μ, and ρ

are constants in the system they can be summarized as the constant C. Rearranging Equation 2.1 to solve for the mass change results in the equation:

$$\Delta m = -\frac{\Delta f}{C} \tag{2.2}$$

Colnatec provided a value of C of $0.22605 \frac{Hz\ cm^2}{ng}$ for the system when Δf is in units of Hz resulting in units of ng/cm^2 for Δm. This system has a resolution of 0.001 Hz or 0.0044 ng/cm^2, which is well below the mass of a monolayer. Figure 2.3 shows the Colnatec QCM interface used with the Gemstar Arradiance 8 tool. The arms of the system allowed the QCM to be directly above the sample in the center of the chamber to ensure the precursor concentrations and temperature between the QCM and the sample were as close as possible.

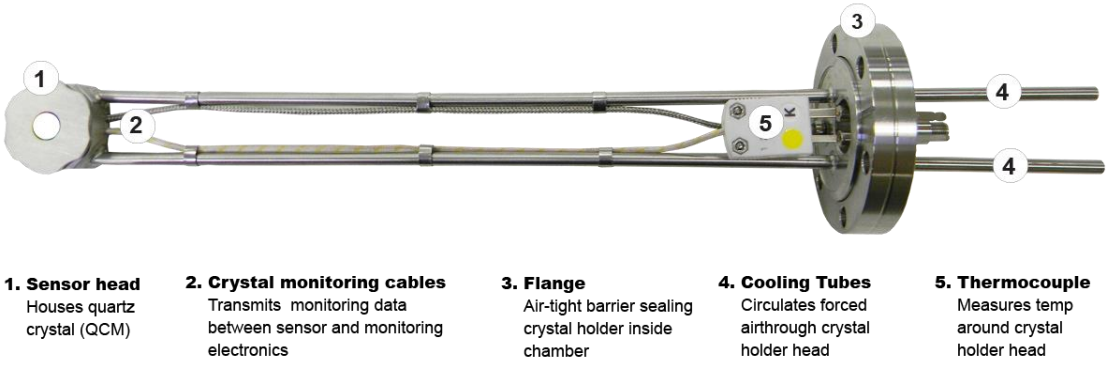

Figure 2.3. An image of the different components of a Colnatec QCM interface [1].

Scanning electron microscopy (SEM) is a powerful tool to characterize the surface morphology of materials with a resolution far exceeding optical microscopy. Due to particle-wave duality, this superior resolution is due to the wavelength of a particle being inversely related to the mass of the particle. This association can be expressed by the following equation:

$$\lambda = \frac{h}{p} = \frac{hc}{pc} \tag{2.3}$$

where λ is the de Broglie wavelength, h is Planck's constant, c is the speed of light, and p is momentum. hc is a constant with the value $1239.85\ eV \cdot nm$. For a photon with $E = 1eV$, and knowing $pc = E, pc = 1\ eV$, therefore, $\lambda = 1240\ nm$. In the case of an electron with a higher mass the energy of the electron can be described by the equation:

$$E = \sqrt{p^2c^2 + m_0^2c^4} \quad \textbf{(2.4)}$$

where m_0 is the rest mass of the electron, a constant, and can be approximated to:

$$pc \approx \sqrt{2 \times KE \times m_0c^2} \quad \textbf{(2.5)}$$

where λ is the de Broglie wavelength, h is Planck's constant and p is momentum. Therefore, an electron with 1 eV of energy, and a rest mass energy of 0.511 MeV, would have a de Broglie wavelength of 1.23 nm, approximately three orders of magnitude less than a photon of the same wavelength. As the resolution of an image is directly related to the wavelength of the particle, electron microscopy provides an enormous advantage over optical microscopy. To take advantage of this phenomenon an SEM utilizes an electron gun which emits a large flux of electrons. The emitted electrons are aligned, condensed and redirected onto the sample as seen in Figure 2.4. By scanning the sample and measuring the intensity of the secondary electrons off of the sample a detailed image can be created.

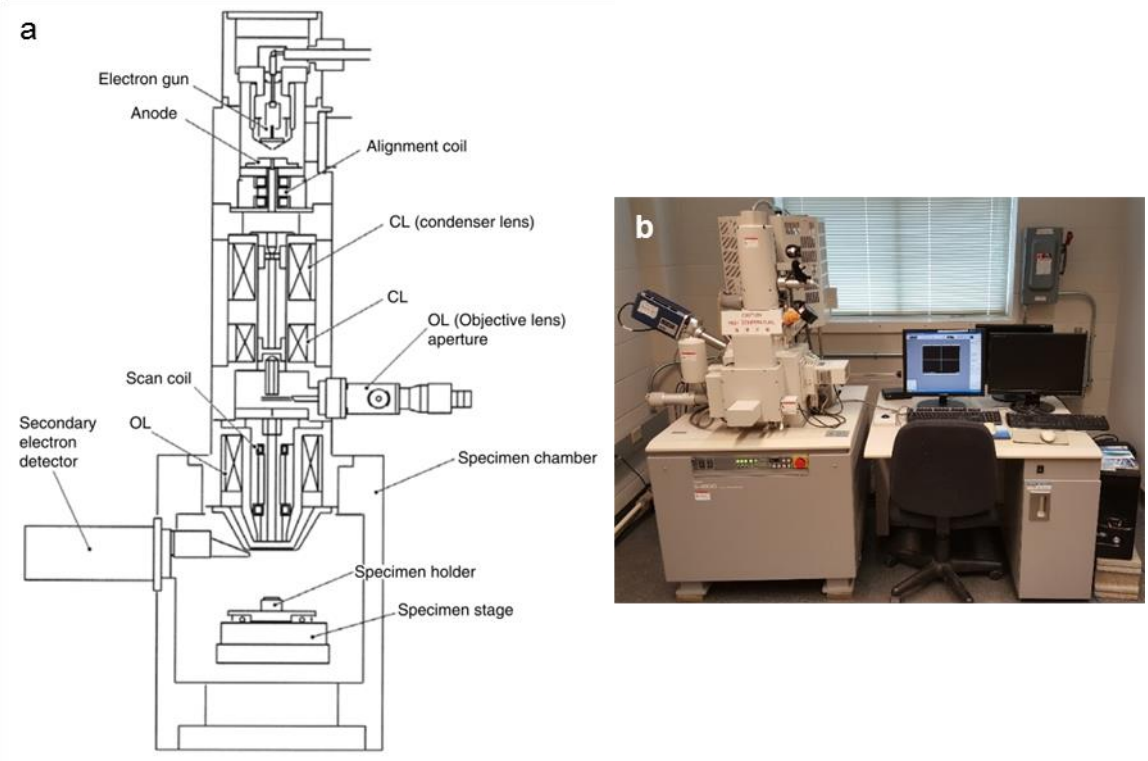

Figure 2.4. (a) A typical configuration of an SEM [2] and (b) SEM Photo of the Hitachi S-4800 scanning electron microscope.

A Hitachi S-4800 high resolution SEM was used to characterize the surface morphology and perform elemental analysis of the materials (Figure 2.4b). An acceleration voltage of 5.0 kV with a working distance of 5 mm was used for collecting the SEM images. In secondary mode, the SEM produced a resolution of ~2 nm. For elemental analysis, an x-ray detector was used for energy-dispersive X-ray spectroscopy (EDX). In this configuration, an acceleration voltage of 20.0 kV with a working distance of 15 mm was employed.

Like SEM transmission electron microscopy (TEM) takes advantage of the high resolution electrons can provide. However, a TEM relies on analyzing electrons which transmit through the sample of interest. If the sample is on the nanometer scale such as a powder it can be dispersed on a copper grid for imaging. Otherwise, a slice of the sample must be cut via focused ion beam (FIB) milling. Similar to SEM a TEM utilizes an electron gun and a series of focusing techniques to create an electron beam to image the sample. As seen in

Figure 2.5a a TEM differs from SEM in the positioning of the detector. Unlike an SEM, which detects the secondary electrons from the sample, a TEM images the primary electrons, which transmit through the sample.

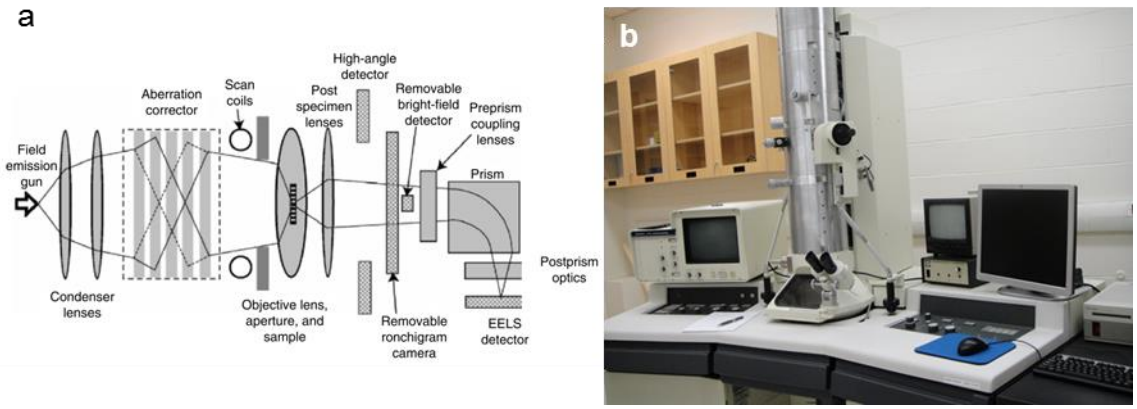

Figure 2.5. (a) A typical schematic of the components of a TEM [3] and (b) photo of the Hitachi H-7000 transmission electron microscope.

To obtain cross sections of the thin films a Hitachi H-7000 TEM was used (Figure 2.5b). An acceleration voltage of 100 kV produced a resolution of ~0.4 nm. Deposition of the MLD thin films onto nanoparticles allowed the imaging of the core particles and the thin film coating for thickness and conformity measurements.

Thermogravimetric analysis (TGA) and differential scanning calorimetry (DSC) are simple, yet powerful tools to gain insight into the composition of a sample. These methods involve the heating of a sample, either under a regular or inert atmosphere. TGA records the mass of the sample during this process whereas DSC records the amount of energy required to heat the sample by 1 °C. This allows the ability to determine the temperature dependence on features such as phase changes and reactions. For mass analysis of MLD thin films during annealing a SDT Q600 was used (Figure 2.6). Using this system allowed the measurement of the mass and heat flux during the annealing process of the porous thin films. Furthermore, the amount of time needed to complete the annealing process and a stable composition could be determined with this method.

Figure 2.6. Photo of the TA Instruments Q600-SDT thermogravimetric analysis system.

Gas-sorption is a powerful technique to measure the surface area of materials by analyzing the physical adsorption of gas molecules onto the material's surface. In this technique, a sample is placed in a vacuum chamber. A gas is slowly introduced in a controlled quantity to allow the comparison of the measured pressure of the chamber and the expected pressure. As some of the gas adsorbs on the surface of the sample the measured pressure is lower than the expected pressure. In Langmuir theory, a single monolayer of gas adsorbs on the surface, however, in reality many layers typically adsorb on the surface. First published in 1938, the method to understand multilayer adsorption is popularly referred to by the authors names as the Brunaur, Emmet and Teller (BET) method [4]. BET has three main assumptions:

(1) infinite layers of the gas molecules adsorb onto a solid surface;
(2) no interaction occurs between the two adsorption layers; and
(3) each layer can be described by Langmuir theory.

From this the BET equation can be derived as:

$$\frac{p}{v(p_0-p)} = \frac{1}{v_m c} + \frac{c-1}{v_m c}\frac{p}{p_0} \qquad \textbf{(2.6)}$$

where p is the equilibrium pressure, p_0 is the saturation pressure at the temperature of adsorption, v is the adsorbed gas quantity, v_m is the monolayer adsorbed gas quantity. c is the BET constant:

$$c = e^{\frac{E_1 - E_L}{RT}} \quad \textbf{(2.7)}$$

where E_1 is the heat of adsorption for the first layer and E_L is the heat of liquefaction for the second layer and up. Plotting $\frac{p}{v(p_0 - p)}$ and $\frac{p}{p_0}$ normally reveals a linear relationship. From this $\frac{c-1}{v_m c}$ can be calculated as the slope and $\frac{1}{v_m c}$ can be calculated as the y-intercept to calculate v_m and c. Finally, the equation to calculate the surface area is:

$$S_{BET} = \frac{v_m N_A s}{Va} \quad \textbf{(2.8)}$$

where N_A is Avogadro's number, s is the adsorption cross-section of the adsorbing species, V is the molar volume of the adsorbate gas and a is the mass of the sample.

For BET surface area analysis of the porous thin films a Micrometrics Tristar II, surface area and porosity measurement tool was used (Figure 2.7). Samples were first prepared by removing any moisture or contamination on the surface. This was achieved by placing the samples in an inert argon atmosphere and heating the sample to 90 °C for one hour followed by three hours at 300 °C. The samples masses were measured and they were placed in the porosity measurement chamber. The chamber was subjected to a vacuum and the temperature was dropped to 77K, by surrounding the chamber with liquid nitrogen. Nitrogen gas was allowed into the chamber at a controlled rate while the pressure was closely monitored. Further details of the sample degas conditions can be found in their respective chapters.

Figure 2.7. Photo of the Micrometrics TriStar II Surface Area and Porosity tool.

Fourier transform infrared spectroscopy (FTIR) is a chemical analysis technique which is used to obtain the infrared spectrum of a sample. In this technique a light beam which contains a large number of frequencies of light is shone onto the sample. The transmitted light is then collected and analyzed. By utilizing a Fourier transform, the intensities of the various wavelengths of the light can be deduced. The adsorption of these wavelengths depend on the resonant frequencies of the chemical bonds in the sample. Many different types of resonances can occur including antisymmetric stretching, scissoring, rocking, wagging and twisting. These vibrations create a change in the dipole of the molecular structure allowing them to be IR active. As many vibration modes have become well documented the IR spectra can provide a detailed understanding of the chemical makeup of a sample.

Infrared active organic materials were measured via a Thermo Scientific Nicolet 380 FT-IR system (Figure 2.8). Thin films deposited on powders were mixed with infrared inactive KBr. To minimize moisture, the powders and KBr were dried under vacuum at 60 °C for 24 hours before measurements. The powder was pressed into a pellet and transmission FTIR measurements were taken. Furthermore, films were deposited on double polished n-type (100) silicon for FTIR spectroscopy.

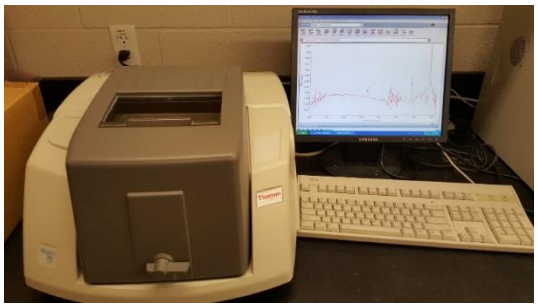

Figure 2.8. Photo of the Thermo Scientific Nicolet 380 FT-IR system.

2.2.2 Electrochemical Characterization Methods

For electrochemical tests, CR-2032 coin cells were prepared in an argon-filled glove box. To ensure no moisture content on the electrodes, the material was dried overnight in a vacuum oven at 60°C. Circular discs were cut from the electrodes with a diameter of 9/16 inches (1.429 cm) and pressed for 3 minutes at 5600 lb to increase the contact between the active material and conducting agent. The electrodes' masses were measured before placing them under vacuum in the glove box transfer chamber to remove any remaining moisture. After one hour in the transfer chamber, the electrodes were transferred into the glove box to assemble the CR-2032 coin cells.

CR-2032 half cells were assembled with the graphite electrode, a lithium reference/counter electrode, a polypropylene separator (Celgard 2400) and a carbonate electrolyte composed of 1 M $LiPF_6$ in an ethylene carbonate, diethyl carbonate and ethylene carbonate solvent (EC:DEC:EMC, 1:1:1 by volume). The cells were fabricated in the following order: the anode cap, two springs, two 0.5 mm spacers, the lithium counter electrode, three drops of electrolyte, the separator, two additional drops of electrolyte, the graphite electrode and a cathode cap (Figure 2.9a). The cells were sealed by crimping them at 50 psi and were left overnight to ensure the electrolyte wetted the separator and electrode.

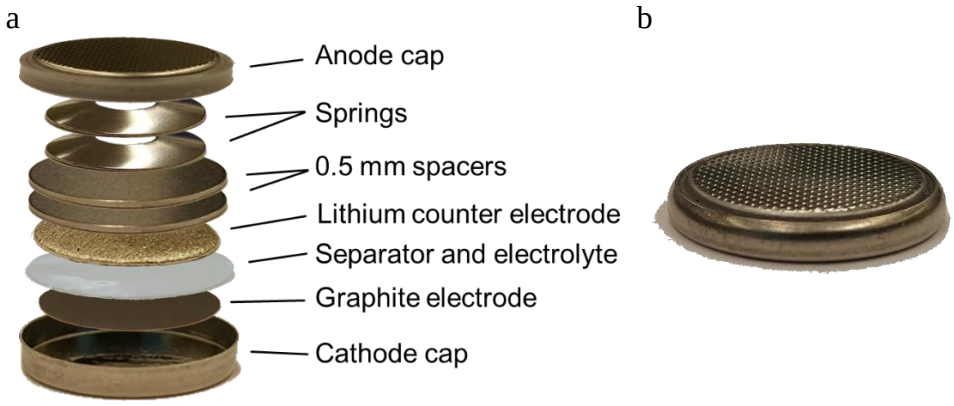

Figure 2.9. (a) Internal components of (b) a CR-2032 coin cell battery.

The CR-2032 half-cells were subjected to galvanostatic charge-discharge, CV and EIS for electrochemical testing. Galvanostatic charge-discharge utilizes a constant current and measures the resulting capacity and voltage of the battery. Once a cut-off voltage is reached, the cells are left to rest for 5 minutes after-which the current is reversed. An Arbin Instruments BT2000 battery testing system was used for galvanostatic testing as seen in Figure 2.10.

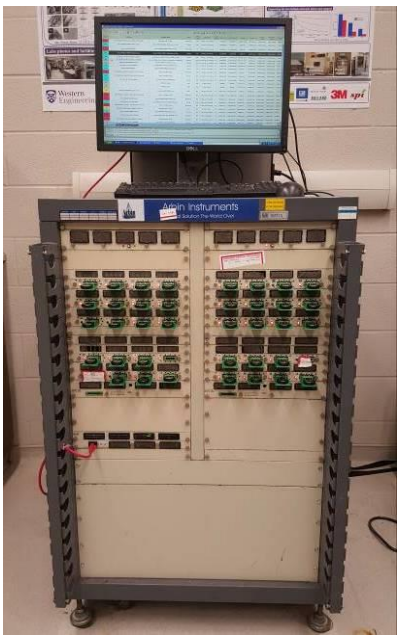

Figure 2.10. Photo of the Arbin Instruments BT-2000 battery testing system.

The current highly affects the resulting capacity of the battery and the amount of time for the batteries to charge/discharge. The current is typically referred to in units of Cs which is the inverse of the amount of time it would take to charge the battery in hours. A C-rate of 1 would be the equivalent of a 1 hour charge and 1 hour discharge whereas a C-rate of 0.1 would be the equivalent of a 10 hour charge and 10 hour discharge. To calculate the C-rate for the graphite electrode material the theoretical specific capacity (q) is first determined via the following equation:

$$q = \frac{xF}{MW} \tag{2.9}$$

Where x is the number of electrons used in the chemical reaction, F is Faraday's constant, and MW is the molecular weight of the active material required for the reduction to proceed. Equation 1.2 shows that six carbon allows the consumption of one electron, therefore, the theoretical capacity of graphite can thus be determined as:

$$q = \frac{1 \times 26\,801 \frac{mAh}{mol}}{12.01 \frac{g}{mol}} = 372 \frac{mAh}{g} \tag{2.10}$$

Therefore, a current of 372 mA/g will theoretically charge a graphite electrode in one hour. Specific charge/discharge rates are specified in in their respective sections.

CV and EIS measurements were taken using a Bio-Logic Multi Potentiostat VMP3. CV performs a voltage sweep across the cells and measures the resulting current. Once a voltage cut-off is reached, the voltage sweep is reversed to replicate the charge-discharge cycles of the cell. Voltages at which SEI formation occurs as well as at which lithium intercalation/deintercalation occurs are of particular interest in this thesis as well as the current densities in these regions.

EIS measurements are performed by subjecting the graphite half-cell to a low-current, low-voltage alternating current (AC). As the different components of the battery have a small capacitive nature a phase shift can be found in the output sinusoidal wave. Measuring this phase shift at different frequencies allows the decoupling of the various impedances and

quantitative analysis of the separate components of the cell. This thesis focuses on the impedance created due to SEI formation on the graphite surface.

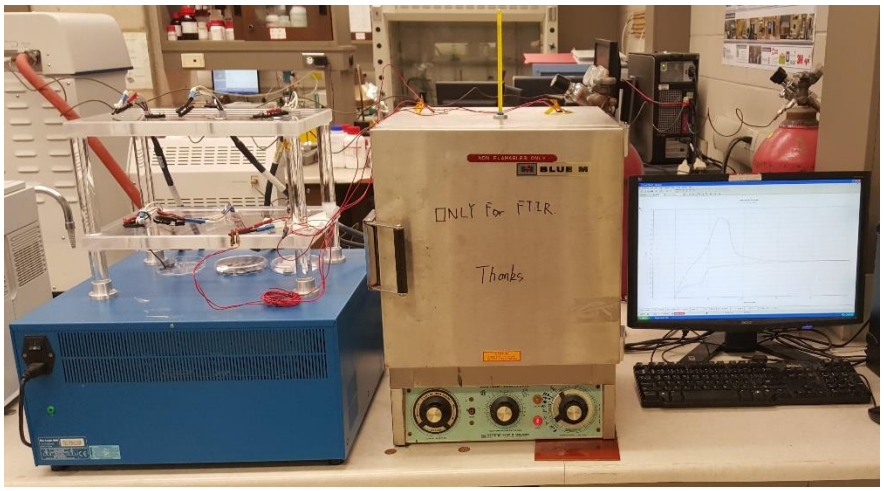

Figure 2.11. Photo of the Bio-Logic Multi Potentiostat VMP3.

References

[1] Colnatec, "Quartz Crystal Microbalance," 2016. [Online]. Available: http://colnatec.com/quartz-crystal-microbalance/. [Accessed: 09-Jun-2016].

[2] W. Zhou, R. Apkarian, Z. L. Wang, and D. Joy, "Fundamentals of Scanning Electron Microscopy (SEM)," in Scanning Microscopy for Nanotechnology, New York, NY: Springer New York, 2006, pp. 1–40.

[3] M. Rozmus, M. Blicharski, and S. Dymek, "Scanning and transmission electron microscopy microstructure characterization of mechanically alloyed NbTiAl alloys," J. Microsc., vol. 224, no. 1, pp. 58–61, Oct. 2006.

[4] S. Brunauer, P. H. Emmett, and E. Teller, "Adsorption of Gases in Multimolecular Layers," J. Am. Chem. Soc., vol. 60, no. 2, pp. 309–319, Feb. 1938.

3 Atomic and Molecular Layer Deposition Coated Graphite Anodes for Li-ion Batteries

Graphite has been the leading anode material for lithium-ion batteries since its first commercialization in the early 1990s. Its electrochemical reversibility is enabled by the in-situ formation of an ultrathin solid film during the discharge process on the battery's first cycle, which is called the solid electrolyte interface (SEI), as a result of the decomposition of the electrolyte. The SEI must fulfil a number of requirements to maintain graphite's stability during cycling, however, its composition is difficult to control due to the highly reducing nature of the graphite's surface. To gain a more precise control of the SEI film, we investigated the deposition ultrathin film coatings via atomic and molecular layer deposition (ALD and MLD) onto the graphite electrode. Using a MLD hybrid organic-inorganic alucone thin film, we demonstrated an improved energy efficiency by reducing the lithium loss due to decomposition of the electrolyte and formation of the SEI, as well as an increased electrode stability over 150 charge-discharge cycles.

3.1 Introduction

An energy storage system, which aims to replace gasoline and diesel engines in transportation vehicles, is gaining demand to decrease greenhouse gas emissions from the transportation sector. Lithium-ion batteries (LIBs) have become the leading rechargeable battery technology in recent years for consumer electronics and have potential to be mass produced for electric vehicles. This is due to their high energy density, high power density, long life-time, low self-discharge and environmental friendliness in comparison to other battery technologies [1], [2]. Despite these advantages, LIBs must overcome a number of issues to compete with gas/diesel engines including their energy density, safety, service life-time, uniformity and cost [1].

Since Sony's introduction of the LIB in 1991 [3], a number of different materials have been used as the cathode material. This includes lithium nickel manganese cobalt oxide (NMC), nickel cobalt aluminum oxide (NCA) and iron phosphate (LFP) [4], meanwhile, graphite and its derivatives have been long used as the commercial anode material throughout the battery's development. This is due to graphite's ability to allow lithium insertion and

removal in and out of its layered structure, without obvious structural changes and with little strain. This allows graphite to lithiate and delithiate consistently, quickly and safely [5]. Furthermore, graphite has a specific capacity of 372 mAh/g, much higher than the capacity of commercial cathode materials, which typically exhibit capacities lower than 200 mAh/g.

Early reports showed that graphite exhibited a poor cycling performance due to the electrolyte solvent, propylene carbonate's (PC), continuous decomposition on its surface [6]. It became apparent that stopping the decomposition of the electrolyte would enable the practical use of graphite in LIBs. This led to the discovery that ethylene carbonate (EC), which only differs from PC by one methyl group, decomposes on the graphite surface, but forms a protective thin film stopping further electrolyte decomposition [7]. This protective thin film, commonly referred to as the solid electrolyte interface (SEI) has become a fundamental aspect in improving graphite's electrochemical performance. By controlling the composition and thickness of the SEI researchers have tried to maximize its ionic conductivity, electronic resistivity, stability, and adhesion to the surface via a number of methods. This has included controlling the composition of the electrolyte [8], additives in the electrolyte [9], as well as pre-treatment of the graphite [10].

Nevertheless, up to now, few works have focused on thin-film surface coatings on the electrode rather than the active material particles to control SEI formation. This is due to two main factors: (1) the electrode contains a polymeric binder which would be destroyed by high temperature methods such as chemical vapour deposition (CVD) and (2) the electrode is highly porous, therefore, line of site methods are not possible as the coating must be conformal, which is challenging for conventional PVD methods. Atomic layer deposition (ALD) provides a way to deposit highly conformal thin-films at low temperatures. Previous studies report that ALD of Al_2O_3 [11]–[13] and TiO_2 [13], [14] on graphite can improve its cycling capabilities. Moreover, previous work on utilizing additives in the electrolyte has shown that an organic SEI allows a more flexible and robust SEI increasing the stability of the graphite's surface [9]. Molecular layer deposition (MLD) is a thin-film deposition method similar to ALD, however, it has the capability to create

hybrid organic-inorganic thin film coating. Therefore, it can be expected that MLD can build a more favorable organic-inorganic SEI for graphite than ALD.

In this study, we prepared ALD and MLD coated graphite electrodes and compared their electrochemical performances. ALD Al_2O_3 films were deposited via alternating exposure of trimethyl aluminum (TMA) and H_2O and MLD "alucone" thin films were deposited via alternating exposure of trimethylaluminum and ethylene glycol. A quartz crystal microbalance (QCM) was used to measure the growth of the thin films and energy-dispersive X-ray spectroscopy (EDX) mapping was used to confirm their conformal nature. Scanning electron microscopy (SEM) determined the coating process had little effect on the micro-scale morphology of the electrodes showing the advantage of the low-temperature ALD and MLD techniques. Analysis of the voltage curves and electrochemical impedance spectroscopy (EIS) measurements of the half-cells helped shed insight to the formation of the SEI. We demonstrate that the deposition of a hybrid organic-inorganic thin-film by MLD results in a superior cycling performance over both the bare and ALD Al_2O_3 coated graphite electrodes. Furthermore, the thin film coatings decreased the degree of side reactions during the cells initial charge-discharge cycles. Methods

3.1.1 Deposition of MLD and ALD Thin-Film Coatings

Deposition of the alucone and aluminum oxide thin films was performed using a Gemstar Arradiance 8 ALD tool. Trimethyl aluminum (TMA, $Al(CH_3)_3$, Strem, 98%) was used as the aluminum precursor in both films and ethylene glycol (EG, $HO(CH_2)_2OH$, Sigma-Aldrich, 99.8%) and deionized water were used as the oxidants for the MLD and ALD films respectively. 10 and 20 cycles of each coating was performed with the parameters as seen in Table 3.1. A base argon flow rate of 20 sccm was used with a purge rate of 100 sccm.

Table 3.1. ALD & MLD Deposition Parameters.

Parameter	TMA and Ethylene Glycol	TMA and H_2O
Chamber Temperature	80 °C	80 °C
Manifold Temperature	115 °C	115 °C
Reductant Temperature	Room Temperature	Room Temperature
Oxidant Temperature	115 °C	Room Temperature
Reductant Pulse Time	50 milliseconds	50 milliseconds
Reductant Hold Time	3 seconds	3 seconds
Reductant Purge Time	10 seconds	10 seconds
Reductant Stabilization Time	15 seconds	15 seconds
Oxidant Pulse Time	50 milliseconds	150 milliseconds
Oxidant Hold Time	3 seconds	3 seconds
Oxidant Purge Time	10 seconds	10 seconds
Oxidant Stabilization Time	10 seconds	20 econds

3.1.2 Electrode and Coin Cell Preparation

The electrode slurry was prepared by mixing graphite (5 μm, Asbury Carbons HPM850), carbon black (BP2000), and a polyvinylidene fluoride binder (Alpha Aesar) was used as the binder in a ratio of 8:1:1 by weight and dry ground for 5 minutes. N-methyl-2pyrrolidone (NMP) was added to the powder mixture in an approximate ratio of 25:1 of NMP:carbon black and wet ground for 3 hours to ensure no agglomeration of the particles and ensure the particles were well dispersed. The slurry was tape cast onto copper foil with two pieces of scotch tape and dried overnight under vacuum at 60 °C. ALD and MLD thin films were deposited with 0, 10 and 20 cycles, herein labelled as bare, 10 ALD, 20 ALD, 10 MLD and 20 MLD. The electrodes were cut into 9/16” discs and pressed under 5600 lb to ensure particle contact before being transferred into the argon filled glove box. CR-2032

coin cells with lithium metal foil as the counter electrode were fabricated with a polypropylene separator and a electrolyte composed of 1M $LiPF_6$ dispersed in EC:DEC:EMC (1:1:1 by volume). The coin cells were stored overnight at room temperature to ensure wetting before testing.

3.1.3 Physical and Electrochemical Characterization

A QCM monitor (Colnatec Eon-LT) was used to measure the mass gain of the ALD and MLD thin films during deposition. Material characterization and elemental analysis was carried out with a field emission SEM (Hitachi S-4800) equipped with an EDX tool. Galvanostatic charge-discharge cycling was performed with an Arbin Instruments BT-2000 battery test station. The batteries were cycled between 0.01 – 2.1 V. Further electrochemical testing was performed with a Bio-Logic Multi Potentiostat VMP3. Again, a voltage range of 0.01 – 2.1 V was used for cyclic voltammetry testing. Electro impedance spectroscopy was performed on the cells, before cycling, by applying a 1 mV AC signal from 10 mHz – 200kHz.

3.2 Results

3.2.1 Physical Characterization

Graphite electrodes were prepared for incorporation into CR-2032 coin cells as described previously [15]. Wet grinding of the electrode slurry ensures a good mixture of the graphite, carbon black and PVdF binder. Figure 3.1a shows an SEM image of the graphite-carbon black-PVdF composite with a good dispersion of the larger graphite particles (~5 μm) and smaller carbon black particles (50 nm). The porous structure is also demonstrated which enables lithium-ion diffusion throughout the electrode material. Investigating the electrode under higher magnification yielded the carbon black particles dispersed on the graphite's surface as seen in Figure 3.1b. The polymeric PVdF binder was confirmed through EDAX imaging of fluorine as seen in Figure S3.1, demonstrating its uniform mixture with the electrode.

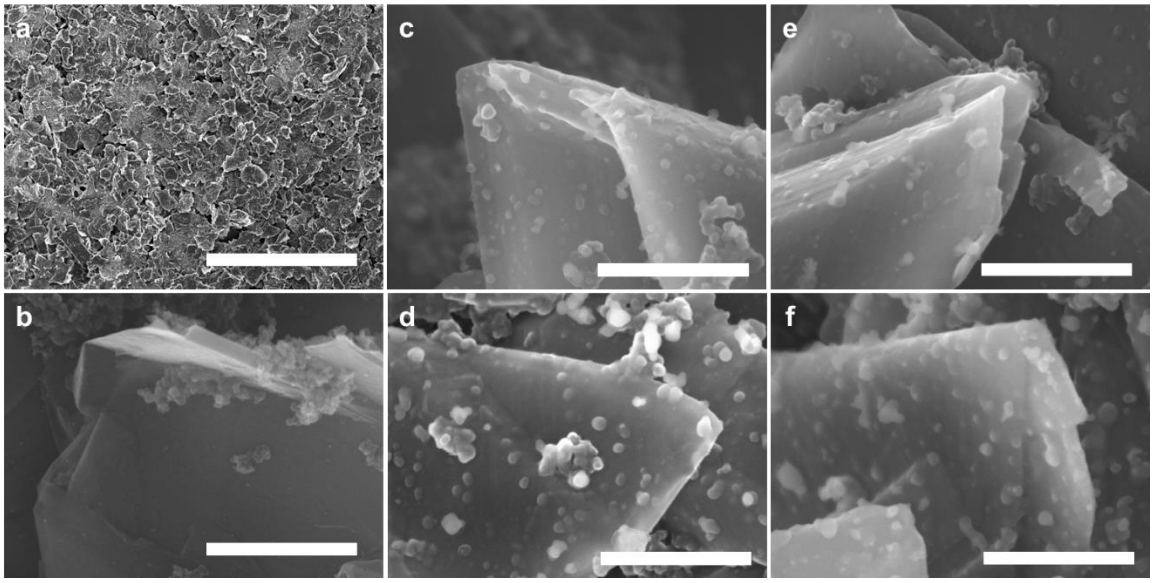

Figure 3.1. SEM images of the graphite anode with (a,b) no coating, (c) 10 ALD cycles, (d) 20 ALD cycles, (e) 10 MLD cycles, (f) 20 MLD cycles. The scale bars represent 500 nm.

Further SEM imaging was conducted upon the samples coated with 10 ALD, 20 ALD, 10 MLD and 20 MLD layers as seen in Figure 3.1(c-f). The 80 °C deposition temperature was well below the melting point of PVdF (177 °C), therefore, little morphology change was expected in the samples as demonstrated in the SEM images. Although the thickness of the thin-film coatings were below the resolution of the SEM and could not be easily imaged, the surface of the graphite with 20 ALD and 20 MLD (Figure 3.1(d,f)) cycles could be seen to be brighter in contrast than the bare graphite as a result of the reduced electronic conductivity of the coating film. The surface features of the coated graphite samples appear to be conformal indicated good conformity of the ALD and MLD coatings. Furthermore, charging of the surface of the sample coated with 20 ALD cycles (Figure 3.1d) indicates the formation of the insulating Al_2O_3 films.

To confirm successful deposition of the ALD and MLD coatings QCM measurements analyzed the mass gain during the depositions. Figure 3.2a shows the resulting mass measurements of a typical TMA-H_2O cycle and a typical TMA-EG cycle. In both curves, the first sharp increase can be attributed to the TMA pulse and are nearly identical. The small decrease in mass after these pulses is due to the slow desorption of the physisorbed

reactant and by-product molecules on the surface. The second sharp increase in mass can be attributed to the H_2O and EG pulses, which differ greatly. H_2O can be seen to have a sharp increase as the methyl groups of the TMA are replaced with hydroxyl groups followed by a stable mass indicating little physisorption of the reactants and by-products. The EG pulse can be seen to have a much larger mass increase due to the larger ethylene glycol molecules reacting with the surface. Furthermore, the large decrease in mass after the EG pulse indicates physisorption of the reactants which can be expected due to increased van der Waals forces from the larger molecules. Mass gains of 38.6 and 34.9 ng/cm^2 per cycle were found for the TMA-EG and TMA-H_2O cycles respectively.

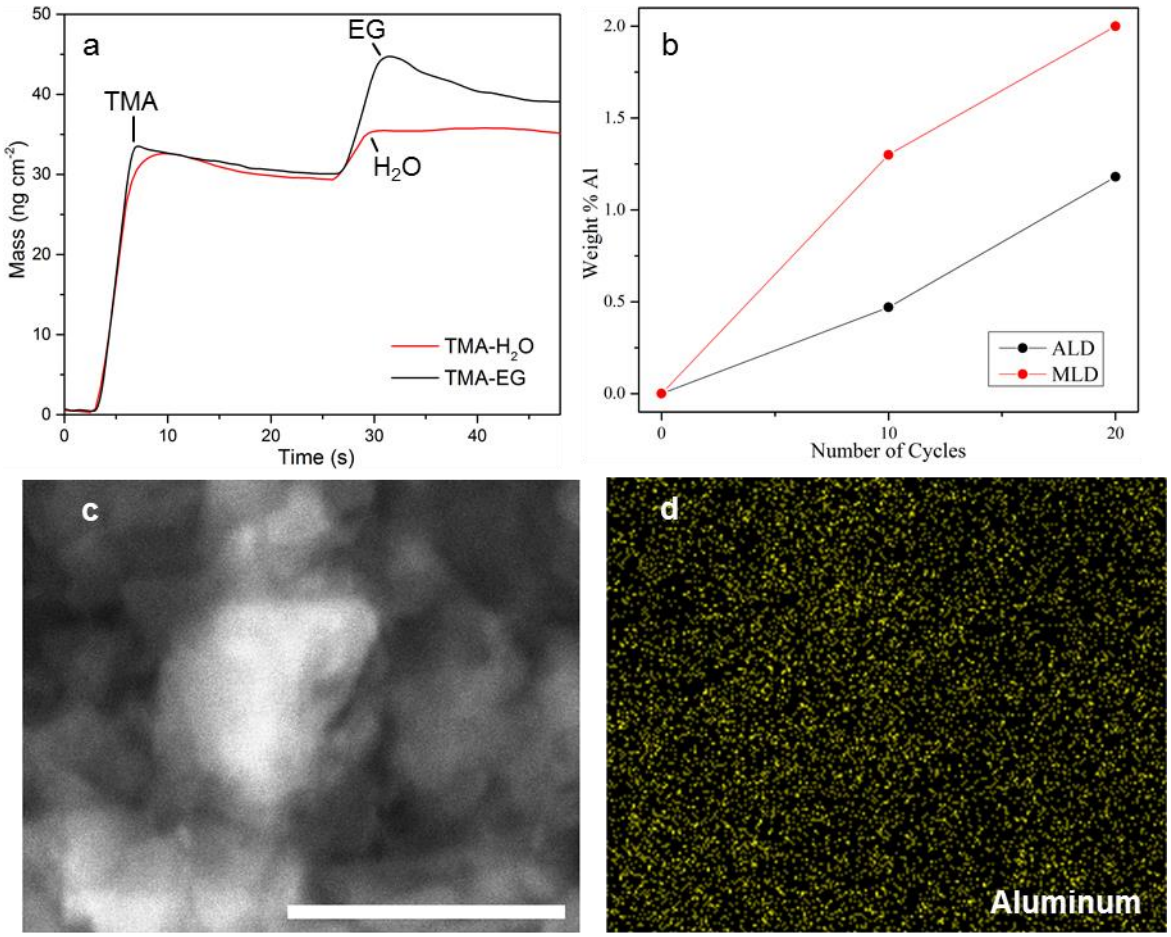

Figure 3.2. (a) QCM measurements of a typical TMA-H_2O and TMA-EG cycle. (b) Aluminum weight percentages from EDX elemental analysis of graphite electrodes with ALD and MLD thin films. (c) The region of interest for EDX measurements on a sample coated with 20 cycles of ALD and (d) EDAX mapping of aluminum on the sample. The scale bar represents 6 µm.

The ALD and MLD processes allow high conformity and controlled thickness of the thin film coatings. To confirm the aluminum based films' growth on the graphite electrodes EDX elemental analysis was performed. Figure 3.2b shows the resulting mass percentage of aluminum from the analysis of the various electrodes. The MLD films exhibited a higher aluminum mass increase per cycle which differs from the measurements from the QCM surface. This can be attributed to: 1) diffusion of TMA into the MLD film [16], and 2) the high porosity of the electrode material making it more difficult to remove physisorbed EG molecules. These phenomena could be mitigated by increasing the deposition temperature,

however, this was limited to avoid oxidizing the copper surface and melting the PVdF binder. The purge time could also be increased, however, this was limited due to time parameters of the ALD system. The MLD growth was deemed sufficient for the purposes of this investigation. To confirm the conformity of the ALD and MLD films EDX mapping was performed. Figure 3.2c shows the region of interest of the graphite electrode coated with 20 ALD cycles. As seen in Figure 3.2d aluminum is dispersed across the particles indicating the conformal nature of the thin film. Figure S3.1 shows the EDX mapping of the other electrodes indicating conformal deposition of the ALD and MLD thin films on the electrodes.

3.2.2 Electrochemical Characterization

Galvanostatic charge-discharge cycling was performed on the graphite CR-2032 coin cells. Rates of 0.1C (10 hour charge and 10 hour discharge) and 0.5C were compared to see the rate performance of the graphite under low and high rates. As seen in Figure S3.2a the cycling capacity of the graphite decreased under a higher rate, however, stable charge-discharge capacities were exhibited in both cases. The capacity loss due to the higher rate is a result of ionic diffusion limitations wherein the graphite cannot be fully lithiated. Furthermore, the higher rate decreases the reduction voltage and increases the oxidation voltage as seen in Figure S3.2c,d. The decrease in specific capacity and operating voltage both decrease the resulting energy density of the battery. CV was performed as seen in Figure S3.2b which had current peaks coinciding with the voltage plateaus of the voltage curves. Most noticeably was the large current peak and voltage plateau at ~0.7V, which coordinates with the formation of the inorganic portion of the graphite's SEI.

Cycling of the coated graphite electrodes was performed at 0.5C to investigate if the thin-film coatings could address the lower capacity and voltage exhibited from the graphite electrode at the higher rate. The discharge capacity curves can be seen in Figure 3.3a,b which show a stable charge-discharge capacity from both the ALD and MLD coated electrodes. Despite all the electrodes showing a stable performance after 150 cycles the 10 ALD and 20 ALD electrodes exhibited a decreased capacity (261 and 252 mAh/g respectively) when compared to the graphite reference (280 mAh/g). The 10 MLD electrode, however, demonstrated a comparable capacity (276 mAh/g) and the 20 MLD

electrode exhibited a slightly higher capacity (289 mAh/g) after 150 cycles. The decrease in capacity from the ALD coated electrodes may be due to the density of Al_2O_3 impeding lithium ion diffusion. This may create "dead" zones in the graphite where lithiation does not occur. The MLD alucone coating, however, has a lower density than the ALD Al_2O_3 coating [17] which may allow for more efficient lithium-ion diffusion. Interestingly, the 10 ALD and 20 MLD samples seem to have an initial decrease in capacity before regulating after ~10 cycles. This does not appear to be in correlation with the coating thickness, therefore, the initial charge-discharge voltage curves were investigated as seen in Figure 3.3c,d. The discharge curve which begins at 2.1 V and decreases to 0V can be seen to have a lithiation plateau at ~0.1 V for the bare electrode, however, it is near 0 V for the ALD and MLD electrodes indicating added resistance from the coatings. Due to this, the cut-off voltage of the battery (0.01V) was reached before the graphite was fully lithiated. The voltage curves of the 100^{th} cycle (Figure 3.3e,f) reveals that the discharge plateaus of the coated electrodes are nearly identical in voltage to those of the bare electrodes. This phenomenon can be also seen in the charge curves of the coated electrodes, which start at 0 V and carry upwards to 2.1 V (Figure 3.3). The increased delithiation plateau voltage in these curves indicated added resistance from the thin film coatings. After the initial cycles, however, the delithiation plateau can be seen to be nearly identical to the bare electrode (Figure 3.3e,f). Interestingly, the coated electrodes appear to have a slow increase in capacity with cycling compared to the bare electrode's slowly diminishing capacity.

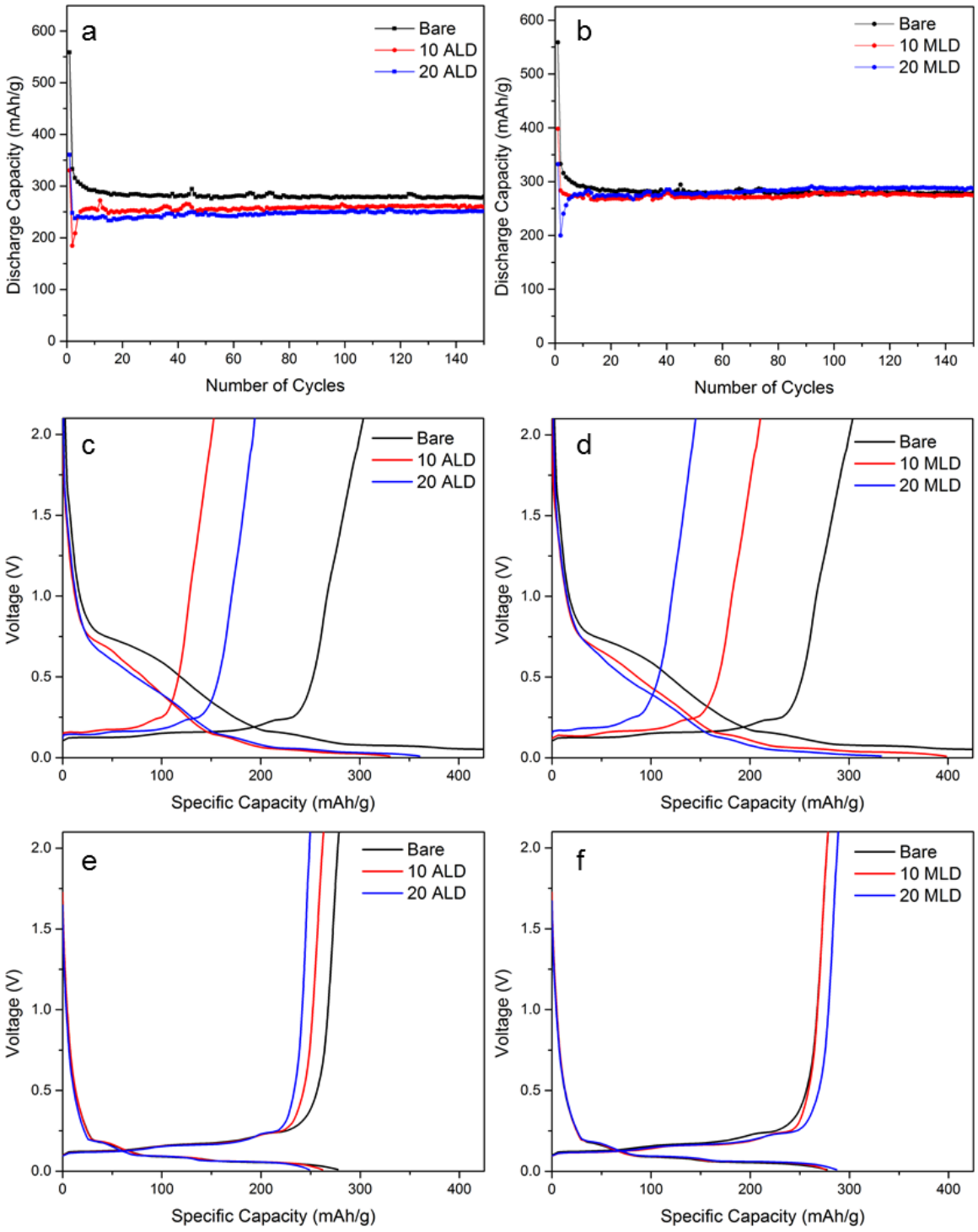

Figure 3.3. Charge-discharge cycling of graphite electrodes coated with (a) 0, 10 and 20 TMA-H_2O ALD cycles and (b) 0, 10 and 20 TMA-EG MLD cycles. Voltage profiles of (c,d) the first cycle of the respective electrodes, and (e,f) the voltage profiles of the electrodes after 100 charge discharge cycles. A rate of 0.5C was used.

The increased cycling performance of the ALD and MLD electrodes can be attributed to their effect on the SEI of the graphite. As seen in Figure 3.3c,d the plateau at ~0.7 V of the lithiation curve was decreased in the case of the coated materials. This plateau is associated with the formation of the inorganic portion of the electrolyte which has been shown to be the unstable portion of the SEI [9]. An additional SEI formation plateau occurs at ~0.1V, however, this is difficult to decouple from the lithiation plateau of the graphite. Therefore, the irreversible capacity loss, the difference in lithiation capacity and delithiation capacity, was calculated to determine how much of the capacity was lost to side reactions. Figure 3.4a,b show the irreversible capacity loss of the electrodes for the first 20 cycles. The first cycle of the bare electrode exhibited an irreversible capacity loss of 255 mAh/g. The 10 ALD and 20 ALD electrodes exhibited an irreversible capacity loss of 178 and 166 mAh/g respectively and the 10 and 20 MLD electrodes exhibited a loss of 188 and 187 mAh/g respectively. The capacity lost to SEI formation decreased due to the coatings. Furthermore, the 20 ALD electrode appeared to have an further impact on the irreversible capacity loss over the 10 ALD electrode, whereas the 10 MLD and 20 MLD electrodes exhibited nearly identical values. This may be due to the electrolyte still penetrating the MLD alucone film regardless of the thickness.

EIS further investigated the thin films' impact on the ionic resistance of the graphite. Figure 3.4c,d shows the resulting Nyquist plots from the EIS measurements of the electrodes. The width of the first semicircle has been shown to coordinate with the charge-transfer resistance of the graphite electrode. Figure S3.3 shows an equivalent circuit to describe the battery and allow calculation of the charge transfer resistance. The charge transfer resistance was found to be 95 Ω for the bare electrode, 126 and 132 Ω for the 10 and 20 ALD electrodes respectively and 120 and 119 Ω for the 10 and 20 MLD electrodes respectively. Figure S3.3b shows a plot of the calculated resistances. The increase in the charge transfer resistance can be attributed to the added coatings on the electrodes and correlates with the decreased SEI formation.

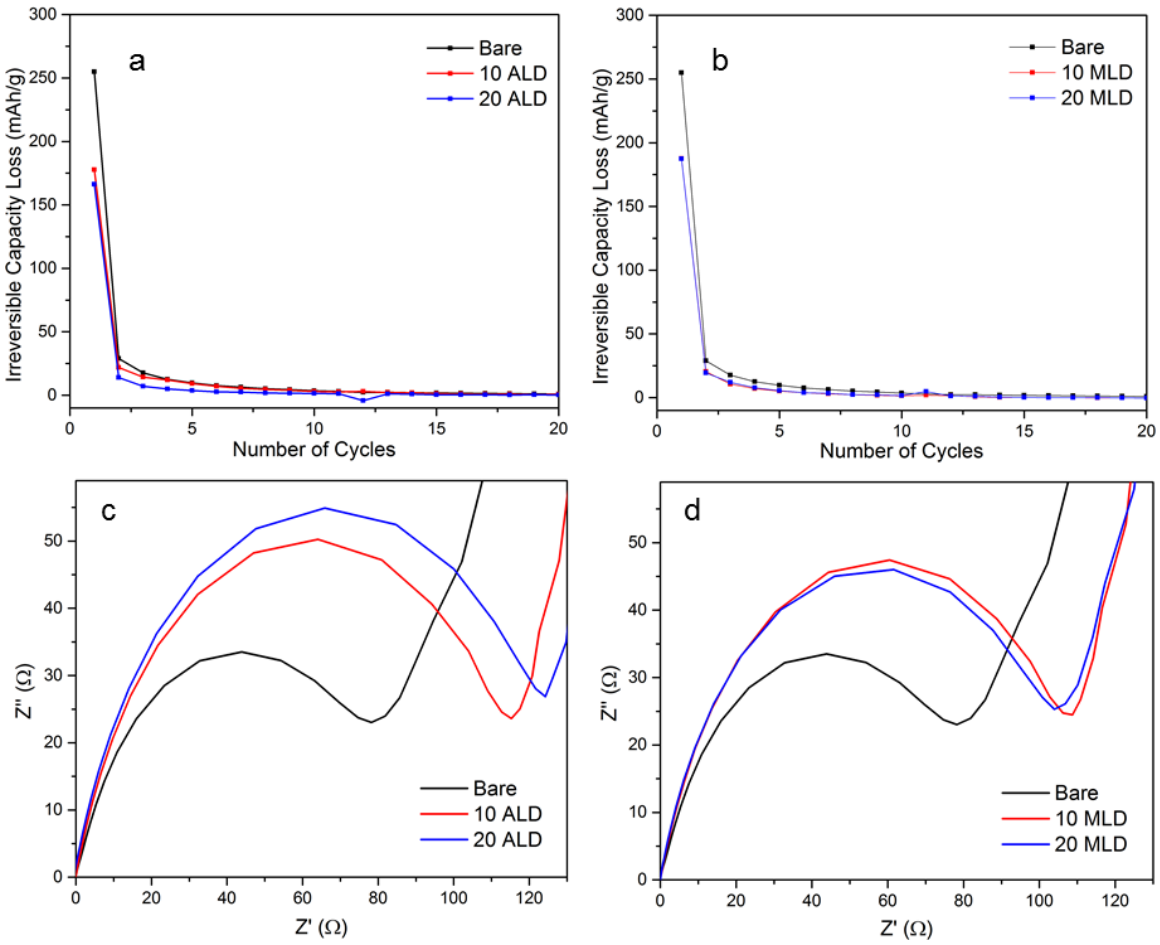

Figure 3.4. Irreversible capacity loss of graphite electrodes coated with (a) 0, 10 and 20 TMA-H_2O ALD cycles and (b) 0, 10 and 20 TMA-EG MLD cycles. EIS measurements of graphite half cells coated with (c) 0, 10 and 20 TMA-H_2O ALD cycles and (d) 0, 10 and 20 TMA-EG MLD cycles.

3.3 Discussion

The superior cycling performance of the MLD alucone coated graphite electrodes can be attributed to the resulting SEI having favourable properties. First, the MLD process creates a conformal film with a uniform morphology and chemical composition. This allows a uniform current distribution and good adhesion to the surface of the graphite. Second, the organic component of the alucone thin film creates a well cross-linked, flexible thin film which allows the coating to stretch and contract with the graphite during lithiation and delithiation. Third, the inorganic components of the alucone film decrease the electron

conductivity of the film reducing the reduction of the electrolyte on the surface of the graphite. Finally, the low density of the film allows lithium-ions to easily diffuse through it to the graphite.

An schematic representation of the SEI formation from the various techniques has been presented in Figure 3.5. Previous studies of the SEI formation of bare graphite electrodes have revealed a hybrid organic-inorganic film, with the surface of the graphite primarily composed of the inorganic components and the outer layer being composed primarily of the organic components [18]. The thin SEI film has good conformity, however, poor SEI performance has been shown to be due to the inner inorganic layer [9].

A similar SEI has been shown via ALD, however, the inorganic Al_2O_3 produces a much thicker inorganic layer decreasing the lithium-ion diffusion of the resulting SEI. This causes dead zones in the graphite decreasing its conductivity. Thicker Al_2O_3 coatings further decreases the capacity of the electrode.

Coating the graphite with a hybrid organic-inorganic alucone thin film produces a superior SEI. This thin film is homogenous in both organic and inorganic components which allows easy diffusion of the lithium-ions while electronically insulating the electrolyte from the graphite. Any electrolyte components which diffuse into the film and are reduced on the graphite's surface are trapped by the interconnected network improving the performance of the SEI. In addition, the organic-inorganic network allows a flexible and robust film which does not deteriorate with graphite's expansion and contraction during cycling.

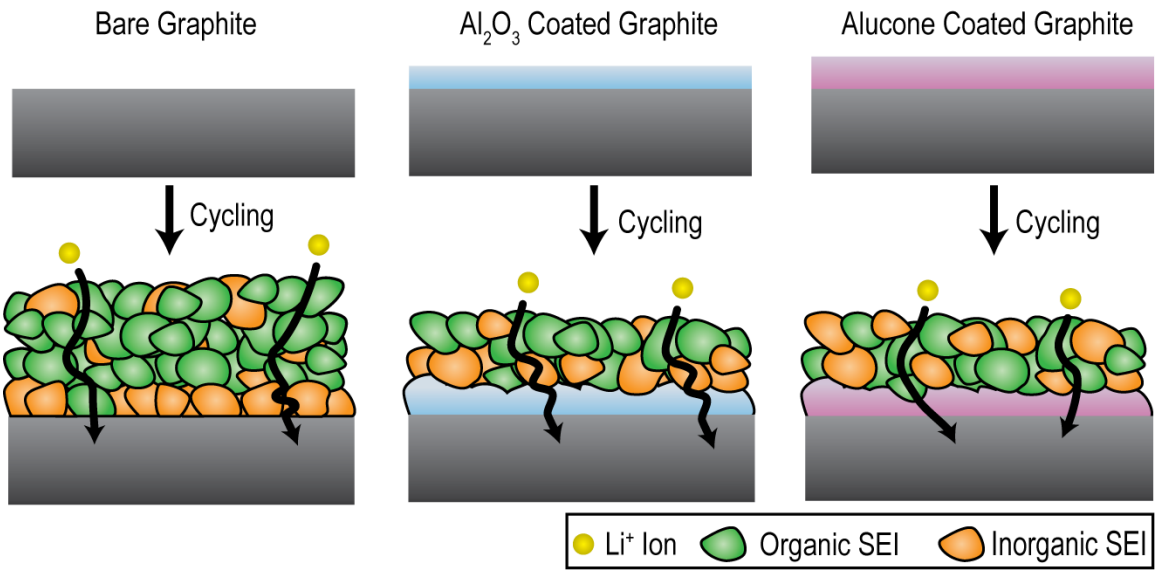

Figure 3.5. A schematic illustration of the SEI formation after cycling a bare graphite electrode, a graphite electrode coated with Al_2O_3 via ALD and a graphite electrode coated with alucone via MLD.

3.4 Conclusions

In conclusion, graphite electrodes were coated with 10 and 20 cycles via both ALD and MLD. The ALD process produced Al_2O_3 thin films by alternating TMA and H_2O pulses and the MLD process produced alucone thin films by alternating TMA and EG pulses. The MLD and ALD techniques resulted in highly conformal, homogenous thin films with a controllable thickness. The deposition processes were confirmed to be in a step-wise fashion via QCM measurements during the deposition and the conformity of the coatings on the electrodes was confirmed via EDX elemental mapping. Galvanostatic charge-discharge cycling revealed the graphite's slowly diminishing capacity with cycling was eliminated with the ALD and MLD coatings. However, the capacity of the ALD coated electrodes was lower than its bare and MLD coated counterparts. The electrodes coated with 20 MLD cycles exhibited initial capacities comparable to the bare electrodes and a superior capacity after cycling. This was attributed to the heavily cross-linked structure of the MLD thin films helping maintain a stable SEI. The coatings were shown to reduce reduction of the electrolyte by analysis of the irreversible capacity loss. Furthermore, EIS measurements revealed the MLD coatings had less impact on the charge transfer resistance

than the ALD coatings indicating a higher lithium-ion diffusivity through coatings. Overall, MLD has been shown to be a viable method to create hybrid organic-inorganic thin films to produce a superior SEI for graphite electrodes.

References

[1] L. Lu, X. Han, J. Li, J. Hua, and M. Ouyang, "A review on the key issues for lithium-ion battery management in electric vehicles," *J. Power Sources*, vol. 226, pp. 272–288, Mar. 2013.

[2] D. Linden and T. Reddy, *Handbook of batteries*, 4th ed. New York: The McGraw-Hill Companies, Inc., 2010.

[3] J.-M. Tarascon and M. Armand, "Issues and challenges facing rechargeable lithium batteries," *Nature*, vol. 414, no. 6861, pp. 359–367, Nov. 2001.

[4] N. Omar, P. Van den Bossche, G. Mulder, M. Daowd, J. M. Timmermans, J. Van Mierlo, and S. Pauwels, "Assessment of performance of lithium iron phosphate oxide, nickel manganese cobalt oxide and nickel cobalt aluminum oxide based cells for using in plug-in battery electric vehicle applications," in *2011 IEEE Vehicle Power and Propulsion Conference*, 2011, pp. 1–7.

[5] D. Fauteux and R. Koksbang, "Rechargeable lithium battery anodes: alternatives to metallic lithium," *J. Appl. Electrochem.*, vol. 23, no. 1, pp. 1–10, Jan. 1993.

[6] M. Arakawa and J.-I. Yamaki, "The cathodic decomposition of propylene carbonate in lithium batteries," *J. Electroanal. Chem. Interfacial Electrochem.*, vol. 219, no. 1–2, pp. 273–280, Mar. 1987.

[7] S. Zhang, M. S. Ding, K. Xu, J. Allen, and T. R. Jow, "Understanding Solid Electrolyte Interface Film Formation on Graphite Electrodes," *Electrochem. Solid-State Lett.*, vol. 4, no. 12, p. A206, 2001.

[8] K. Xu, "Nonaqueous Liquid Electrolytes for Lithium-Based Rechargeable Batteries," *Chem. Rev.*, vol. 104, no. 10, pp. 4303–4418, Oct. 2004.

[9] S. S. Zhang, "A review on electrolyte additives for lithium-ion batteries," *J. Power Sources*, vol. 162, no. 2, pp. 1379–1394, Nov. 2006.

[10] T. Tsumura, "Surface modification of natural graphite particles for lithium ion batteries," *Solid State Ionics*, vol. 135, no. 1–4, pp. 209–212, Nov. 2000.

[11] Y. S. Jung, P. Lu, A. S. Cavanagh, C. Ban, G.-H. Kim, S.-H. Lee, S. M. George, S. J. Harris, and A. C. Dillon, "Unexpected Improved Performance of ALD Coated LiCoO 2 /Graphite Li-Ion Batteries," *Adv. Energy Mater.*, vol. 3, no. 2, pp. 213–219, Feb. 2013.

[12] a. Tokranov, B. W. Sheldon, P. Lu, X. Xiao, and A. Mukhopadhyay, "The Origin of Stress in the Solid Electrolyte Interphase on Carbon Electrodes for Li Ion Batteries," *J. Electrochem. Soc.*, vol. 161, no. 1, pp. A58–A65, Nov. 2013.

[13] H.-Y. Wang and F.-M. Wang, "Electrochemical investigation of an artificial solid electrolyte interface for improving the cycle-ability of lithium ion batteries using an

atomic layer deposition on a graphite electrode," *J. Power Sources*, vol. 233, pp. 1–5, Jul. 2013.

[14] M.-L. Lee, C.-Y. Su, Y.-H. Lin, S.-C. Liao, J.-M. Chen, T.-P. Perng, J.-W. Yeh, and H. C. Shih, "Atomic layer deposition of TiO2 on negative electrode for lithium ion batteries," *J. Power Sources*, vol. 244, pp. 410–416, Dec. 2013.

[15] Y. S. Jung, A. S. Cavanagh, L. a Riley, S.-H. Kang, A. C. Dillon, M. D. Groner, S. M. George, and S.-H. Lee, "Ultrathin Direct Atomic Layer Deposition on Composite Electrodes for Highly Durable and Safe Li-Ion Batteries," *Adv. Mater.*, vol. 22, no. 19, pp. 2172–2176, Apr. 2010.

[16] D. Seghete, R. A. Hall, B. Yoon, and S. M. George, "Importance of Trimethylaluminum Diffusion in Three-Step ABC Molecular Layer Deposition Using Trimethylaluminum, Ethanolamine, and Maleic Anhydride," *Langmuir*, vol. 26, no. 24, pp. 19045–19051, Dec. 2010.

[17] A. A. Dameron, D. Seghete, B. B. Burton, S. D. Davidson, A. S. Cavanagh, J. A. Bertrand, and S. M. George, "Molecular Layer Deposition of Alucone Polymer Films Using Trimethylaluminum and Ethylene Glycol," *Chem. Mater.*, vol. 20, no. 10, pp. 3315–3326, May 2008.

[18] E. Peled, "Advanced Model for Solid Electrolyte Interphase Electrodes in Liquid and Polymer Electrolytes," *J. Electrochem. Soc.*, vol. 144, no. 8, p. L208, 1997.

Supporting Information

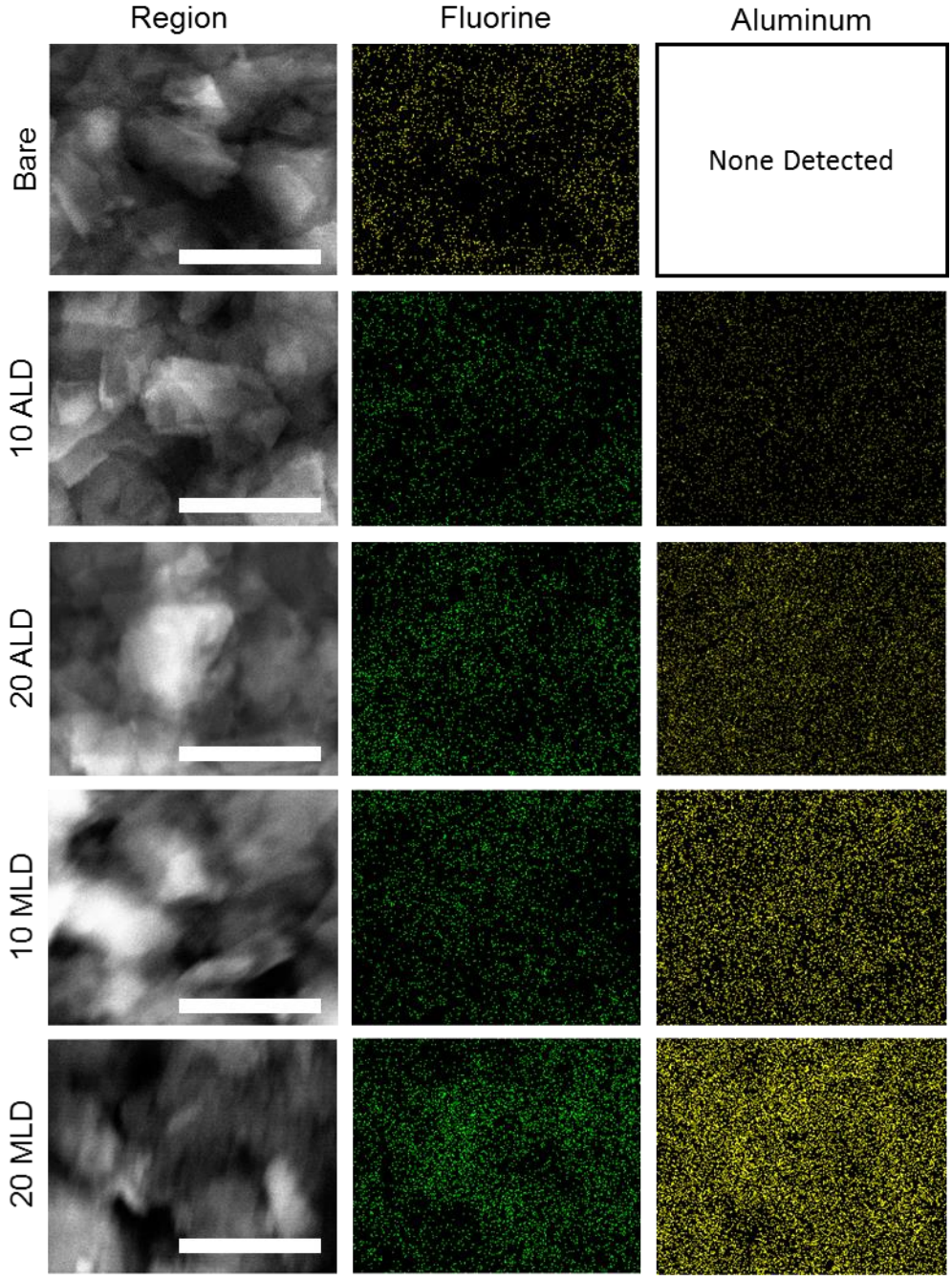

Figure S3.1. EDX mapping of the electrodes coated with ALD and MLD thin films. The left images show the SEM image of where the mapping was performed. The center images show mapping of fluorine indicating conformal PVdF mixing on all the samples. The right images show the mapping of the aluminum indicating good conformity of the ALD and MLD thin films. Scale bars are 6 µm.

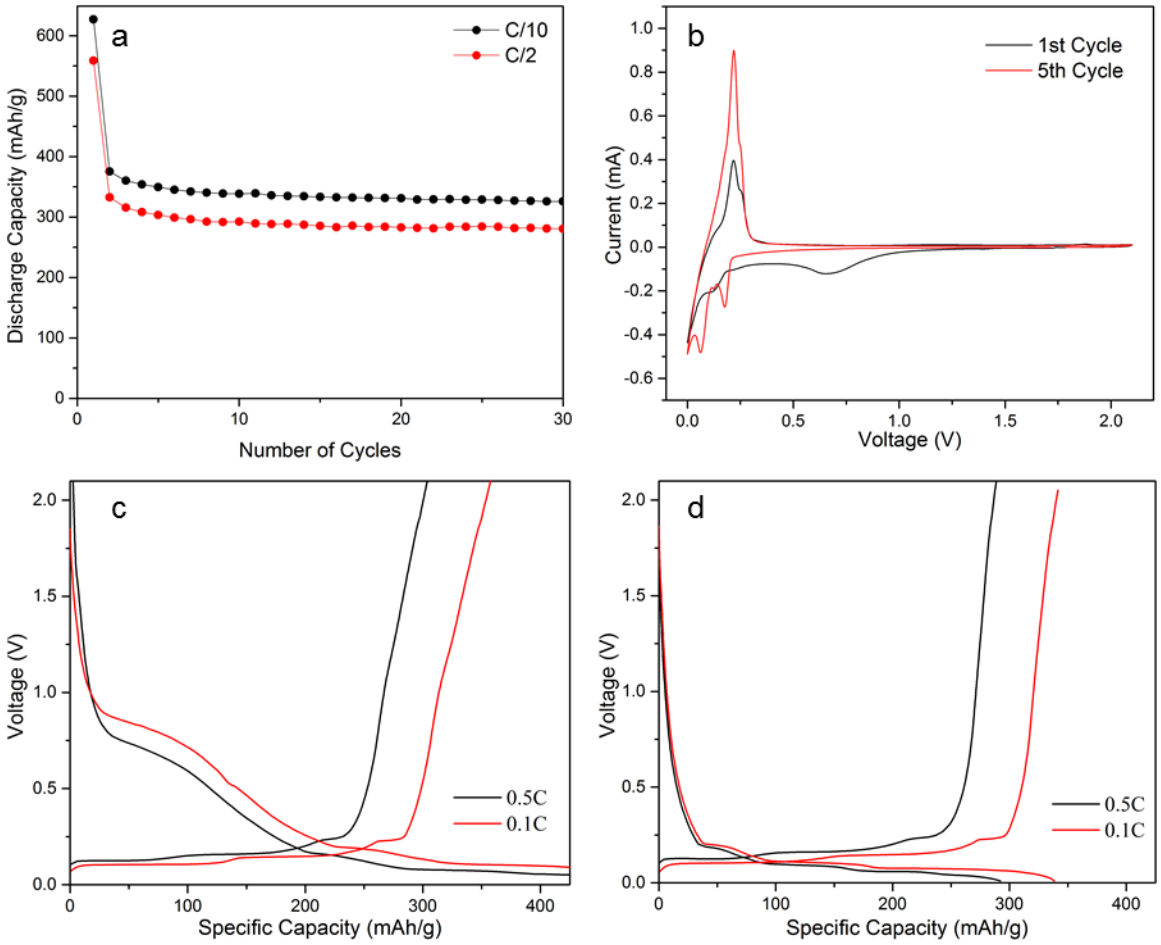

Figure S3.2. (a) Cycling performance of a bare graphite electrode with a 10 hour charge and 10 hour discharge (C/10) and 2 hour charge and 2 hour discharge (C/2). (b) Cyclic voltammetry curves of the reference graphite electrode. Voltage curves of the graphite electrode at different C/2 and C/10 during (a) the first and (b) 10th charge-discharge cycles.

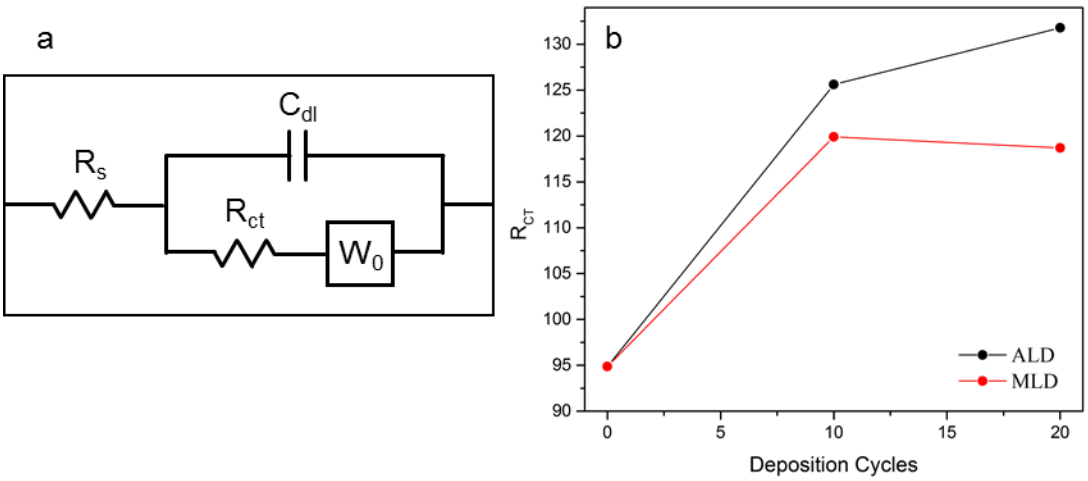

Figure S3.3. (a) Equivalent circuit of a half-cell composed of the series resistance R_s, double layer capacitance (C_{dl}), charge transfer resistance (R_{ct}) and the Warburg impedance (W_0). (b) The calculated charge transfer resistances of the bare and coated graphite electrodes before the first cycle.

4 A Controlled Surface Area Thin-Film via Molecular Layer Deposition

Microporous thin films have the potential to be in LIBs as they can provide unique material surface properties. Utilizing a thin-film coating can alter specific chemical/physical properties of a bulk material. For consistent properties, this thin film should be highly conformal, with a controlled porosity and thickness to have precise control of the bulk material's overall surface properties. Hybrid organic-inorganic molecular layer deposited thin films are excellent candidates to create highly conformal thin films with a controlled thickness, however, up until now no work has reported a method to control the thin film's microporosity. To gain control of the porosity of the ultrathin films we investigated the effect of the number of organic subcycles during the molecular layer deposition process. We demonstrated the number of organic subcycles have a direct impact on the surface area of the thin films increasing the surface area from 134 m^2/g with a single organic subcycle to 235 m^2/g with 5 organic subcycles.

4.1 Introduction

Microporous thin films have recently been shown to have potential applications for selectivity [1], anti-corrosion [2], anti-reflection [3] and drug-delivery [4]. Coating a material with a microporous thin film allows the enhancement of specific chemical and/or physical properties for these applications, therefore, this thin-film may prove to be useful for LIBs. Molecular layer deposition (MLD) thin-films has been demonstrated to produce microporous thin films with tunable thickness and high conformity after annealing [5], [6], however, up until now no work has reported a method to control the structure of the pores. MLD involves exposure of a substrate to two complementary precursors. Alternating the exposure of these precursors to the substrate allows layer-by-layer growth. It is important that these two precursors are not self-reactive to avoid a continuous CVD reaction on the surface and that they react with the complementary precursor on the surface of the substrate.

Inorganic films have traditionally been created via atomic layer deposition (ALD), however, recently the inclusion of organic precursor molecules has allowed the fabrication

of organic and hybrid organic-inorganic thin films. Liang et al deposited a hybrid organic-inorganic MLD film, alucone, by the introduction of an aluminum precursor, trimethyl-aluminum (TMA), and an organic linker, ethylene glycol (EG) [7]. By performing a post-water or annealing treatment, the organic component of the alucone could be removed from the film leaving a microporous aluminum oxide thin film. The microporous thin films exhibited a pore-size of 0.6 nm with little variance. Qin et al further investigated the effect of post annealing alucone films deposited onto copper and found the copper diffused to the outer surface of the microporous structure [8].

The control of the pore-size has been intensively investigated in bulk microporous materials as it affects the chemical and physical properties such as the catalytic performance, selectivity as a molecular sieve, gas diffusion rate and drug release rate [9]–[12]. Angstrom level control of the pore-size is needed to optimize the performance of these materials and has been done by controlling their composition [10], synthesis parameters [13] and post treatment [9]. In particular, a method to create microporous oxide structures via the sol-gel method is the removal of an organic template [14]. By controlling the length of the polymer chains between the inorganic portions the resulting pore size after an annealing process can be controlled. We have recently demonstrated the ability to control the chain length between inorganic sections of hybrid organic-inorganic MLD films [15]. This is achieved by introducing three precursors in an AB-CB pattern. In this case, precursor A is an inorganic compound and precursors B and C are organic components. By repeating the CB "subcycle", the chain length of the polymer between the inorganic components can be controlled.

Herein we introduce a method to control the surface area of annealed MLD thin films by controlling the number of organic subcycles. This method uses three precursors in an AB-CB pattern in which the first AB subcycle contains an inorganic Al_2O_3 portion and the second CB subcycle produces a purely organic linker. The number of both subcycles can be controlled independently. The inorganic AB subcycle is composed of trimethylaluminum (TMA) and ethylene glycol (EG) pulses, followed by the organic subcycle composed of terephthaloyl chloride (TC) and EG pulses, herein named as TMA-EG-(TC-EG). 20 super cycles of TMA-EG-$(TC\text{-}EG)_x$ with x = 1,3,5 produced films of

increasing organic content. This was followed by an annealing process in air at 400°C for one hour to remove the organic component of the thin films. To investigate the properties of the film *in-situ* thermogravimetric analysis analyzed the mass loss during the annealing process of the film. *Ex-situ* transmission electron microscopy (TEM), energy dispersive X-ray spectroscopy (EDX), Fourier transform infrared spectroscopy (FTIR), and Brunauer-Emmett-Tller (BET) surface area measurements allowed further characterization of the thin-films.

4.2 Methods

4.2.1 Thin-film Preparation

Silicon dioxide nanoparticles (Sigma Aldrich, 20-30 nm, 99.5%) were used as the deposition substrate due to their high stability, and high surface area. The nanoparticles were prepared for deposition by sonicating in an ethanol solution for 30 minutes (1:10 v/v) before dispersing on aluminum foil. The dispersion was allowed to dry overnight leaving a thin coating of nanoparticles across the aluminum's surface.

Deposition of the MLD thin films was performed using a Gemstar Arradiance 8 ALD tool. The hybrid organic-inorganic thin films with a controlled organic content was achieved by cycling inorganic and organic subcycles in an AB-CB fashion. The AB subcycle consisted of pulses of trimethyl aluminum (TMA, $Al(CH_3)_3$, Strem, 98%) and ethylene glycol (EG, $HO(CH_2)_2OH$, Sigma-Aldrich, 99.8%). This was followed by the purely organic subcycle, which consisted of alternating pulses of terepthaloyl chloride (TC, $C_8H_4Cl_2O_2$, Sigma-Aldrich, 99%) and EG. Figure 4.1 shows a schematic depicting the deposition process to produce the inorganic-organic thin films. TMA-EG to TC-EG subcycles were controlled in ratios of 1:1, 1:3 and 1:5 for investigation of the varying organic content.

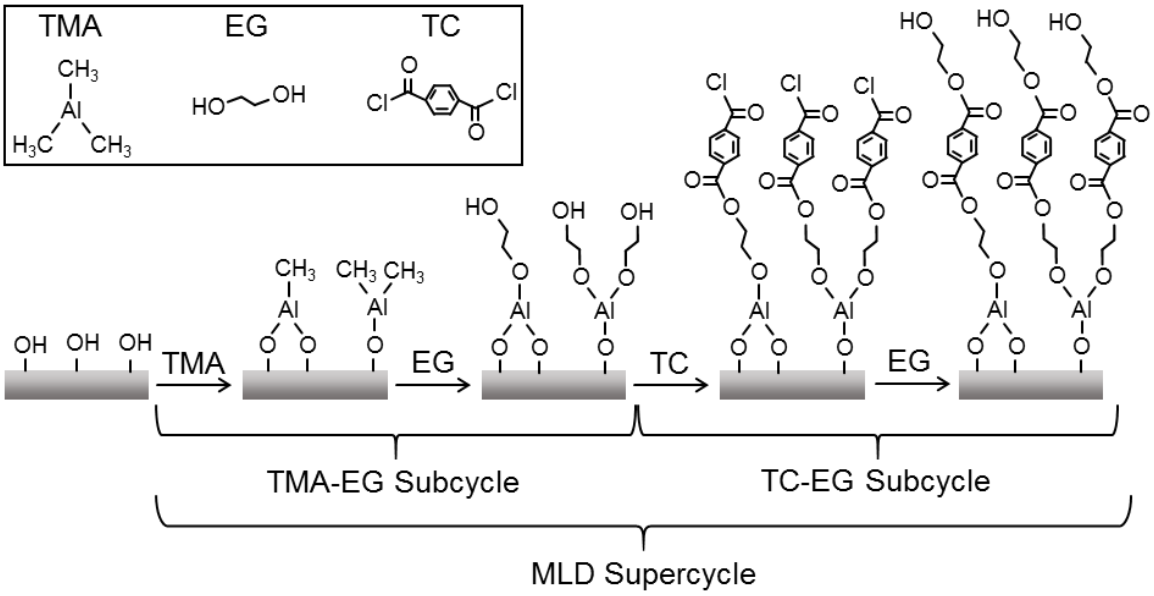

Figure 4.1. Schematic showing the process to produce hybrid inorganic-organic MLD thin-films using trimethyl aluminum (TMA), ethylene glycol (EG) and terephthaloyl chloride (TC).

20 supercycles of each ratio was performed at a temperature of 130 °C with a manifold temperature of 120 °C. Precursors were pulsed into the system for a set time after which the vacuum was closed holding the precursor in the system to create a precursor "bath". To remove any precursor or by-products the vacuum was opened and the gas flow rate was increased to a rate of 100 sccm purging the system. The chamber was then set back to initial conditions with a flow rate of 10 sccm, and left to stabilize. Details of the precursor deposition parameters are in Table 4.1. It should be noted that the pulse time of the TC was due to its low volatility resulting in a lower vapour pressure.

Table 4.1. MLD Deposition Parameters.

	TMA	EG	TC
Temperature (°C)	Room Temperature	90	110
Pulse Time (milliseconds)	50	50	500
Hold Time (seconds)	3	3	3
Purge Time (seconds)	10	10	10
Stabilization Time (seconds)	10	10	10

The coated nanoparticles were heated with a ramp rate of 10 °C per minute to 400 °C under atmosphere. The chamber was held at 400 °C for one hour before cooling to room temperature.

4.2.2 Characterization

A QCM monitor (Colnatec Eon-LT) was used to measure the mass gain of the MLD thin-films during deposition. Physical characterization of the coatings was carried out with a field emission SEM (Hitachi S-4800) and cross-section imaging was performed with a TEM (Hitachi 7000). I*n-situ* measurements of the coating's mass during the annealing treatment were carried out with a TA Instruments Q600-SDT TGA system. A Thermo Scientific Nicolet 380 FTIR system was used for *ex-situ* characterization of the infrared active components of the thin-films before and after the annealing treatment. A Micrometrics TriStar-II tool was used to obtain gas-sorption isotherms of the samples and to calculate the BET surface area of the thin films after the annealing process. For gas-sorption preparation samples were heated 90 °C for one hour followed by 3 hours at 300 °C to ensure no surface species on their surfaces.

4.3 Results

SiO_2 nanoparticles were cast onto aluminum foil for preparation for deposition of the MLD thin films. For confirmation of MLD growth during the deposition process QCM measurements analyzed the mass gain. Figure 4.2a shows the resulting mass measurements of a typical TMA-EG-$(TC-EG)_x$, x = 1,3,5 cycle. The first mass gain is due to the TMA

pulse. This pulse can be seen to have a slight decrease in mass during the purging time, however, it is relatively stable. Furthermore, a larger mass increase is found with the TMA pulse of the TMA-EG-$(TC-EG)_5$ recipe. This may be due to the additional TC-EG subcycles creating additional reactive sites for the TMA as well as diffusion of the TMA into the additional TC-EG layers [16]. Following the initial TMA-EG cycle a larger mass gain can be seen with each pulse in the films with higher TC-EG subcycles, again, likely due to the additional reaction sites and additional absorption. The TC and EG pulses can be seen to have a large mass decrease during the purge time. This is due to the larger TC and EG organic molecules physisorbing on the surface of the surface before being pulled off by the following vacuum. Furthermore, a lower mass gain can be seen after the first TC-EG subcycle. Due to the steric hindrance of the larger TC molecules, as well as double reactions of the TC and EG molecules to TMA a lower deposition rate can be expected. The following TC-EG subcycles can be seen to be linear in growth after the initial post-ALD-EG subcycle. An overall mass gain of 54.8, 84.9 and 121.8 ng/cm^2 per cycle was found for the TMA-EG-$(TC-EG)_1$, TMA-EG-$(TC-EG)_3$ and TMA-EG-$(TC-EG)_5$ films respectively.

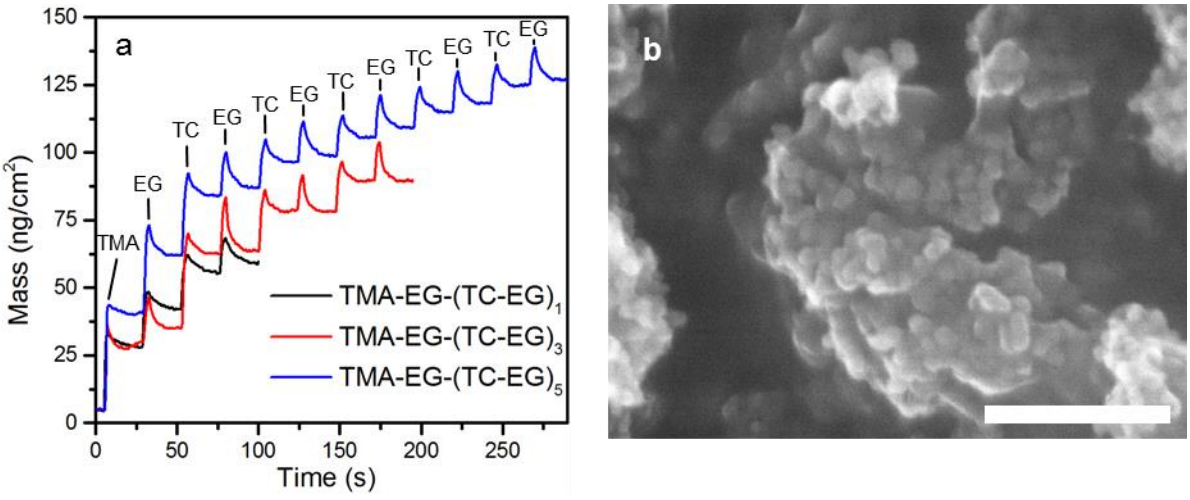

Figure 4.2. (a) QCM measurements of a typical MLD deposition cycle of TMA-EG-$(TC-EG)_x$, x = 1, 3, 5. (b) SEM image of SiO_2 nanoparticles coated with TMA-EG-$(TC-EG)_1$. Scale bar represents 200 nm.

For confirmation of the surface morphology of the sample SEM was performed. Figure 4.2b shows the SEM image of the SiO_2 nanoparticles coated with 20 cycles of TMA-EG-(TC-EG)$_1$. The MLD coating can be seen to be blanketed across the particles, and it appears that the particles were not individually coated. This is likely due to the drop casting method for the sample preparation causing the nanoparticles to clump. In addition, the SEM characterization was damaging to the electrodes slowly melting the thin-film coatings during prolonged exposure causing further congregation of the particles. To minimize this, the acceleration voltage was reduced from 20 kV to 5 kV and images were taken immediately. For individual coating of the nanoparticles fluidized bed reactors have shown to be practical [17], however, the casting method was deemed sufficient for testing of the surface area control of the resulting thin films. Further imaging of the particles coated with 20 cycles of TMA-EG-(TC-EG)$_3$ and TMA-EG-(TC-EG)$_5$ were attempted, however, the samples proved to be highly sensitive to the electron beam and melted almost immediately upon investigation. This is likely due to the higher TC-EG sub-cycles in these samples creating a softer, more polymer-like composition.

To gain insight into the cross section of the thin films TEM characterization was performed and the results are seen in Figure 4.3. The bare SiO_2 nanoparticles can be seen to range in size from 20-30 nm in Figure 4.3a. A core-shell structure can be seen Figure 4.3(b-d) with the coating have good conformation on the particles. Analysis of the films from TEM imaging revealed average thicknesses of 5.3, 7.2 and 9.7 nm for the TMA-EG-(TC-EG)$_1$, TMA-EG-(TC-EG)$_3$ and TMA-EG-(TC-EG)$_5$ coated samples respectively. Calculated deposition rates of 2.7, 3.6 and 4.9 Å per supercycle of the respective coatings correlate well with previous work [15].

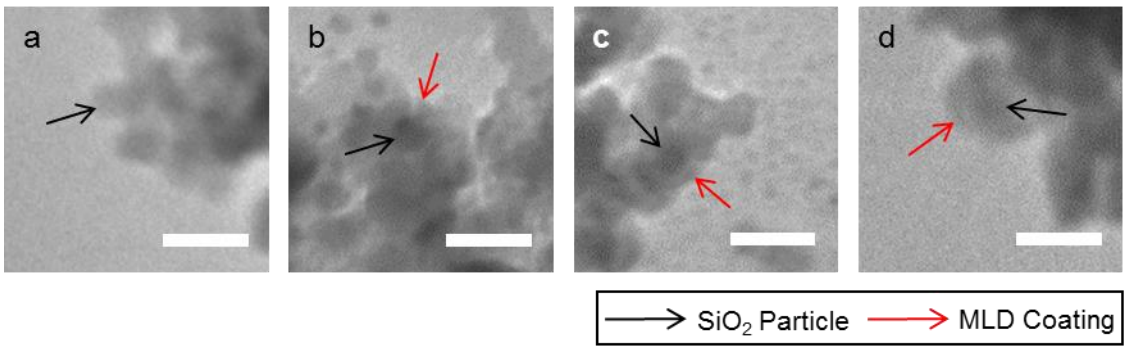

Figure 4.3. TEM images of (a) bare SiO_2 nanoparticles and SiO_2 nanoparticles coated with 20 cycles of (b) TMA-EG-(TC-EG)$_1$, (c) TMA-EG-(TC-EG)$_3$ and (d) TMA-EG-(TC-EG)$_5$. Scale bar is 30 nm.

TGA and DSC measurements were taken during the annealing process of the MLD films to analyze the mass lost. Figure 4.4a shows the relative masses of the samples. A ramp rate of 10 °C / minute was used as shown by the dotted line followed by isothermal conditions at 400 °C for the following hour. A sharp decrease in mass loss can be seen until the temperature reaches above 100 °C which can be associated with surface moisture loss off the samples. The bare SiO_2 can be seen to have the highest mass drop due to moisture loss indicating its surface is highly hydrophilic. The bare SiO_2 can also be seen to have a steady decrease in mass with time, despite the temperature reaching isothermal conditions after 45 minutes. This is likely due to the small SiO_2 particle size and being caught by the passing air flow. The other samples exhibited similar phenomena under isothermal conditions indicating this is the case. Higher TC-EG subcycles can be seen to increase the mass loss during the annealing process. Figure 4.4b shows the mass loss of the samples after the annealing process. This can be seen to be nearly linear which is indicative of stepwise MLD deposition during the TC-EG subcycles.

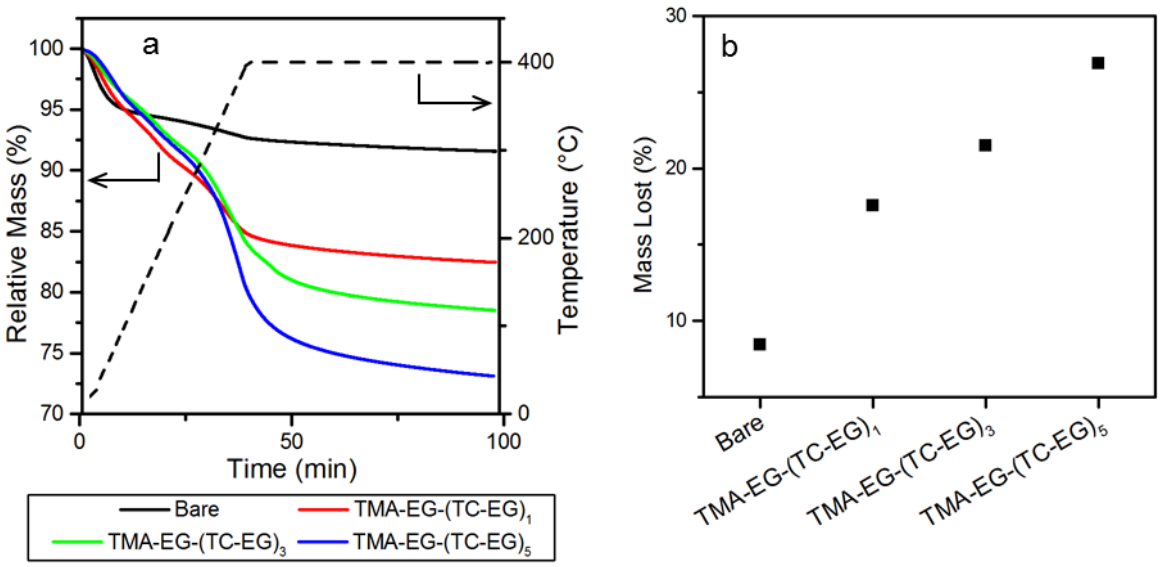

Figure 4.4. (a) TGA measurements during the annealing process of SiO_2 nanoparticles treated with different MLD coatings. The dotted line shows the temperature profile of the process. (b) The resulting mass loss after the annealing processes.

DSC characterization of the coatings was also found and can be seen in Figure S4.2. From this there can be seen to be an heat flux at ~300 °C which coordinates with the combustion of the carbon content of the thin-film. Furthermore, this peak can be seen to increase with the number of TC-EG subcycles, with 5 TC-EG subcycles having the highest heat flow at this point. From this it can be seen that by the time the temperature reaches 400 °C the combustion of the carbon has completed. Maintaining the temperature at 400 °C for one hour ensures the complete removal of the carbon.

FTIR measurements were used to detect the organic composition of the all the MLD coated samples before and after the annealing treatment. A strong absorption could be found in all the samples at 1101 cm^{-1} with a small shoulder coordinating with the longitudinal and transversal optical mode of the Si-O-Si asymmetric stretching vibrations [18]. All spectra were normalized with respect to this peak as the SiO_2 nanoparticles were consistent amongst all the samples. The peaks at 1631 cm^{-1}, 802 cm^{-1} and 474 cm^{-1} are also observed, coordinate with the O-Si-O bond [18], which was confirmed via FTIR analysis of the bare

SiO_2 nanoparticles as seen in Figure S4.1. The bands at 1724 cm^{-1} (red), 1263 cm^{-1} (green) and 729 cm^{-1} (blue) have been well documented for MLD films and coordinate with vibrations of the C=O, CH_2 and aromatic vibrations respectively [19], [20]. These bands can be seen in all MLD coated samples before the annealing treatment, however, they are completely gone after the annealing process. This further confirms the removal of the organic component of the thin films through the annealing process. Meanwhile, the organic compounds' absorption bands can be seen to increase with the number of TC-EG subcycles indicative of increasing organic content in the films. Furthermore, some minor peaks can be seen to begin to appear in the 1550-1450 cm^{-1} range. These peaks are attributed to skeletal vibrations in the aromatic ring [19]. A small absorption band can be seen to develop at 875 cm^{-1} which has been associated with O=C-Cl stretching [20]. This indicates incomplete reactions of the C-Cl bond of TC which may be due to hanging bonds on the surface of the film, or incomplete removal of physisorbed TC. Despite this, the absorption band in relation to the other absorption bands is relatively small when compared to previous results [21], indicating only a small portion of the precursor didn't react.

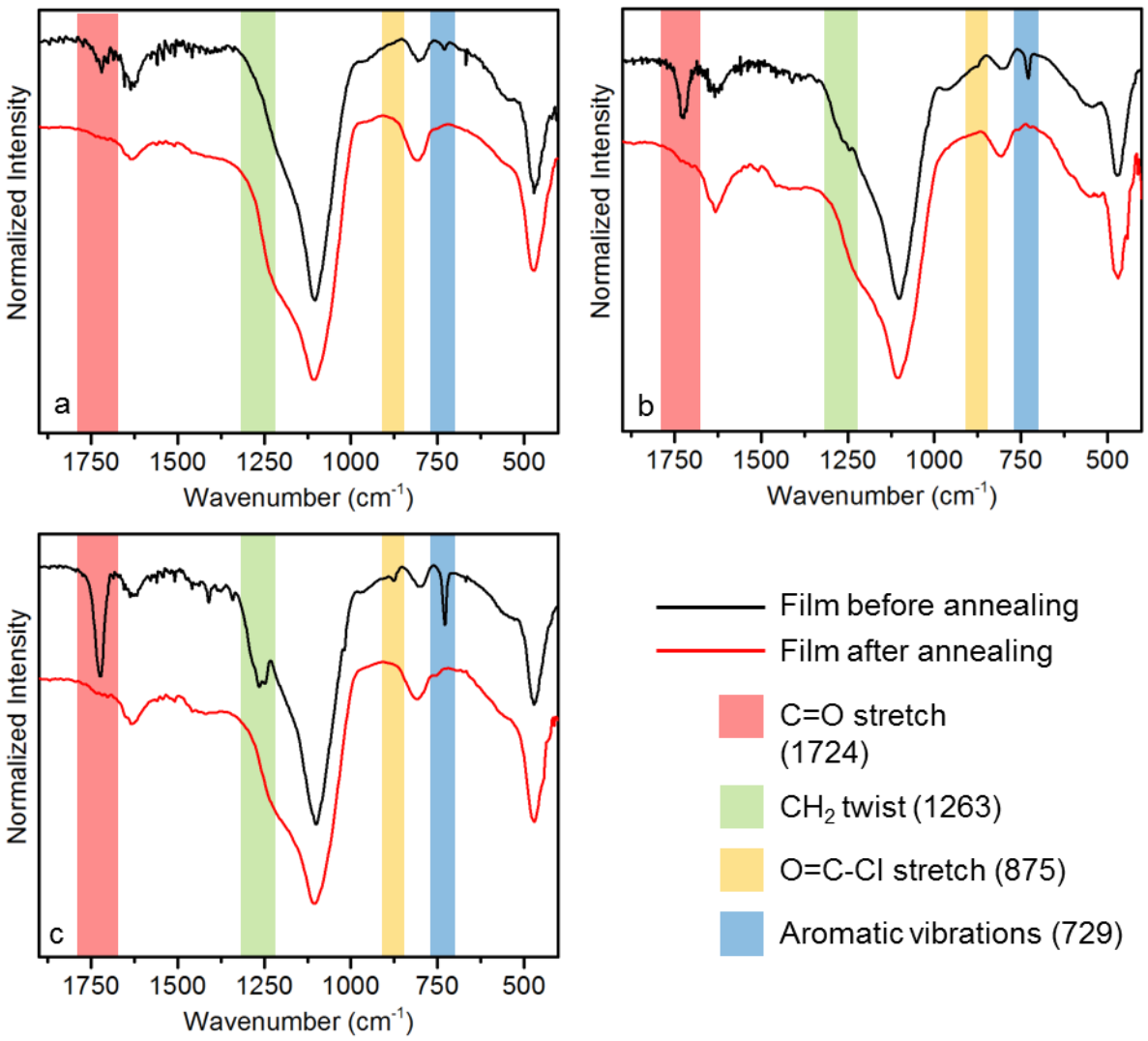

Figure 4.5. FTIR measurements before and after the annealing process of SiO_2 nanoparticles treated with 20 MLD cycles of (a) TMA-EG-(TC-EG)$_1$, (b) TMA-EG-(TC-EG)$_2$ and (c) TMA-EG-(TC-EG)$_3$.

The gas-sorption isotherms were measured for the bare SiO_2 nanoparticles and particles coated with 20 cycles of TMA-EG-(TC-EG)$_x$, x = 1,2,3 as seen in Figure 4.6. A sharp increase of surface area can be seen with low P/P_0 ratios flowed slow increase from ~0.1 to ~0.8 P/P_0. The adsorption sharply increases again as P/P_0 approaches 1. The region above 0.5 P/P_0 is indicative of a type IV isotherm [22], which is due to the condensation of nitrogen at the higher pressures. This is likely due to droplets spanning the larger pores between the SiO_2 nanoparticles. The hysteresis that is found in the higher pressure is

indicative of condensation across the pores. In the lower pressure region below 0.1 P/P_0 the quantity absorbed is dependent upon monolayer growth of the nitrogen. This sharp increase is due to the micropores quickly reaching saturation [23]. Therefore, the amount absorbed in this region is indicative of the microporous surface area of the samples. Increasing the number of TC-EG subcycles can be seen to increase the quantity of nitrogen absorbed in this region indicating an increased microporous surface area. The surface areas of the material was calculated by the system utilizing BET theory and can be seen in Figure 4.6b. show an increase in surface area with TC-EG subcycles. Surface areas of 60.3, 134.3, 191.5 and 235.2 m^2/g were calculated for the bare, TMA-EG-$(TC\text{-}EG)_1$, TMA-EG-$(TC\text{-}EG)_3$ and TMA-EG-$(TC\text{-}EG)_5$ films respectively. This indicates that the number of TC-EG subcycles directly controls the surface area of the films.

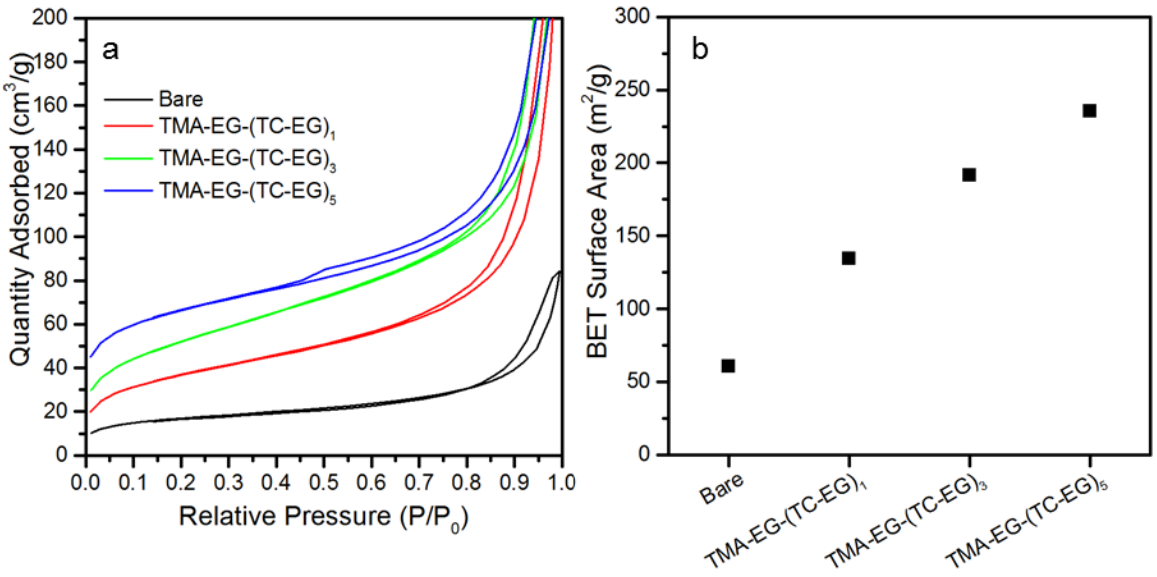

Figure 4.6. (a) Gas-sorption isotherms of the MLD coated silicon dioxide nanoparticles after the annealing process. (b) Resulting BET measurements calculated from the isotherms of the samples.

4.4 Discussion

The porous thin films created via annealing MLD coatings is superior to other methods such as the sol-gel method and template method in a number of ways. First, the number of organic subcycles during the deposition process directly controls the microporous surface

area of the coating. Second, the MLD process allows a highly conformal thin film to be created, which can be deposited on high aspect substrates. This allows the possibility of developing the film coating on a number of substrates, provided the substrate is stable in atmosphere at 400 °C. Finally, the uniform nature of the thin film allows for it to exhibit consistent properties.

A simplified schematic of the thin films is proposed in Figure 4.7 which depicts 3 cycles of each recipe opposed to 20 cycles used in the process. Due to the additional TC-EG subcycles a thicker organic component of the thin films creating a thicker film and larger space between the inorganic layers of the film. As the organic portion of the film gets thicker TMA molecules are more likely to diffuse into the film as demonstrated from the QCM measurements. After the annealing process the organic portion of the films is completely removed with only the inorganic component remaining. Due to the thinner and more compact structure of the film with one TC-EG subcycle a much denser porous film results after the process. Increasing the number of TC-EG subcycles creates a less dense film forms with higher porosity, and likely larger pores. This results in an highly conformal, ultrathin film coating with a controlled porosity.

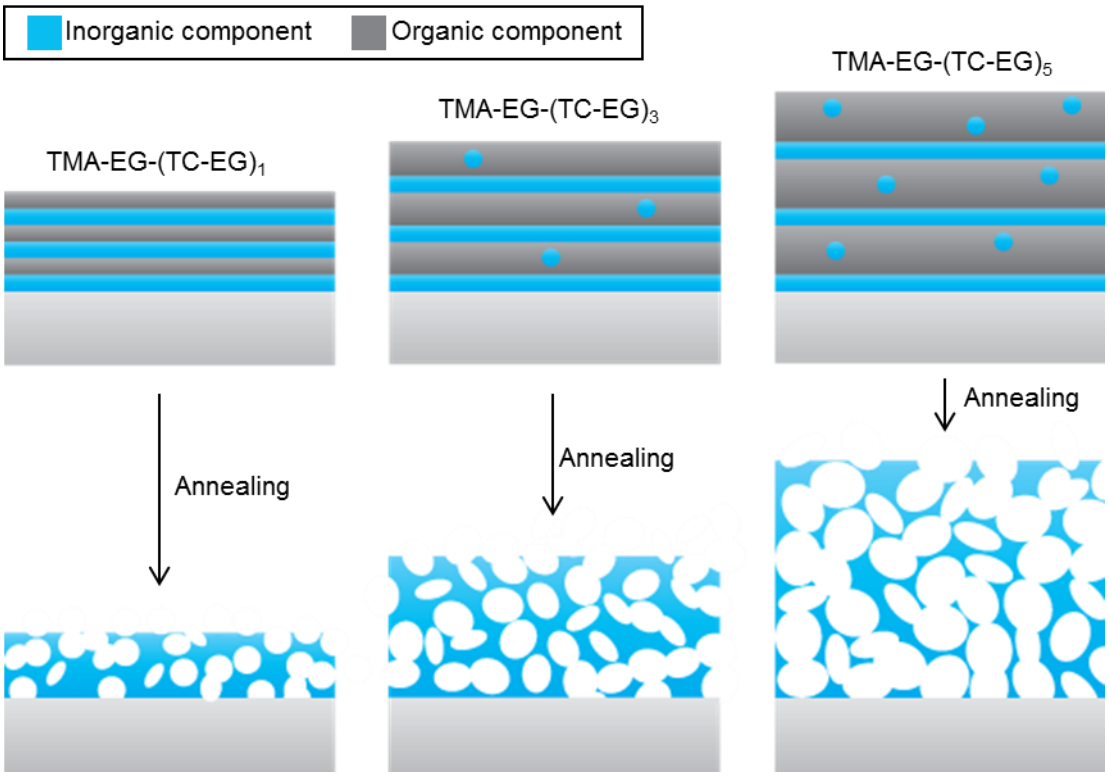

Figure 4.7. Schematic of 3 supercycles of TMA-EG-(TC-EG)$_x$, x=1,3,5 before and after the annealing process.

4.5 Conclusions

In conclusion, a series of ultrathin film with controllable surface areas were created on SiO_2 nanoparticles via MLD. This was achieved by first depositing 20 super cycles of TMA-EG-(TC-EG)$_1$, TMA-EG-(TC-EG)$_3$ and TMA-EG-(TC-EG)$_5$. Increasing the number of TC-EG subcycles allowed the control of the carbon content of the thin film. The deposition process was confirmed via QCM measurements showing the step-wise deposition of the MLD process. SEM characterization revealled a conformal thin film on the nanoparticles, however, some clumping of particles was found, likely due to the substrate preparation process. TEM characterization gained further insight to the thickness and conformity of the thin films confirming the increased growth rate with more TC-EG subcycles. To create a porous thin-film the samples were annealed in air at 400 °C, where *in-situ* TGA showed an increased mass loss with increasing TC-EG subcycles indicating removal of the organic component of the films. Removal of the organic components was further confirmed via

FTIR spectroscopy in which the bands associated with the organic bonds disappeared with annealing. Finally, BET analysis revealed that increasing the TC-EG subcycles resulted in an increase in the microporous surface area of the annealed thin films. Overall, MLD with a controlled organic subcycle has been shown to be a viable method to create ultrathin porous films with a controlled microporosity. These thin-films have potential to be used as coatings for LIBs as the micropores can enable ionic diffusion while blocking larger electrolyte molecules.

References

[1] C.-Y. Tsai, S.-Y. Tam, Y. Lu, and C. J. Brinker, "Dual-layer asymmetric microporous silica membranes," *J. Memb. Sci.*, vol. 169, no. 2, pp. 255–268, May 2000.

[2] S. V. Lamaka, M. L. Zheludkevich, K. A. Yasakau, R. Serra, S. K. Poznyak, and M. G. S. Ferreira, "Nanoporous titania interlayer as reservoir of corrosion inhibitors for coatings with self-healing ability," *Prog. Org. Coatings*, vol. 58, no. 2–3, pp. 127–135, Feb. 2007.

[3] J. Hiller, J. D. Mendelsohn, and M. F. Rubner, "Reversibly erasable nanoporous anti-reflection coatings from polyelectrolyte multilayers," *Nat. Mater.*, vol. 1, no. 1, pp. 59–63, Sep. 2002.

[4] J.-F. Chen, H.-M. Ding, J.-X. Wang, and L. Shao, "Preparation and characterization of porous hollow silica nanoparticles for drug delivery application," *Biomaterials*, vol. 25, no. 4, pp. 723–727, Feb. 2004.

[5] Y. Qin, Y. Yang, R. Scholz, E. Pippel, X. Lu, and M. Knez, "Unexpected Oxidation Behavior of Cu Nanoparticles Embedded in Porous Alumina Films Produced by Molecular Layer Deposition," *Nano Lett.*, vol. 11, no. 6, pp. 2503–2509, Jun. 2011.

[6] X. Liang, M. Yu, J. Li, Y.-B. Jiang, and A. W. Weimer, "Ultra-thin microporous–mesoporous metal oxide films prepared by molecular layer deposition (MLD)," *Chem. Commun.*, no. 46, p. 7140, Dec. 2009.

[7] X. Liang and A. W. Weimer, "An overview of highly porous oxide films with tunable thickness prepared by molecular layer deposition," *Curr. Opin. Solid State Mater. Sci.*, vol. 19, no. 2, pp. 115–125, Apr. 2015.

[8] Y. Qin, Y. Yang, R. Scholz, E. Pippel, X. Lu, and M. Knez, "Unexpected oxidation behavior of Cu nanoparticles embedded in porous alumina films produced by molecular layer deposition.," *Nano Lett.*, vol. 11, no. 6, pp. 2503–9, Jun. 2011.

[9] M. Ito, H. Nishihara, K. Yamamoto, H. Itoi, H. Tanaka, A. Maki, M. T. Miyahara, S. J. Yang, C. R. Park, and T. Kyotani, "Reversible Pore Size Control of Elastic Microporous Material by Mechanical Force," *Chem. - A Eur. J.*, vol. 19, no. 39, pp. 13009–13016, Sep. 2013.

[10] M. E. Davis and R. F. Lobo, "Zeolite and molecular sieve synthesis," *Chem. Mater.*,

vol. 4, no. 4, pp. 756–768, Jul. 1992.

[11] A. W. Thornton, T. Hilder, A. J. Hill, and J. M. Hill, “Predicting gas diffusion regime within pores of different size, shape and composition,” *J. Memb. Sci.*, vol. 336, no. 1–2, pp. 101–108, Jul. 2009.

[12] C. a. Aerts, E. Verraedt, R. Mellaerts, A. Depla, P. Augustijns, J. Van Humbeeck, G. Van den Mooter, and J. a. Martens, “Tunability of Pore Diameter and Particle Size of Amorphous Microporous Silica for Diffusive Controlled Release of Drug Compounds,” *J. Phys. Chem. C*, vol. 111, no. 36, pp. 13404–13409, Sep. 2007.

[13] M. J. Kim and R. Ryoo, “Synthesis and Pore Size Control of Cubic Mesoporous Silica SBA-1,” *Chem. Mater.*, vol. 11, no. 2, pp. 487–491, Feb. 1999.

[14] C. J. Brinker, R. Sehgal, S. L. Hietala, R. Deshpande, D. M. Smith, D. Loy, and C. S. Ashley, “Sol-gel strategies for controlled porosity inorganic materials,” *J. Memb. Sci.*, vol. 94, no. 1, pp. 85–102, Sep. 1994.

[15] A. Lushington, J. Liu, M. N. Bannis, B. Xiao, S. Lawes, R. Li, and X. Sun, “A novel approach in controlling the conductivity of thin films using molecular layer deposition,” *Appl. Surf. Sci.*, vol. 357, pp. 1319–1324, Dec. 2015.

[16] D. Seghete, R. A. Hall, B. Yoon, and S. M. George, “Importance of Trimethylaluminum Diffusion in Three-Step ABC Molecular Layer Deposition Using Trimethylaluminum, Ethanolamine, and Maleic Anhydride,” *Langmuir*, vol. 26, no. 24, pp. 19045–19051, Dec. 2010.

[17] D. M. King, J. A. Spencer, X. Liang, L. F. Hakim, and A. W. Weimer, “Atomic layer deposition on particles using a fluidized bed reactor with in situ mass spectrometry,” *Surf. Coatings Technol.*, vol. 201, no. 22–23, pp. 9163–9171, Sep. 2007.

[18] R. Al-Oweini and H. El-Rassy, “Synthesis and characterization by FTIR spectroscopy of silica aerogels prepared using several Si(OR)4 and R′′Si(OR′)3 precursors,” *J. Mol. Struct.*, vol. 919, no. 1–3, pp. 140–145, Feb. 2009.

[19] T. V. Ivanova, P. S. Maydannik, and D. C. Cameron, “Molecular layer deposition of polyethylene terephthalate thin films,” *J. Vac. Sci. Technol. A Vacuum, Surfaces, Film.*, vol. 30, no. 1, p. 01A121, 2012.

[20] N. M. Adamczyk, a a Dameron, and S. M. George, “Molecular Layer Deposition of Poly(p-phenylene terephthalamide) Films Using Terephthaloyl Chloride and p -Phenylenediamine,” *Langmuir*, vol. 24, no. 5, pp. 2081–2089, Mar. 2008.

[21] Y. Umar and S. Abdalla, “Experimental FTIR and Theoretical Investigation of the Molecular Structure and Vibrational Spectra of Terephthaloyl Chloride by Density Functional Theory,” *IOSR J. Appl. Chem. I*, vol. 8, no. 9Ver, pp. 26–34, 2015.

[22] R. Schmidt, M. Stöcker, E. Hansen, D. Akporiaye, and O. H. Ellestad, “MCM-41: a model system for adsorption studies on mesoporous materials,” *Microporous Mater.*, vol. 3, no. 4–5, pp. 443–448, Jan. 1995.

[23] E. Maglara, A. Pullen, D. Sullivan, and W. C. Conner, “Characterization of Microporous Solids by Adsorption: Measurement of High-Resolution Adsorption Isotherms,” *Langmuir*, vol. 10, no. 11, pp. 4167–4173, Nov. 1994.

Supporting Information

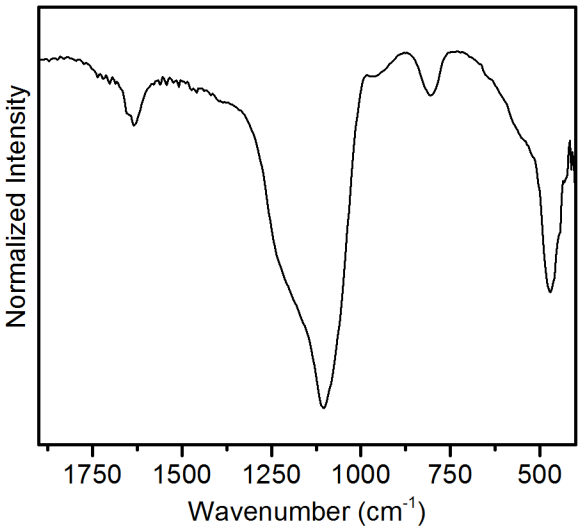

Figure S4.1. FTIR spectroscopy of bare SiO_2 nanoparticles.

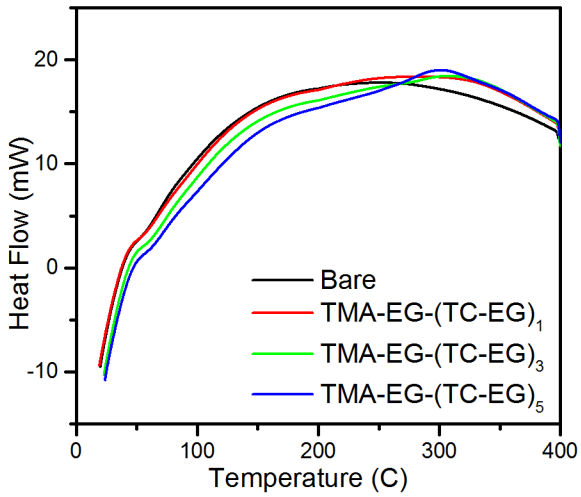

Figure S4.2 Differential scanning calorimetry of SiO_2 nanoparticles heated to 400°C at 10°C/minute.

5 Conclusions and Future Work

5.1 Conclusions

In this thesis, two studies were conducted revolving around MLD of hybrid organic-inorganic alucone thin films with two main objectives: (1) demonstrate that MLD is superior to ALD as a coating method to improve the stability of graphite in LIBs and (2) develop a MLD derived porous thin-film with a controlled surface area by controlling the thin film's inorganic-organic ratio. The first is a study focused on meeting the first objective by investigating the influence of the MLD coating on graphite, the current commercial anode material for lithium-ion batteries. The physical and electrochemical properties of the electrodes were compared to both bare and ALD coated electrodes. The second study is a study focused on meeting the second objective by annealing MLD thin films with a controlled organic chain length.

In the first study, 0, 10 and 20 cycles via ALD and MLD directly onto graphite electrodes. This was accomplished by alternating pulses of TMA and H_2O for the ALD thin-films and TMA and EG for the MLD thin films. The deposition of the thin films on the electrodes were first characterized. Step-wise growth of the thin films was found with a higher mass increase per cycle via MLD due to the larger EG molecules. The ALD and MLD processes produced conformal ultrathin-films on the graphite electrodes and did not have any effect on the microscale morphology of the samples due to their low deposition temperatures. Once the deposition of the thin films on the electrodes was confirmed the electrodes were subjected to electrochemical testing to investigate the effect of the thin-film coatings.

Cycling of the cells revealed both the ALD and MLD thin-film coatings decreased the irreversible capacity loss of the graphite electrodes. Furthermore, both thin-film coated electrodes did not exhibit the characteristic diminishing capacity the bare graphite electrode did. Despite these advantages, the ALD coated electrodes had a lower cycling capacity, likely due to regions becoming inactive from the denser coating. A superior cycling performance from the MLD coated electrodes was demonstrated, which had a cycling capacity higher than both the bare and ALD coated electrodes after 150 cycles. The graphite electrode coated with 20 MLD cycles gave the best results indicating the MLD

coating increases the stability of the SEI. It was revealed that the thin-film coatings exhibited an increased ionic resistance to the bare electrode, however, after stabilization of the SEI, this was eliminated.

In the second study, an MLD thin-film was deposited with control of the carbon content. This was achieved by having an inorganic sub-cycle of TMA and EG, followed by an organic sub-cycle of TC and EG. The TMA-EG and TC-EG sub-cycles were controlled in ratios of 1:1, 1:3 and 1:5 respectively to create a combined super-cycle. To create the thin-films the super-cycle was repeated 20 times. All films were found to grow in a stepwise manner, with the TMA-EG to TC-EG ratio of 1:5 producing the fastest growth per super-cycle. Further chemical and physical characterization revealed that the thin-films contained increasing organic content with the TC-EG sub-cycles. Upon confirmation of the increasing organic content in the thin-films, the samples were subjected to the annealing treatment.

To create a porous thin film with a controllable surface area the thin films were annealed in air to burn off their organic component. Chemical and physical characterization revealed complete removal of the organic portion of the films leaving an aluminum oxide structure. Testing the surface area of the thin-films demonstrated an increasing surface area with TC-EG sub-cycles showing that the surface area of the thin films could be controlled by changing the organic content in the thin films.

Overall, the two studies in this thesis have demonstrated MLD as a viable method to improve the performance of the lithium-ion battery anode, graphite, as well as create an ultrathin high surface area coating. MLD is a powerful tool as it can produce a thin-film with excellent control over its thickness and composition. Additionally, this thin-film is excellent for high aspect substrates as it has a high conformity, and has a deposition temperature much lower than conventional thin film techniques. My work shows that despite MLD films being ultra-thin they can have an very large impact on the electrochemical performance of a graphite in lithium-ion batteries. This opens the possibility to explore other thin-film compositions deposited via MLD which can further optimize the SEI formed on the graphite during cycle. Additionally, these thin films can

have a large impact on the surface area of a material, opening the possibility for their deposition on various substrates to develop “hybrid materials”. These porous thin-films have potential application as coating materials for lithium-ion battery electrodes, photocatalysts, drug delivery coatings and anti-reflection coatings. In conclusion, this thesis demonstrates the power of MLD to control the electrochemical performance and surface morphology of materials which has potential application for LIB electrode materials.

5.2 Recommendations for Future Work

Molecular layer deposition is a relatively new field having only been developed since the early 1990s [1]. However, since its initial introduction it has been found to be an incredibly versatile tool to deposit a wide range of both organic and hybrid organic-inorganic thin-films due to various chemistries [2]. This has allowed an excellent platform to expand its application in LIBs. Furthermore, treatment of these thin-films can provide many unique surface properties. A number of possible future sudies based on the work in this thesis is presented below.

Graphite has been used for commercial LIBs for over 20 years due to its high stability, low voltage potential, reasonable capacity and low cost. Due to the capacity of the metal oxide cathode being the most limiting factor towards the battery’s capacity a large amount of work has gone towards enabling high capacity cathode materials such as sulfur and oxygen [3]. However, these cathodes use non-carbonate based electrolytes, disallowing stable SEI formation on graphite during the first charge-discharge cycle, resulting in a low stability. As this thesis has shown an MLD coating on the electrode has a drastic effect on SEI formation, therefore, a logical step would be to investigate the capability of MLD coatings to enable a stable SEI in alternative electrolytes allowing graphite’s practicality for future battery systems.

Another interesting project would be to apply MLD coatings to battery anode materials with have superior capacities to graphite. A recent study has shown the use of MLD can drastically improve the cycling performance of silicon, which has a theoretical specific capacity much greater than graphite [4]. Lithium metal, the typical anode material paired

with sulfur and oxygen cathodes has an unstable surface during cycling. Recent studies have shown ALD as a tool to improve the stability of lithium metal [5], [6]. Due to the higher flexibility and control of mechanical properties MLD has to offer it is an excellent candidate for lithium-metal coatings.

In terms of the use of MLD for porous thin-film, many avenues for future projects are possible. Coating the active material of a battery with a porous thin-film would be a very interesting study to follow. The porous nature of the thin-film may allow formation of ion-conducting channels as well as create a bi-functional thin-film. Due to the high temperature treatment required to create the porous thin-film the coating could not be deposited directly on the electrode composite as performed in this thesis. Instead, it would need to be deposited on the active material powder, followed by the annealing treatment, which could then be mixed with the polymeric binder and conducting agent. The investigation of a thin film, with a controlled structure, would be very novel in this field.

A logical next step for the use of a porous thin-film with a controlled surface area would be investigating how the variation of surface area impacts its use for various applications. Porous thin-films have been shown to be practical for applications such as photocatalysts [7], drug delivery [8] and anti-reflection coatings [9]. Control of the structure of the thin-films may allow optimization of the porous thin-films. Furthermore, this method allows the variation of substrates enabling further control of the material.

In general, MLD is a new field in which a large number of compositions and chemistries have been realized, however, their application for use in batteries remains to be investigated. Furthermore, its ability to combine different processes to create hybrid thin-films offers an even wider range of thin-films with varying chemical and physical properties. Already, MLD has been shown to improve the electrochemical performance of various anode and cathode materials in lithium-ion batteries [4], [10]–[12]. With the transportation sector largely contributing to greenhouse gasses it is fundamental that more advanced batteries are realized for use in electric vehicles. Molecular layer deposition has shown that it can be a valuable tool for this development, and is expected to contribute further to this field in the future.

References

[1] T. Yoshimura et al., “Polymer films formed with monolayer growth steps by molecular layer deposition,” *Appl. Phys. Lett.*, vol. 59, no. 4, p. 482, 1991.

[2] P. Sundberg et al., “Organic and inorganic–organic thin film structures by molecular layer deposition: A review,” *Beilstein J. Nanotechnol.*, vol. 5, pp. 1104–1136, Jul. 2014.

[3] M. M. Thackeray et al., “Electrical energy storage for transportation—approaching the limits of, and going beyond, lithium-ion batteries,” *Energy Environ. Sci.*, vol. 5, no. 7, p. 7854, 2012.

[4] D. M. Piper et al., “Reversible High-Capacity Si Nanocomposite Anodes for Lithium-ion Batteries Enabled by Molecular Layer Deposition,” *Adv. Mater.*, vol. 26, no. 10, pp. 1596–1601, Mar. 2014.

[5] E. Kazyak et al., “Improved Cycle Life and Stability of Lithium Metal Anodes through Ultrathin Atomic Layer Deposition Surface Treatments,” *Chem. Mater.*, vol. 27, no. 18, pp. 6457–6462, Sep. 2015.

[6] A. C. Kozen et al., “Next-Generation Lithium Metal Anode Engineering via Atomic Layer Deposition,” *ACS Nano*, vol. 9, no. 6, pp. 5884–5892, Jun. 2015.

[7] C. Chen et al., “Nanoporous Nitrogen-Doped Titanium Dioxide with Excellent Photocatalytic Activity under Visible Light Irradiation Produced by Molecular Layer Deposition,” *Angew. Chemie Int. Ed.*, vol. 52, no. 35, pp. 9196–9200, Aug. 2013.

[8] J.-F. Chen et al., “Preparation and characterization of porous hollow silica nanoparticles for drug delivery application,” *Biomaterials*, vol. 25, no. 4, pp. 723–727, Feb. 2004.

[9] J. Hiller et al., “Reversibly erasable nanoporous anti-reflection coatings from polyelectrolyte multilayers,” *Nat. Mater.*, vol. 1, no. 1, pp. 59–63, Sep. 2002.

[10] X. Li et al., “Safe and Durable High-Temperature Lithium–Sulfur Batteries via Molecular Layer Deposited Coating,” *Nano Lett.*, vol. 16, no. 6, pp. 3545–3549, Jun. 2016.

[11] X. Li et al., “Superior stable sulfur cathodes of Li–S batteries enabled by molecular layer deposition,” *Chem. Commun.*, vol. 50, no. 68, p. 9757, Jul. 2014.

[12] A. J. Loebl et al., “Solid Electrolyte Interphase on Lithium-Ion Carbon Nanofiber Electrodes by Atomic and Molecular Layer Deposition,” *J. Electrochem. Soc.*, vol. 160, no. 11, pp. A1971–A1978, Sep. 2013.

Curriculum Vitae

Name: Craig Langford

Post-secondary Education and Degrees:
B.A.Sc., Nanotechnology Engineering
University of Waterloo
Waterloo, Ontario, Canada
2008 - 2013

Honours and Awards:
Queen Elizabeth II Graduate Scholarship in Science and Technology
2015-2017

Western University Graduate Scholarship
2013-2015

Ontario Society of Professional Engineers Personal Scholarship
2016

Related Work Experience
Teaching Assistant
The University of Western Ontario
2013-2016

Battery R&D Co-op
General Motors
Warren, Michigan, USA
05/2015 – 08/2015

Publications:

[Co-author] Q. Sun, H. Yadegari, M. Banis, J. Liu, B. Xiao, X. Li, **C. Langford**, R. Li, X. Sun, J. Phys. Chem. Lett. (2015).

[Acknowledged] J. Wang, X. Sun, Energy Environ. Sci. 00 (2015) 1.

[Co-author] B. Xiao, X. Li, X. Li, B. Wang, **C. Langford**, R. Li, X. Sun, J. Phys. Chem. C 118 (2014) 881.